AD-A229 922

AD_____

CONTRACT NO.: DAMD17-87-C-7139

TITLE: Cutaneous Toxicity of Mustard and Lewisite on The Isolated Perfused Porcine Skin Flap

PRINCIPAL INVESTIGATOR: Nancy A. Monteiro-Riviere
CO-AUTHORS: John R. King
Jim E. Riviere

CONTRACTING ORGANIZATION: North Carolina State University
College of Veterinary Medicine
Cutaneous Pharmacology and Toxicology Center
Raleigh, North Carolina 27606

REPORT DATE: April 1, 1990

TYPE OF REPORT: Midterm Report

PREPARED FOR: U.S. ARMY MEDICAL RESEARCH AND DEVELOPMENT COMMAND Fort Detrick, Frederick, Maryland 21702-5012

DISTRIBUTION STATEMENT: Approved for public release; distribution unlimited

DTIC
ELECTE
DEC 13 1990

The findings in this report are not to be construed as an official Department of the Army position unless so designated by other authorized documents.

REPORT DOCUMENTATION PAGE

Form Approved
OMB No. 0704-0188

1a. REPORT SECURITY CLASSIFICATION	1b. RESTRICTIVE MARKINGS

2a. SECURITY CLASSIFICATION AUTHORITY	3. DISTRIBUTION/AVAILABILITY OF REPORT
2b. DECLASSIFICATION/DOWNGRADING SCHEDULE	Approved for public release; distribution unlimited

4. PERFORMING ORGANIZATION REPORT NUMBER(S)	5. MONITORING ORGANIZATION REPORT NUMBER(S)

6a. NAME OF PERFORMING ORGANIZATION	6b. OFFICE SYMBOL (If applicable)	7a. NAME OF MONITORING ORGANIZATION
College of Veterinary Medicine North Carolina State Univ.		

6c. ADDRESS (City, State, and ZIP Code)	7b. ADDRESS (City, State, and ZIP Code)
Box 8401 Raleigh, North Carolina 27606	

8a. NAME OF FUNDING/SPONSORING ORGANIZATION U.S. Army Medical Research & Development Command	8b. OFFICE SYMBOL (If applicable)	9. PROCUREMENT INSTRUMENT IDENTIFICATION NUMBER DAMD17-87-C-7139

8c. ADDRESS (City, State, and ZIP Code)	10. SOURCE OF FUNDING NUMBERS			
Fort Detrick Frederick, MD 21702-5012	PROGRAM ELEMENT NO. 61102A	PROJECT NO. 3M1 61102BS11	TASK NO. AA	WORK UNIT ACCESSION NO. 055

11. TITLE (Include Security Classification)

Cutaneous Toxicity of Mustard and Lewisite on the Isolated Perfused Porcine Skin Flap

12. PERSONAL AUTHOR(S)
Monteiro-Riviere, N.A., King, J.R., and Riviere, J.E.

13a. TYPE OF REPORT Midterm	13b. TIME COVERED FROM 9/30/87 TO 4/1/90	14. DATE OF REPORT (Year, Month, Day) 1990, April 01	15. PAGE COUNT 144

16. SUPPLEMENTARY NOTATION

17.	COSATI CODES		18. SUBJECT TERMS (Continue on reverse if necessary and identify by block number)
FIELD	GROUP	SUB-GROUP	pig, skin, flap, porcine, integument, absorption, pharmaco- logy, histology, electron microscopy, toxicology, mustard, lewisite, vesication, glucose utilization, vascular response,
06	15		
06	04		

RAV

19. ABSTRACT (Continue on reverse if necessary and identify by block number)

This report describes the utilization of the isolated perfused porcine skin flap (IPPSF) to characterize the cutaneous toxicity of sulfur mustard (XHD) and lewisite (XL). The IPPSF is an humane, alternative, in vitro, animal model consisting of an isolated perfused skin preparation with intact and viable epidermis and dermis in association with a functional microcirculation. Task 1 of the present contract was to characterize the dose-response profile of both vesicants in 53 IPPSFs using biochemical, physiological, and morphological (light and transmission electron microscopy) endpoints. Twenty-four IPPSFs were treated with 200 μl of either 5.0, 2.5, 1.25, 0.2, 0.14, or 0.07 mg/ml XL, and 29 IPPSFs were treated with 200 μl of either 10.0, 5.0, 2.5, 1.25, 0.5 or 0.2 mg/ml XHD. At least four replicates were performed per compound, and four untreated IPPSFs served as controls. Experiments lasted 8 hours. Both XL and XHD resulted in a reduction in the cumulative glucose utilization and an increased vascular resistance as compared to controls. The high-dose groups for both agents consistently showed a marked alteration in both parameters.

20. DISTRIBUTION/AVAILABILITY OF ABSTRACT ☐ UNCLASSIFIED/UNLIMITED ☐ SAME AS RPT ☐ DTIC USERS	21. ABSTRACT SECURITY CLASSIFICATION Unclassified
22a. NAME OF RESPONSIBLE INDIVIDUAL Mrs. Virginia M. Miller	22b. TELEPHONE (Include Area Code) (301) 663-7325 22c. OFFICE SYMBOL SGRD-RMI-S

DD Form 1473, JUN 86   Previous editions are obsolete.   SECURITY CLASSIFICATION OF THIS PAGE

19. ABSTRACT (continued)

Morphologically, both XL and XHD produced macroscopic and microscopic blisters in a dose-dependent fashion. In conclusion, these studies suggest that the IPPSF is an appropriate _in vitro_ model with which to study cutaneous vesication of XL and XHD treatment, since the dose-dependent biochemical, physiological, and morphological changes seen were similar to previously reported _in vivo_ findings.

FOREWORD

Opinions, interpretations, conclusions, and recommendations are those of the author and are not necessarily endorsed by the U.S. Army.

Name Where copyrighted material is quoted, permission has been obtained to use such material.

N/A Where material from documents designated for limited distribution is quoted, permission has been obtained to use the material.

Name Citations of commercial organizations and trade names in this report do not constitute an official Department of Army endorsement or approval of the products or services of these organizations.

Name In conducting research using animals, the investigator(s) adhered to the "Guide for the Care and Use of Laboratory Animals," prepared by the Committee on Care and Use of Laboratory Animals of the Institute of Laboratory Resources, National Research Council (NIH Publication No. 86-23, Revised 1985).

N/A For the protection of human subjects, the investigator(s) adhered to policies of applicable Federal Law 45 CFR 46.

_____   4/1/90
PI - Signature   DATE

4

ACKNOWLEDGMENT

TABLE OF CONTENTS

TABLE OF CONTENTS (continued)

TABLE OF CONTENTS (continued)

Figures

TABLE OF CONTENTS (continued)

<u>Figures</u>

TABLE OF CONTENTS (continued)

<u>Figures</u>

INTRODUCTION

The isolated perfused porcine skin flap (IPPSF) is an _in vitro_ model that has been utilized for percutaneous absorption studies (Carver et al., 1989) and for the pharmacokinetic modeling of xenobiotics (Williams et al., 1990; Williams and Riviere, 1989). In addition, the histology and biochemical responses of this model have been evaluated as markers of viability and cutaneous toxicity (Monteiro-Riviere et al., 1987; Riviere et al., 1986a; Riviere et al., 1986b; Riviere et al., 1987). Advantages of this system include: (1) a viable, full-thickness skin preparation, (2) an intact vasculature, (3) a relatively large surface area for dosing, (4) ease in sample collection and in measurement and control of experimental parameters, and (5) the lack of systemic immune system mediation (Riviere and Carver, 1991, Monteiro-Riviere, 1990). Also, this preparation offers an alternative animal model to many of the classic _in vivo_ models used for cutaneous toxicity studies. Pig skin has been shown to be morphologically similar to human skin and has been offered as a good model for the study of cutaneous absorption and toxicity (Meyer et al., 1978; Monteiro-Riviere, 1986; Monteiro-Riviere and Stromberg, 1985; Montagna and Yun, 1964; Reifenrath et al., 1984).

Evidence of the use of sulfur mustard (HD) in the Iran-Iraq war (United Nations Report, 1984) has resulted in a renewed focus on the need for research on the mechanisms of vesicant injury, as well as for improved protective and therapeutic strategies. A major concern of this research has been the inability to identify an _in vivo_ or _in vitro_ model that possesses cutaneous tissue structurally and functionally similar to human skin and that reproduces the characteristic, grossly vesicated skin lesions that are typical of human exposure to vesicants. Historically, vesicles or vesicle-like lesions have been produced in a few animal model systems, including bird skin, frog skin, canine mammary gland skin, rabbit ear skin, and thermally-burned re-epithelialized guinea pig skin (Renshaw, 1946). More

11

recent research has suggested that microvesicles can occur in pigs treated topically with neat butyl mustard (Westrom, 1987). Another recent study showed that in vivo cutaneous exposure of pigs to the vesicants HD and lewisite resulted in microvesicle formation, but not grossly vesicated lesions (Micheltree et al., 1989). Also, microvesicles have been elicited in the haired (Marlow et al., 1989; Vogt et al., 1984) and euthymic hairless guinea pig (Marlow et al., 1989; Petrali et al., 1989; Wade et al., 1989) and in the human skin grafted athymic nude mouse model (Papirmeister et al., 1984a; Papirmeister et al., 1984b) on exposure to HD and in the human skin grafted athymic nude mouse model after exposure to vesicant arsenicals (McGown et al., 1987). Of in vitro systems, the full-thickness human skin organ culture model has demonstrated the ability to develop microscopic, epidermal-dermal separation on exposure to HD (Mol et al., 1989b). However, none of these newer models have reported the macroscopic blisters that are typical of reports of human exposure to vesicant compounds (Requena et al., 1988).

Previous studies utilized the IPPSF to biochemically and morphologically assess the dermatotoxicity of 2-chloroethyl methyl sulfide (CEMS), a monofunctional analogue of the vesicant, sulfur mustard. In these studies, distinct biochemical, physiologic, and morphologic changes occurred as a result of topical exposure to this vesicant (King and Monteiro-Riviere, 1990). These changes included the formation of gross vesicles and bullae in CEMS treated IPPSF's. Light microscopy revealed subepidermal vesicle formation above the basement membrane and extensive basal cell pyknosis in all IPPSF's treated with CEMS. No macroscopic or microscopic lesions were noted in the control flaps. Transmission electron microscopy revealed separation between the lamina lucida and lamina densa of the basal lamina, with intracellular vacuolization and mitochondrial swelling occurring in the stratum basale and stratum spinosum cells of IPPSF's treated with CEMS. These lesions are similar to those described after human exposure to sulfur mustard. The objective of this

study was to explore the potential utility of the IPPSF as a model of cutaneous vesication by evaluation of the effects of XHD and lewisite (XL) on the biochemical viability, vascular response, and morphology of the IPPSF. The studies conducted in the initial phase of this contract (Technical Objective 1) were performed to characterize the cutaneous toxicity of lewisite and sulfur mustard on the IPPSF. The biological indices utilized to assess vesication were based on the earlier results obtained with CEMS and other cutaneous toxicants. These include cumulative glucose utilization, glucose/lactate ratio, lactate dehydrogenase (LDH) production, and changes in vascular resistance and morphology using light and transmission electron microscopy. The results presented in this report are those of a dose-response study for both vesicants using these parameters as the response.

MATERIALS AND METHODS

Weanling, female, Yorkshire pigs were purchased commercially and acclimated for at least 1 week prior to surgery. They were housed in a temperature (72°C) and light-dark-cycle (12:12 hour) controlled facility with elevated pen floors. Water was provided ad libitum, and the animals were fed 15% protein pig and sow pellets (Wayne Feeds Division, Chicago, IL) daily.

Anesthetic induction was accomplished with ketamine hydrochloride (10 mg/kg) and xylazine hydrochloride (4 mg/kg), after pre-dosing with atropine sulfate. Tracheal intubation was performed, and anesthesia was maintained with halothane. The surgical procedure is described in detail elsewhere (Bowman et al., 1991; Monteiro-Riviere, 1989). Briefly, it was conducted in two stages, with two IPPSF's created on each pig. Previous studies have shown the area of skin flap preparation to be vascularized primarily by the caudal superficial epigastric artery and its paired venae comitantes. The first surgical stage consisted of the formation of two, axial pattern, tubed skin flaps. Two days later, the flaps were removed from the pig and their arterial supply cannulated. The flaps were flushed with heparinized saline to clear the vasculature of blood and were placed in a Riviere Skin Flap Chamber (Diamond Research, Raleigh, NC) for perfusion (Figure 1). The perfusion chambers were contained in a fume hood.

The IPPSF's were perfused with a medium containing bovine serum albumin, glucose, and Krebs-Ringer bicarbonate buffer. The chamber perfusion apparatus consisted of a closed recirculating system (Figure 1). The media was oxygenated during perfusion with $95\%O_2/ 5\%CO_2$ via a silastic oxygenator. Media temperature, flow rate, pH, and chamber humidity were monitored and controlled throughout the experiment and were constant overall. Target ranges for these parameters were: media temperature of 36 to 38°C, flow rate of 1.5 to 2.0 ml/min, pH of 7.3 to 7.5, and chamber relative humidity of 50 to 60 per

14

cent. Samples were taken of the arterial media and the venous effluent on an hourly basis, and these were analyzed for glucose and lactate content. Glucose values were based on the rate of oxygen consumption as determined using a Beckman Glucose Analyzer 2 (Beckman Instruments, Fullerton, CA). Lactate was measured on a Multistat III Plus clinical chemistry analyzer (Instrumentation Laboratory Lexington, MA) using a spectrophotometric assay (Stat-Pack Rapid Lactate Test, Behring Diagnostics Inc., Somerville, NJ). LDH content was evaluated on a Monarch 2000 clinical chemistry analyzer (Instrumentation Laboratory, Lexington, MA) which utilized a spectrophotometric assay (IL Test LD-L/LDH-L-Instrumentation Laboratory).

After 1 hour of stabilization, each IPPSF was either treated with XL or XHD or served as an untreated control. The agent treated flaps were dosed inside a flexible, plastic template (Stomahesive, ConvaTec-Squibb, Princeton, NJ) having a 5 cm² dosing area. Agent was applied to the dosing area using a positive displacement pipette system (Gilson Microman-Gilson Medical Electronics, France). This system offered the advantages of disposable pipette tips and plungers, thus allowing for the immediate decontamination of the dosing system and preventing cross-contamination between flaps. The XL or XHD was applied to the skin surface one drop at a time along the length of the dosing area until the complete dose was dispensed (usually within a minute). Then, the liquid agent was gently and evenly spread over the dosing surface with the blunt tip of the pipette. The dosed region of the IPPSF was not occluded. The chamber temperature, airflow, and relative humidity were constant for all exposures. The untreated controls (n=4) had an identical template applied but received no treatment.

We have completed 53 isolated perfused porcine skin flap (IPPSF) experiments. Twenty-four IPPSF's were treated with 200 μl of either 5.0 mg/ml, 2.5 mg/ml, 1.25 mg/ml, 0.2 mg/ml, 0.14 mg/ml, or 0.07 mg/ml of lewisite (XL) in ethanol (n=4/treatment). In

addition, 29 IPPSF's were treated with 200 μl of either 10.0 mg/ml (n=5), 5.0 mg/ml, 2.5 mg/ml, 1.25 mg/ml, 0.5 mg/ml, or 0.2 mg/ml of sulfur mustard (XHD) in ethanol (n=4/treatment). The 0.2 mg/ml XHD experiments were repeated (n=4) due to variability in the original results. Four IPPSF's served as controls for both the XHD and XL treatment groups.

After perfusion, the entire dosed region of skin was excised, and tissue samples were taken for light microscopy (LM) and transmission electron microscopy (TEM). LM samples were fixed in cold (4°C), 10% neutral buffered formalin for 24-48 hours. TEM samples were minced into 1-mm^3 pieces and fixed in cold (4°C), modified Karnovsky's fixative (2.0% paraformaldehyde, 2.5% glutaraldehyde in 0.1 M cacodylate buffer, pH=7.2) for 24 hours. (Monteiro-Riviere and Manning, 1987). The LM samples were processed routinely and embedded in paraffin. They were then sectioned at 6 μm and stained with either Harris's hematoxylin and eosin (H&E) or periodic acid-Schiff (PAS). The TEM samples were post-fixed with 1% osmium tetroxide for 1 hour, dehydrated through a graded series of ethanols, and infiltrated and embedded in Spurr's resin. Thick sections, approximately 1 μm in thickness, were stained with 1% toluidine blue for orientation and localization of lesions. Thin sections of 800-1,000 Å were picked up on copper grids, post-stained with uranyl acetate and lead citrate, and examined on a transmission electron microscope (Philips 410L, Philips Electronics, Mahwah, NJ).

Cumulative glucose utilization (CGU) and the ratio of lactate production to glucose utilization (L/GU ratio) have been characterized for the IPPSF and were used as indicators of biochemical viability in previous studies (Carver et al., 1989; Riviere et al., 1986a; Riviere et al., 1987; Monteiro-Riviere, 1989). In this study, these parameters were used to determine the biochemical effects of XL or XHD on IPPSF metabolism and to evaluate IPPSF viability. Hourly glucose utilization was used as the sole parameter of biochemical viability

prior to dosing, and an hourly glucose utilization of less than 10 mg/hour/IPPSF or a plateau in the upward slope of GU indicated a loss of viability in the skin flap preparation. In addition, after the first 1-3 hours of perfusion, any marked deviation from a constant L/GU ratio was associated with loss of IPPSF viability. During the initial hours of perfusion, this typical linear relationship between lactate production and glucose utilization was not seen, apparently, due to the release of endogenous lactate. However, by 3 hours of perfusion, this relationship stayed constant, unless IPPSF viability was compromised. Statistical comparisons of the viability parameters were performed by calculation of the average rate of change for these parameters over the time course of perfusion (slope). Differences between treatments were analyzed by the General Linear Model procedure (Proc GLM) (SAS Institute Inc., Cary, NC), and multiple comparison tests were performed using Student's (Least Significant Differences) t-test to control for Type I comparisonwise error and the Ryan-Einot-Gabriel-Welsch multiple F test to control for Type I experimentwise error. The vascular response of the IPPSF was characterized using the physiological parameter vascular resistance (VR). This parameter was calculated using the formula:

$$VR \ (mmHg \cdot min/ml) = \frac{arterial\ pressure\ (mmHg)}{flow\ (ml/min)}.$$

RESULTS

The results of these studies will be reported separately for XL and XHD. Within these sections, the presentation will be further divided into biochemical/physiological data and then morphological findings. Although all of these studies were conducted and analyzed within compounds and within biochemical or morphological findings, a global analysis of these data across compounds and types of data has not yet been conducted.

Lewisite - XL

Biochemical and Physiological Evaluation

Glucose utilization has been used as a marker of cell viability in a variety of in vitro test systems, and the partial suppression of cellular glucose utilization in these systems has been associated with exposure to XHD. Also, cumulative glucose utilization (units = mg glucose/gm tissue) has been characterized in the IPPSF as a marker of biochemical viability and glucose metabolism. Previous studies have shown that an analogue of sulfur mustard (2-chloroethyl methyl sulfide) caused suppression of CGU in the IPPSF (King and Monteiro-Riviere, 1990).

After exposure to XL, CGU for the 0.07 mg/ml IPPSF's was slightly lower than control from the fourth to fifth hour after dosing until the termination of perfusion at 8 hours (Figure 2). The 0.14 mg/ml XL treatment resulted in decreased CGU at the same time after dosing, but the effect was more pronounced than the 0.07 mg/ml treatment (Figure 3). The 0.2 mg/ml XL flaps closely approximated the 0.14 mg/ml group, with suppression of CGU from approximately the fourth hour after dosing (Figure 4). The 1.25 mg/ml XL dose had a similar effect on CGU, but the effect began earlier (approximately 3 hours after dosing) (Figure 5). The 2.5 mg/ml XL IPPSF's closely approximated the controls throughout the post-dosing period (Figure 6). The 5.0 mg/ml XL flaps showed the most prominent suppression of CGU over the course of perfusion, with lowered CGU noted

18

from 2 to 3 hours after dosing (Figure 7). Figure 8 shows CGU for all XL-treated IPPSF's versus control. Statistical analysis of the average rate of change in CGU (slope) for each of the XL treatment groups showed the 5.0 mg/ml group to have a significantly lowered rate of CGU versus control ($p < 0.05$). All statistical analyses in this report were done using the Proc GLM of SAS, and multiple comparison tests were performed using Student's (Least Significant Differences) t-test at the 95% confidence level.

Vascular resistance (VR) is a physiological parameter that has been used in previous IPPSF studies to evaluate vascular response to cutaneous toxins. This has been shown to increase (versus control) after treatment with the mustard analogue 2-chloroethyl methyl sulfide. Figure 9 shows that, within 1 hour after dosing, vascular resistance increased with XL treatment at the 0.07 mg/ml dose. This response leveled at approximately 4 hours after dosing. A similar, but more pronounced, response was seen at the 0.14 mg/ml dose (Figure 10). A generally less pronounced response was seen with the 0.2 mg/ml XL flaps (Figure 11). The 1.25 mg/ml XL IPPSF's demonstrated an increase in VR, with an apparent plateau about 4 hours after dosing (Figure 12). The 2.5 mg/ml XL dose resulted in an initial increase in VR followed by a plateau at approximately 2 hours (Figure 13). VR was increased in the 5.0 mg/ml XL IPPSF's, with a plateau around 6 to 7 hours after dosing (Figure 14). This dose produced terminal VR levels that were similar to those produced by the 0.14 mg/ml and the 0.07 mg/ml doses. VR for all treatment groups is shown in Figure 15. All treatments resulted in mean VR values that were significantly higher than control ($p < 0.05$).

The ratio of lactate production to glucose utilization (L/GU ratio) has been used as another indicator of biochemical viability in the IPPSF. Typically, a constant (linear) ratio is noted after the first 2 to 3 hours of perfusion. Variation from a linear ratio, or from the control profile, is indicative of an alteration in normal pathways of IPPSF glucose

19

metabolism. Figures 16-21 show that all XL-treated groups demonstrated linear ratios after the first 3 hours of perfusion. In addition, none of the groups showed mean L/GU ratios that were significantly different from control ($p > 0.05$). Figure 22 compares all groups to control and includes the first 2 hours after dosing. Again, the linearity of the ratio for all treatments is apparent, as well as the similarity to control. The lack of linearity during the first 2 hours after dosing is typical for the IPPSF and is due to the release of endogenous lactate during the early hours of perfusion.

Lactate dehydrogenase (LDH) (units = IU/gm tissue) is an oxidative enzyme that has been used in numerous studies and in vitro systems, including other isolated organ systems, as an indicator of cell death. The use of this enzyme to evaluate cell viability in the IPPSF after exposure to cutaneous toxins has not been well described. Figure 23 shows that LDH release in the IPPSF's treated with 0.07 mg/ml XL was essentially the same as control until late in perfusion. Within 3 hours after dosing, LDH release was generally higher than control for the 0.14 mg/ml flaps (Figure 24). LDH profiles for the 0.2 mg/ml and the 1.25 mg/ml XL flaps were similar to control (Figures 25 and 26). The 2.5 mg/ml XL treatment group showed an overall increase in LDH versus control (Figure 27). The 5.0 mg/ml IPPSF's showed the most pronounced increase in LDH, with a continuing increase in LDH release noted between 2 and 8 hours after dosing (Figure 28). All treated groups are plotted against control in Figure 29, and the increase in the terminal-phase LDH values of the 5.0 mg/ml and the 2.5 mg/ml groups is apparent. Although the increase in LDH seen with the highest dose (5.0 mg/ml) appeared significant in the later hours of perfusion, comparisons of the mean LDH values for the entire post-dosing period did not elicit any significant difference between the treatment groups and control ($p > 0.05$).

Morphological Evaluation:

After perfusion, the entire XL dosed region of skin was excised from the IPPSF and

20

samples were taken for light microscopy (LM), transmission electron microscopy (TEM), and enzyme histochemistry. Macroscopic, LM, and TEM observations will be reported at this time.

Macroscopic observations are presented in Table 1. Many of the XL-treated IPPSF's demonstrated the formation of gross vesicles and/or bullae. Of the 5.0 mg/ml IPPSF's, 4/4 showed macroscopic blisters. Only 1/4 of the 2.5 mg/ml XL flaps showed macroscopic lesions. In the 1.25 mg/ml dosing group, 3/4 developed visible blisters. Of the lower doses, 2/4 of the 0.2 mg/ml flaps blistered grossly, while only 1/4 of the 0.14 mg/ml IPPSF's showed any signs of macroscopic blisters. Also 1/4 of the 0.07 mg/ml treated flaps developed blisters. Typically, at the higher doses (5.0 and 2.5 mg/ml), these lesions were noted initially as small vesicles that coalesced into bullae and covered large portions of the dosing surface (5 cm^2) by the end of perfusion. These bullae were filled with a clear fluid and often resulted in marked elevation of the skin surface. At the lower doses (1.25, 0.2, 0.14, and 0.07 mg/ml), most of these lesions did not coalesce as readily and tended to remain smaller and more discrete. Of the IPPSF's developing visible blisters, the shortest mean times to blister formation were seen in the 5.0 mg/ml XL flaps at 4.30 hours (n=4) and the 2.5 mg/ml flaps at 2.0 hours (n=1). The 1.25 mg/ml dosing group had a mean time to blister formation of 4.7 hours (n=3), and the longest mean time for visible blister development was seen for the 0.2 mg/ml group at 7.5 hours (n=2). The flaps that blistered in the 0.14 and 0.07 mg/ml developed lesions at 6.3 and 4.3 hours respectively. Based on time to blister formation and the severity of the lesions formed, there did appear to be an agent-induced formation of macroscopic lesions. The time for a macroscopic blister to form was shorter for the highest concentrations (5.0 mg, 2.5 mg).

TABLE I. Macroscopic and microscopic observations of XL treated skin flaps.

Flap Number	XL Concentration	Gross Blister	LM or TEM BM Separation
614	5.0 mg/ml	2.4 h	+
629	5.0 mg/ml	3.0 h	+
677	5.0 mg/ml	5.7 h	+
683	5.0 mg/ml	6.5 h	+
634	2.5 mg/ml	NO	-
671	2.5 mg/ml	2.0 h	+
676	2.5 mg/ml	NO	+
688	2.5 mg/ml	NO	+
696	1.25 mg/ml	5.0 h	+
702	1.25 mg/ml	6.2 h	+
704	1.25 mg/ml	NO	+
705	1.25 mg/ml	3.0 h	+
670	0.2 mg/ml	NO	+
682	0.2 mg/ml	NO	+
689	0.2 mg/ml	7.1 h	+
697	0.2 mg/ml	8.0 h	+
738	0.14 mg/ml	6.3 hr	+
745	0.14 mg/ml	NO	+
746	0.14 mg/ml	NO	+
747	0.14 mg/ml	NO	+
615	0.07 mg/ml	NO	-
624	0.07 mg/ml	NO	+
739	0.07 mg/ml	4.3 hr	+
744	0.07 mg/ml	NO	-

Light microscopic observations of hematoxylin and eosin (H&E) and/or periodic acid-Schiff (PAS) stained, paraffin embedded sections (as well as toluidine blue stained, plastic sections) showed microvesicles to be present in 18/24 of the XL-treated IPPSFs. TEM revealed microvesicles in three more skin flaps and resulted in a combined microscopic documentation of microvesicle formation in 21/24 of the XL-treated flaps. Treatment with 5.0 mg/ml of XL resulted in marked separation of the epidermis from the dermis at the epidermal-dermal junction (Figure 30). Numerous pyknotic cells were noted in the stratum basale and lower stratum spinosum layers of the epidermis (Figure 30). All of the flaps in this group demonstrated microvesicles on LM evaluation.

Figure 31 demonstrates that intercellular epidermal edema occurred, primarily in the stratum basale and stratum spinosum layers in the 2.5 mg/ml group. Figure 32 shows that the 1.25 mg/ml dose resulted in intercellular edema in the stratum basale and stratum spinosum layers. This degree of intercellular edema was common at all dosing levels. This dose resulted in microvesicles in all of the treated skin flaps on LM evaluation and were not seen in the control flaps.

Figure 33 illustrates that XL caused well-organized microvesicles and epidermal-dermal separation at the 0.2 mg/ml dose, with only half of the IPPSF's treated with this dose exhibiting LM evidence of microvesicles. However, TEM evaluation identified microvesicles in the other skin flaps in this group. The need for ultrastructural identification of these lesions was an indication of the decreasing severity and frequency of the lesions at this dose. Similar findings were noted at the 0.14 mg/ml dose, when LM showed 3/4 with microvesicles (Figure 34). The 0.07 mg/ml dose resulted in microvesicles in 1/2 of the flaps on LM (Figure 35).

TEM revealed a number of interesting insights into the lesions produced in the IPPSF by XL. Figure 36 shows the typical ultrastructural lesions seen at the 5.0 mg/ml XL

dose. Separation of the epidermal-dermal junction was common. This occurred at the level of the lamina lucida, but the lamina densa (basal lamina) remained predominantly intact. When the epidermal-dermal junction was intact, there appeared to be an increase in the deposition of intracellular lipid and glycogen in the basal cells (Figure 37). Also, membranous structures were noted in the basale layer and appeared to be remnants of intracellular membranes, possibly from degenerative organelles. Increased intracellular glycogen and lipid can be seen in response to cell injury or when epidermal metabolism is altered. Since arsenic can have a direct toxic effect on the glycolytic pathway, it is plausible that this could be an effect of the arsenic component of lewisite.

Figure 38 demonstrates some of the ultrastructural lesions seen with the 2.5 mg/ml dose. At this dose, intercellular edema was common. Blown-out mitochondria with ruptured cristae were noted in many of the basal and lower spinosum cells. Accumulation of intracellular lipid and the formation of intracellular clefts were seen (Figure 38). Such clefts could be sites of cellular disruption. In addition, chromatin clumping around the nucleolus was noted. In some areas, disruption of basal cells occurred at the epidermal-junction, resulting in focal separation of the cells from the basal lamina (Figure 39).

At the 1.25 mg/ml XL dose, similar lesions were seen. Swollen and disrupted mitochondria were numerous in the basal cells (Figure 40). Intracellular lipid was commonly seen, and chromatin clumping around the nucleoli was noted. Focal disruption of the basal cells from the epidermal-dermal junction was noted, and paranuclear clefts were sometimes present (Figure 41).

Epidermal-dermal separation was noted in all of the IPPSF's treated with 0.2 mg/ml XL, and numerous intracellular vacuoles representing disrupted mitochondria, were present at this dose (Figure 42). Remnants of cellular membranes that formed lamellar structures along the epidermal-dermal junction were sometimes present at the 0.2 mg/ml XL (Figure

24

43). Intracellular lipid did not appear as often at this dose. The 0.14 mg/ml XL resulted in intercellular edema and intracellular clefts (Figure 44) and paranuclear vacuoles in the stratum basale cells (Figure 45). The 0.07 mg/ml XL-treated flaps showed few ultrastructural changes, except for mild intercellular edema, chromatin clumping, and nuclear envelope blebbing (Figure 46).

Sulfur Mustard - XHD

Biochemical and Physiological Evaluation:

Cumulative glucose utilization (CGU), in milligrams/gram (mg/gm), of 0.2 mg/ml of XHD-treated IPPSF's compared to controls showed that the 0.2 mg/ml group had a decrease in glucose utilization from 1 hour through 8 hours after dosing (Figure 47). In an another experiment with 0.2 mg/ml of XHD (n=4), the new 0.2 mg/ml had a gradual increase in CGU from 1 hour through 8 hours (Figure 48). The 0.5 mg/ml of XHD-treated IPPSF's had an initial increase in CGU through 3 hours and tended to decrease through 8 hours compared to controls (Figure 49). The 1.25 mg/ml of XHD group showed a continual but slow increase in CGU, when compared to controls (Figure 50). The 2.5 mg/ml of XHD-treated IPPSF's showed an initial increase in glucose utilization (GU) up to 3 hours, followed by a slow decrease around 4 hours compared to control (Figure 51). The CGU of 5.0 mg/ml of XHD-treated IPPSF's was similar to that of the 2.5 mg/ml of XHD in that an initial increase in GU was followed by a decrease compared to control (Figure 52). The 10.0 mg/ml of XHD-treated IPPSF's (n=5) demonstrated a dramatic change in CGU when compared to controls and to the 0.2 mg/ml, 0.50 mg/ml, 1.25 mg/ml, 2.5 mg/ml, and the 5.0 mg/ml XHD-treated IPPSF's. There was an initial decrease in CGU from the first hour after dosing that continued to decrease through 8 hours (Figure 53). Although the agent induced changes in CGU appear minor, based on our experience with over 1,000 other IPPSF's, any deviation from linearity is significant.

In Figure 54, all XHD-treated IPPSF's were plotted against control flaps to give a better understanding of CGU between these flaps. By 4 hours, most XHD-treated flaps (0.2 mg/ml, 0.5 mg/ml, 2.5 mg/ml, 5.0 mg/ml, and the 10.0 mg/ml) demonstrated a decrease in CGU compared to the control flaps, except for the new 0.2 mg/ml and the 1.25 mg/ml, which demonstrated an increase in CGU. The 10.0 mg/ml XHD flaps had the lowest CGU, followed by the 0.2, 5.0, 2.5, 0.5, 1.25, and the new 0.2 mg/ml. Initially, this data demonstrated a graded, good dose response at higher doses, with the exception of the 0.2 mg/ml of XHD dose. Therefore, an attempt was made to establish a new 0.2 mg/ml of XHD and to compare that to the control. Based on an analysis of all the data, the new 0.2 mg/ml group appeared correct, since a more appropriate dose response was noted. The 10.0 mg/ml, 5.0 mg/ml, and 0.2 mg/ml IPPSF's were statistically different from the controls (p < 0.05).

The ratio of lactate production to glucose utilization (L/GU) in the IPPSF has been characterized previously in our laboratory and used as an indicator of biochemical viability in our previous studies. In Figures 55-61, the lactate/glucose ratios for the new 0.2 mg/ml, 0.2 mg/ml, 0.5 mg/ml, 1.25 mg/ml, 2.5 mg/ml, 5.0 mg/ml, and 10.0 mg/ml were very linear compared to the controls. Figure 62 compares the L/GU ratio between all treatment groups showing a linear response. The statistical analysis for lactate using the General Linear Model Procedure (Proc GLM) in SAS showed no significant difference in lactate production between all XHD-dosed IPPSF's and controls.

In comparing the vascular resistance of the new 0.2 mg/ml and the 0.2 mg/ml of XHD and control, there was an increase in VR around 1 hour after dosing, this response continued to increase until 4 hours, where it then plateaued until 8 hours (Figures 63-64). The 0.5 mg/ml slowly increased in VR until 6 hours, where it plateaued through 8 hours (Figure 65). The 1.25 mg/ml showed a slow increase in VR up to 4 hours where it leveled

off until 8 hours (Figure 66). The 2.5 mg/ml showed an initial decrease until 1 hour after dosing, then a steady increase in VR up to 6 hours, where it plateaued until 8 hours (Figure 67). Figure 68, depicts the 5.0 mg/ml of XHD, which resembles that of the 2.5 mg/ml (Figure 67). The last group, comparing 10.0 mg/ml of XHD with controls, shows a dramatic increase in VR from 1 hour through 4 hours, where it levels off (Figure 69). An overall comparison of VR between all doses of XHD-treated IPPSF's to controls can be seen in Figure 70, which shows that there was an overall increase in VR with 0.5 mg/ml having the highest increase, followed by 1.25 mg/ml, 10.0 mg/ml, 0.2 mg/ml, 5.0 mg/ml, new 0.2 mg/ml, 2.5 mg/ml, and then control. Statistical analysis for VR using the Student's t-test shows that all the concentrations of XHD were significantly different from the controls ($p < 0.05$).

Lactate dehydrogenase (LDH) for the new 0.2 mg/ml of XHD slowly increased during the 8 hours of perfusion (Figure 71) The 0.2 mg/ml initially increased until 1 hour, then decreased to 3 hours; it then increased up to 6 hours, then slowly decreased to 8 hours (Figure 72). The LDH for the 0.5 mg/ml of XHD slowly increased up to 5 hours, then decreased at the sixth hour, and continued to rise through the remaining 2 hours (Figure 73). The LDH for the 1.25 mg/ml increased after 1 hour and continued to rise through the sixth hour, then decreased at 7 hours with an increase on the last hour of perfusion (Figure 74). The 2.5 mg/ml increased after 1 hour and continued to slowly increase up to 8 hours (Figure 75). The 5.0 mg/ml continued to show an increase in LDH throughout the entire 8 hours of perfusion (Figure 76). Also, the 10.0 mg/ml demonstrated an increase in LDH for the entire 8 hours of perfusion (Figure 77). The LDH for all concentrations can be seen in Figure 78. Statistical analysis for LDH using the Proc GLM in SAS showed a statistically significant difference with the 10.0 mg/ml and the new 0.2 mg/ml of XHD compared to controls ($p < 0.05$).

27

<u>Morphological Evaluation:</u>

Macroscopic observations (see Table II) revealed that 3/4 flaps treated with 0.2 mg/ml of XHD blistered. The new 0.2 mg/ml of XHD flaps showed no blisters in 0/4 flaps. This supports the biochemical and vascular resistance data that the new 0.2 mg/ml is correct and justifies the repeating of this group. In the 0.50 mg/ml of XHD-treated flaps 2/4 had blistered; and the 1.25 mg/ml of XHD showed that 1/4 flaps had blistered. Only 1/4 of the 2.5 mg/ml of XHD blistered, and 2/4 of the 5.0 mg/ml of XHD blistered, while 4/5 of the high-dose 10.0 mg/ml of XHD blistered.

Light microscopic observations of hematoxylin and eosin (H&E) paraffin embedded samples demonstrated some interesting findings. The 0.2 mg/ml of XHD-treated IPPSF's consistently had both intracellular epidermal edema (Figure 79) and intercellular epidermal edema (Figure 80). Of the IPPSF's that had blistered at 0.2 mg/ml of XHD, some focal basement membrane separation had occurred between the epidermis and the dermis (Figure 81). Transmission electron microscopy of the 0.2 mg/ml treated IPPSF's demonstrated the typical intercellular epidermal edema, and typical nucleolar pleomorphism seen in normal IPPSF's, and blown-out mitochondria (Figure 82). TEM of another 0.2 mg/ml of XHD-treated flaps showed normal epidermal-dermal junctions and dilated endoplasmic reticulum in the stratum basale cells forming a cleft (Figure 83). The 0.5 mg/ml of XHD showed slight intercellular and intracellular epidermal edema (Figure 84). Transmission electron microscopy showed a normal epidermal-dermal junction, lipid inclusions in the stratum basale cells, and nucleolar margination (Figure 85). Another 0.5 mg/ml of XHD-treated flaps showed nucleolar margination and nucleolar caps. Most nucleoli had enlarged granular centers surrounded by a dense fibrillar components (Figure 86). Light microscopy of the 1.25 mg/ml of XHD-treated IPPSF's demonstrated a normal stratum corneum, with intercellular and intracellular edema (Figure 87). Transmission

28

TABLE II. Macroscopic and microscopic observations of XHD treated skin flaps.

Flap Number	XHD Concentration	Gross Blister	LM or TEM BM Separation
603	0.2 mg/ml	6.5 h	+
608	0.2 mg/ml	8.0 h	-
613	0.2 mg/ml	6.8 h	+
652	0.2 mg/ml	NO	-
736	N0.2 mg/ml	NO	-
737	N0.2 mg/ml	NO	+
740	N0.2 mg/ml	NO	+
741	N0.2 mg/ml	NO	-
711	0.50 mg/ml	2.6 h	+
716	0.50 mg/ml	8.0 h	+
721	0.50 mg/ml	NO	-
726	0.50 mg/ml	NO	-
710	1.25 mg/ml	NO	+
717	1.25 mg/ml	NO	+
720	1.25 mg/ml	NO	-
727	1.25 mg/ml	2.7 h	+
658	2.5 mg/ml	3.8 h	-
659	2.5 mg/ml	NO	-
664	2.5 mg/ml	NO	-
665	2.5 mg/ml	NO	+
640	5.0 mg/ml	NO	-
641	5.0 mg/ml	NO	+
646	5.0 mg/ml	8.4 h	+
647	5.0 mg/ml	7.5 h	+
602	10.0 mg/ml	3.1 h	+
609	10.0 mg/ml	6.1 h	+
612	10.0 mg/ml	7.2 h	+
653	10.0 mg/ml	NO	+
733	N10.0 mg/ml	3.1 h	+

N = additional IPPSF experiment.

electron microscopy showed a normal basement membrane, with normal stratum basale, stratum spinosum (Figure 88), stratum granulosum, and stratum corneum cells (Figure 89). The flaps treated with 2.5 mg/ml of XHD showed primarily intracellular epidermal edema and very slight intercellular epidermal edema, and only one flap showed basement membrane separation. In Figure 90, a Langerhans cell process can be seen traversing the stratum basale and stratum spinosum cell layers. The basement membrane is unaffected and most cytoplasmic organelles appear normal in this 2.5 mg/ml treated IPPSF. A few mitochondria have no cristae, and nuclear envelope separation has occurred in two of the stratum basale cells. Also, a few lipid inclusion bodies are present in some cells. Figure 91 is another example of a 2.5 mg/ml treated IPPSF showing a dark degenerative stratum basale cell with large cytoplasmic vacuoles, which are probably remnants of damaged mitochondria. Figures 92, 93, and 94 give us a better understanding of what occurred with the 5.0 mg/ml of XHD. Characterization of these lesions showed multiple focal areas of subepidermal vesiculation, with separation occurring above the basement membrane and basal cell degeneration (Figure 92). In Figure 93, both intracellular and intercellular edema were present, along with basement membrane separation. These lesions were focal, where one area may appear fairly normal and yet adjacent areas exhibit separation of the epidermis and dermis (Figure 94). Figure 95 is a representative electron micrograph of a 5.0 mg/ml treated IPPSF. Note the numerous damaged mitochondria present in the stratum basale, stratum spinosum, and the Langerhans cell. It appears that the damaged mitochondria became so swollen that they eventually coalesced, thereby forming a large, crescent-shaped vacuole that may correspond to the perinuclear cap seen by other investigators.

The effects seen in the 10.0 mg/ml flaps were more severe than those in the previous

doses. All skin flaps had both intracellular and intercellular epidermal edema that extended as far as the stratum granulosum area. Although 4 out of 5 flaps treated with 10.0 mg/ml showed macroscopic blisters, 5 out of 5 showed microscopic blisters. Figures 96 and 97 show typical basement membrane separation, with pyknotic stratum basale cells and some inflammatory cells (Figure 97). The 10.0 mg/ml flaps showed severe degeneration of the stratum basale cells, damaged mitochondria, intercellular epidermal edema and separation of the basement membrane (Figure 98). In Figure 99, the stratum basale cells became separated from the basement membrane. In the space between the separation, note the amorphous substance containing cytoplasmic remnants of organelles. Vacuoles were also present in the cells, along with dilated, rough endoplasmic reticulum.

It is important to note that all three indicators of vesication (e.g. gross, light and ultrastructure) are needed to precisely identify morphological evidence of agent induced vesication. In many cases the gross observations alone are not adequate because microvesicles obviously connect be detected. In contrast, due to sampling limitations, basement membrane separation may be missed when gross blisters are present (e.g. flaps 608, 658).

DISCUSSION

The results of both XL and XHD treatment of IPPSF's clearly indicate that distinctive biochemical, physiological, and morphological changes occurred. In general, the response of both XL and XHD treated IPPSF's are similar, except for the more severe epidermal sloughing seen with XL. Before the general summary, the results of the XL and XHD experiments will be separately addressed.

<u>Lewisite - XL</u>

The results of the biochemical and physiological parameters in these experiments yielded several key findings. Perhaps the most consistent finding was the presence of the 5.0 mg/ml dosing group in the "most effected" position for all of the parameters in which differences were noted. This treatment resulted in the lowest average rate of cumulative glucose utilization, one of the highest terminal levels of vascular resistance, and the highest values for LDH release. Although a dose-related sensitivity in response was not apparent for these parameters at other concentrations (2.5 mg/ml gave an abnormally low response), the 5.0 mg/ml dose consistently resulted in changes that were quite different from control.

The lack of dose-related separation of responses was not observed at the other levels of XL treatment could be a factor of either the dosing concentrations that were tested or a lack of sensitivity of these parameters to XL-induced changes. The presence of significant differences at the 5.0 mg/ml dose suggests that this concentration was the most effective at producing measurable differences from control for these parameters. It seems possible that experiments with even higher concentrations of XL might result in more pronounced and separable levels of these responses. An example of lack of parameter sensitivity is seen with the LDH results. While these results suggest that monitoring such enzymes may be appropriate in XL experiments, the level of LDH release in this model was not high enough

32

and did not show the sensitivity necessary to achieve a statistical, dose-related differentiation in response. Possibly, more sensitive indicators of XL-induced changes may be identified through consideration of different measures of enzyme activity, such as enzyme histochemistry, or by media levels of other enzymes. The poor sensitivity of these biochemical parameters to low doses of applied agent may be a result of the relatively small proportion of total skin area dosed in these studies (approximately 15%). By increasing the dosing surface area to greater than 5 cm^2, more skin would be affected.

Another key finding of these experiments was the presence of increased vascular resistance at all XL dosing levels versus control, making this a very sensitive biological parameter for assessing decontaminant strategies. This suggests that topical application of a variety of concentrations of XL had either direct or indirect effects on the IPPSF vasculature. While XHD has been shown to affect the cutaneous vascular endothelium and to cause the release of a variety of vasoactive mediators, little work has been done on the vascular effects of vesicant arsenicals. The mechanism of the XL-related vascular response seen in these studies is unknown. However, future IPPSF experiments may allow us to explore this interesting response and may give new insight into the pathogenesis of lewisite injury.

Evaluation of XL-induced morphological changes did appear to provide a more sensitive measure of dose response than the previously described biochemical and physiologic parameters. The 5.0 mg/ml dose consistently produced some of the more severe changes noted in this study. However, both macroscopic and microscopic lesions demonstrated differing levels of response, depending on XL concentration. Again, the 2.5 mg/ml dose appeared to be out of phase with the other doses, and this dose group will be repeated. Ultrastructural findings suggested that intracellular glucose and fatty acid

33

metabolism may be affected by this compound, and TEM evaluation allowed the identification of lethal and sublethal cellular changes that may be precursors to or directly responsible for the macroscopic lesions seen.

Mustard - XHD

The XHD studies demonstrated biochemical and morphological changes qualitatively similar to the XL lesions just described. The magnitude of the change in CGU appeared to be less dramatic than that induced by XL. The LM and TEM observations of XHD were very similar to those reported for CEMS (King and Monteiro-Riviere, 1990). Unlike XL-treated samples, XHD samples (when the new 0.2 mg/ml dose was considered) clearly demonstrated a graded dose-response relationship for some of the parameters at the higher doses.

General

In documenting the response of isolated perfused porcine skin to exposure to XL and XHD, this model demonstrated the ability to respond biochemically, physiologically, and morphologically to cutaneous exposure by vesicant compounds. The results of the biochemical parameters support the relevance of this model for the study of cutaneous vesication due to arsenical or mustard compound exposure. Most agent-treated flaps demonstrated an average rate of GU that was significantly lower than control. A similar, incomplete suppression of GU has been described in cultured human epidermal keratinocytes (Mol et al., 1989a) and in the full-thickness, human skin organ culture model (Mol et al., 1989b) after exposure to XHD. Other in vitro studies in skin have demonstrated that anaerobic glycolysis is a primary pathway of energy production for skin and that lactate is a major end product of epidermal glycolysis (Freinkel, 1983). The L/GU ratio was found to be constant both for controls and for XL and XHD-treated flaps, and no significant

34

differences were noted between the treated groups and their respective controls. This suggests that, although glucose utilization was decreased, typical pathways of IPPSF epidermal glucose metabolism were maintained after vesicant treatment.

XL and XHD treatment resulted in an overall increase in vascular resistance. The VR profiles of the treated IPPSF's showed an increase shortly after dosing, and a plateau was noted in the VR profile for some agent concentrations. A biphasic vascular response to high doses of XHD has been described in both rabbit and guinea pig skin in vivo (Vogt et al., 1984). In that study, an early response of the vascular endothelium to XHD resulted in vascular leakage within the first hour after dosing. This appeared reversible, as permeability changes returned to normal by 2 to 3 hours. However, a second phase of vascular response occurred between 3 to 8 hours, during which time there occurred a marked increase in vascular permeability, which resulted in diffuse leakage and dermal edema. This study suggested that the first phase was the result of reversible endothelial damage to the superficial microvasculature and the second phase of vascular response was caused by the release of vasoactive mediators. Later studies identified specific proteinases, proteases, and hydrolases released from XHD-produced skin lesions in rabbits (Harada et al., 1987; Higuchi et al., 1988). These studies point to the fact that the cutaneous vasculature can be affected rapidly by topically applied mustard compounds and that vasoactive products are released by HD-induced lesions. Based on these findings, it would seem that the rapid increase in VR seen in this study may be due to an early primary effect of vesicants on the vasculature, and that the plateau noted in the flaps may be due to a second phase in vascular response caused by the release of vasoactive mediators.

The IPPSF responded with the formation of macroscopic and microscopic lesions similar to those seen after human exposure to HD (Requena et al., 1988). Histologically,

35

these lesions were similar to those seen in the euthymic, hairless guinea pig (Wade et al., 1989; Marlow et al., 1989), the human skin grafted athymic nude mouse model (Papirmeister et al., 1984a; McGown et al., 1987), the full-thickness human skin organ culture model (Mol et al., 1989b), and in in vivo studies with pigs (Micheltree et al., 1989) in response to cutaneous exposure to vesicants such as HD, lewisite, and lewisite analogs. Ultrastructural findings supported the LM evaluation of these lesions and were similar to those described in both the euthymic, hairless guinea pig (Marlow et al., 1989; Petrali et al., 1989) and the human skin grafted athymic nude mouse model (Papirmeister et al., 1984b; McGown et al., 1987). A key finding in the IPPSF was the formation of characteristic gross blisters in treated flaps.

These findings show that XHD produced biochemical and morphological responses in the IPPSF model that are strikingly similar to those described for neat HD in humans and in various in vitro and in vivo models. The ability of the IPPSF to form gross blisters in response to vesicant exposure is unique among in vitro test systems and many of the in vivo models that have been studied.

The rapid occurrence of gross blisters in IPPSF is both an advantage and disadvantage of this in vitro model. There are conflicting observations on the ability of pig skin to form gross blisters in vivo. Microvesication is observed by all to occur in vivo and is identical to that seen in the IPPSF. This supports a similar mechanism of action. The formation of gross blisters in the IPPSF is probably due to increased pressure seen in an in vitro perfused model which accentuates any lesion produced. Since these only occur after vesicant exposure, this makes the IPPSF a more sensitive model.

In addition, characteristic mustard-induced changes in glucose utilization and vascular resistance were quantitated in this model. The IPPSF appears to be a useful and relevant

in vitro model with which to investigate cutaneous vesicant toxicity, and it offers a humane alternative to classic in vivo studies. Full characterization of the morphological and biochemical changes seen after topical exposure of the IPPSF to vesicants may shed light on the pathogenesis of cutaneous toxicity of these compounds in vivo and may serve as a model to assess protective strategies against vesicant exposure.

Although the biochemical parameters did not provide as sensitive a characterization of dose response as did the morphological changes, XL did create consistent treatment-related changes in glucose utilization and lactate dehydrogenase release at high doses (5.0 mg/ml). XHD resulted in a graded dose-response for some parameters, with severe blistering consistently seen at the high dose (10.0 mg/ml). Re-evaluation of these and other potential parameters may lead to more sensitive biochemical indices of vesicant-induced changes. In addition. the ability to evaluate vascular changes in an isolated system which contains an in'ar microcirculation provides a unique opportunity to explore the vascular component in the pathogenesis of cutaneous vesicant injury. The use of vesicant-induced changes in vascular resistance appears especially promising as a biological marker of both L and HD exposure, since this parameter increased at all doses of both compounds. It is noteworthy that when other chemicals or treatments are applied to the IPPSF, vascular resistance does not change. Among these chemicals and treatment are many pesticides, solvent vehicle systems, and alkylating platinum containing cancer chemotherapeutic drugs (cisplatin, carboplatin). Although sufficient time was not available to further analyze this data, work is presently being conducted on constructing a multivariate toxicologic index which would combine biochemical, physiologic, and morphologic indices. However, even without such analysis, the occurrence of XL or XHD-induced cutaneous vesication appears readily detectable.

37

Based upon the work reported here, there does not appear to be a clear-cut dose-response relationship for XL exposure (one dose appears anomalous) or for very low-dose XHD exposure in the IPPSF. The major reason for this phenomenon may be that all doses used in this study were below the linear portion of a classic logarithmic dose-response relationship. However, we are precluded from using higher doses in our studies because our laboratory is restricted to dilute agent work (XCSM). An alternative explanation is that there is more than one mechanism responsible for the changes seen. For example, the vascular changes seen could be a result of a direct vesicant effect on the vasculature or could be secondary to epidermal damage associated with a concomitant release of vasoactive mediators. If two independent processes are present, then, a priori, one would not expect a linear dose-response relationship. Repetition of the 2.5 mg/ml dose of XL should be performed before seriously entertaining these hypotheses.

Another possible explanation for the lack of a graded dose-response relates to XL and low-dose XHD penetration, distribution, metabolism, and capillary uptake kinetics (i.e. cutaneous disposition kinetics). This is especially important if the penetrating chemical (or its metabolite) is vasoactive, since different patterns of cutaneous disposition may be expressed when threshold concentrations for vasodilation/constriction are exceeded. When the responses of an integrated system are studied these nonlinearities in penetration kinetics, coupled with multiple sites of vesicant action, result in an irregular dose-response relationship. In simple in vitro systems, where disposition kinetics are absent and only a single site of action exists, such complex behavior would not be expected. This hypothesis could be addressed by (1) integrating the dose-response data with the time series results when available, (2) conducting the multiple parameter modelling as described earlier, and (3) attempting to assay XL or XHD flux in perfusate and formulating a toxicokinetic model

of vesicant agent penetration and action. Options 1 and 2 will be addressed, since they are consistent with this contractual agreement. The high degree of IPPSF reproducibility observed in these studies suggest that this goal is achievable. In order to address these concerns further, it is important to correlate the biochemical and physiologic changes over time with morphological data to determine the temporal pattern of vesicant damage. We feel that in the absence of this data, planned for the second phase of this grant, and without the results of a multivariate analysis of all of the parameters, more detailed mechanistic discussions would be speculative.

The final conclusions which could be drawn from this work relate to the criteria which should be used in selecting an appropriate animal model for vesicant research. The first criterion should be an ability to form blisters after exposure. If, as the present work seems to strongly suggest, vascular changes are an integral part of vesicant-induced damage, the model should be able to respond to vascular toxins, an attribute that rules out many in vitro test systems. Based on these criteria and the similarity of results seen in this study to those reported in the open literature, the IPPSF appears to be a humane alternative animal model for studying XL and XHD-induced cutaneous vesication. Further studies in progress, conducted under the auspices of the present contract, will further define the underlying mechanisms operative and should establish the protocol necessary to use the IPPSF as a tool for assessing decontamination strategies.

The technical goal of this contract was to "develop a standardized dosing protocol of vesicant agents which would produce a specific lesion of a defined severity based on morphologic and biochemical criteria." Based upon an analysis of the data presented in this report, this goal has been achieved for both XL and XHD, since characteristic blisters and a specific biochemical and physiologic profile is consistently seen after high-dose vesicant

39

exposure. This should provide a useful, humane, alternative in vitro animal model system for further mechanistic studies and future evaluation of decontamination protocols.

REFERENCES

BOWMAN, K.F., MONTEIRO-RIVIERE, N.A., AND RIVIERE, J.E. (1991). Development of surgical techniques for preparation of in vitro isolated porcine skin flaps for percutaneous absorption studies. Am. J. Vet. Res. (In Press).

CARVER, M.P., WILLIAMS, P.L., AND RIVIERE, J.E. (1989). The isolated perfused porcine skin flap III. Percutaneous absorption pharmacokinetics of organophosphates, steroids, benzoic acid, and caffeine. Toxicol. Appl. Pharmacol. 97, 324-337.

FREINKEL, R.K. (1983). Carbohydrate metabolism of the epidermis. In Biochemistry and Physiology of the Skin I (L.A. GOLDSMITH, ed.), pp. 328-337. Oxford Univ. Press, New York.

HARADA, S., DANNENBERG, A.M., VOGT, R.F., JR., MYRICK, J.E., TANAKA, F., REDDING, L.C., MERKHOFER, R.M., PULA, P.J., AND SCOTT, A.L. (1987). Inflammatory mediators and modulators released in organ culture from rabbit skin lesions produced in vivo by sulfur mustard II. Electophoretic protein fractions, trypsin-inhibitor capacity, α_1-proteinase inhibition and α_1- and α_2-macroglobulin proteinase inhibitors of culture fluids and serum. Am. J. Pathol. 126:148-163.

HIGUCHI, K., KAJIKI, A., NAKAMURA, M., HARADA, S., PULA, P.J., SCOTT, A.L., AND DANNENBERG, A.M. (1988). Proteases released in organ culture by acute dermal inflammatory lesions produced in vivo in rabbit skin by sulfur mustard. Inflam. 12(4), 311-334.

KING, J.R. AND MONTEIRO-RIVIERE, N.A. (1990). Cutaneous toxicity of 2-chloroethyl methyl sulfide in isolated perfused porcine skin. Toxicol. Appl. Pharmacol. 104:167-179.

MARLOW, D.D., MERSHON, M.M., MITCHELTREE, L.W., PETRALI, J.P., AND JAAX, G.P. (1989) Evaluation of euthymic hairless guinea pigs [Cr1:IAF(HA)BR] as an animal model for vesicant injury. In Proceedings of the 1989 Medical Defense Bioscience Review. August, 1989, pp. 561-568.

McGOWN, E.L., VAN RAVENSWAAY, T., AND DUMLAO, C.R. (1987). Histologic changes in nude mouse skin and human skin xenografts following exposure to sulfhydryl reagents: arsenicals. Toxicol. Pathol. 15, 149-156.

MEYER, W., SCHWARZ, R., AND NEURAND, K. (1978). The skin of domestic mammals as a model for the human skin, with special reference to the domestic pig. Curr. Probl. Dermatol. 7, 39-52.

MICHELTREE, L.W., MERSHON, M.M., WALL, H.G., AND PULLIAM, J.D. (1989). Microblister formation in vesicant-exposed pig skin. J. Toxicol.--Cut. & Ocular Toxicol. 8 (3), 309-319.

MOL, M.A.E., van de RUIT, A.B.C., AND KLUIVERS, A.W. (1989a). NAD+ levels and glucose uptake of cultured human epidermal cells exposed to sulfur mustard. Toxicol. and Appl. Pharmacol. 98, 159-165.

MOL, M.A.E., van de RUIT, A.B.C., AND KLUIVERS, A.W. (1989b) The response of sulphur mustard-treated pieces of human skin on nicotinamide treatment. In Proceedings of the 1989 Medical Defense Bioscience Review. August, 1989, pp. 57-61.

MONTAGNA, W. AND YUN, J. (1964). The skin of the domestic pig. J. Invest. Dermatol. 43, 11-21.

MONTEIRO-RIVIERE, N.A. (1986). Ultrastructural evaluation of the porcine integument. In Swine in Biomedical Research. (M.E. TUMBLESON, Ed.), pp. 641-655.

42

MONTEIRO-RIVIERE, N.A. AND MANNING, T.O. (1987). The effects of different fixatives on the porcine integument. In Proceedings of the 45th Annual Meeting of the Electron Microscopy Society of America. (G.W. BAILEY, Ed.) pp. 948-949, San Francisco Press, San Francisco, CA.

MONTEIRO-RIVIERE, N.A. AND STROMBERG, M.W. (1985). Ultrastructure of the integument of the domestic pig (Sus scrofa) from one through fourteen weeks of age. Anat. Histol. Embryol. 14, 97-115.

MONTEIRO-RIVIERE, N.A., BOWMAN, K.F., SCHEIDT, V.J., AND RIVIERE, J.E. (1987). The isolated perfused porcine skin flap II. Ultrastructural and histological characterization of epidermal viability. In Vitro Toxicol. 1, 241-252.

MONTEIRO-RIVIERE, N.A. (1990). Specialized Technique: Isolated perfused porcine skin flap. In Methods for Skin Absorption. (B.W. Kemppainen and W.G. Reifenrath, Eds.). CRC Press, Inc. Chap. 11, pp. 175-189.

PAPIRMEISTER, B., GROSS, C.L., PETRALI, J.P., AND HIXSON, C.J. (1984a). Pathology produced by sulfur mustard in human skin grafts on athymic nude mice. I. Gross and light microscopic changes. J. Toxicol.--Cut. & Ocular Toxicol. 3, 371-391.

PAPIRMEISTER, B., GROSS, C.L., PETRALI, J.P., AND MEIER, H.L. (1984b). Pathology produced by sulfur mustard in human skin grafts on athymic nude mice. II. Ultrastructural changes. J. Toxicol.--Cut. & Ocular Toxicol. 3, 393-408.

PETRALI, J.P., OGLESBY, S.B., AND MILLS, K.R. (1989). Ultrastructural correlates of sulfur mustard toxicity. In Proceedings of the 1989 Medical Defense Bioscience Review. August, 1989. pp. 49-52.

REIFENRATH, W.G., CHELLQUIST, E.M., SHIPWASH, E.A., AND JEDERBERG, W.M. (1984). Evaluation of animal models for predicting skin penetration in man. Fundam. Appl. Toxicol. 4, S224-S230.

RENSHAW, B. (1946). Mechanisms in production of cutaneous injuries by sulfur and nitrogen mustards. In Chemical Warfare Agents and Related Chemical Problems. Technical summary report of Division 9, National Defense Research Committee, Washington, DC, Vol. 1, Part III-VI, Chap. 23, pp. 479-487.

REQUENA, L., REQUENA, C., SANCHEZ, M., JAQUETI, G., AGUILAR, A., SANCHEZ-YUS, E., AND HERNANDEZ-MORO, B. (1988). Chemical warfare. Cutaneous lesions from mustard gas. J. Am. Acad. Dermatol. 19, 529-536.

RIVIERE, J.E., BOWMAN, K.F., MONTEIRO-RIVIERE, N.A., DIX, L.P., AND CARVER, M.P. (1986a). The isolated perfused porcine skin flap (IPPSF) I. A novel in vitro model for percutaneous absorption and cutaneous toxicology studies. Fundam. Appl. Toxicol. 7, 444-453.

RIVIERE, J.E., BOWMAN, K.F., AND MONTEIRO-RIVIERE, N.A. (1986b). The isolated perfused porcine skin flap: A novel model for cutaneous toxicological research. In Swine in Biomedical Research. (M.E. TUMBELSON, Ed.) pp. 657-666, Plenum, New York.

RIVIERE, J.E., BOWMAN, K.F., AND MONTEIRO-RIVIERE, N.A. (1987). On the definition of viability in isolated perfused skin preparations. Brit. J. Dermatol. 116, 739-741.

RIVIERE, J.E. AND CARVER, M.P. (1991). Isolated perfused skin flap and skin grafting techniques. In Fundamentals and Methods of Dermal and Ocular Toxicology, Chap. 10. (D.W. DOBSON, Ed.). The Telford Press, Caldwell, New Jersey. (In Press)

UNITED NATIONS REPORT OF THE SPECIALISTS APPOINTED BY THE SECRETARY-GENERAL TO INVESTIGATE ALLEGATIONS BY THE ISLAMIC REPUBLIC OF IRAN CONCERNING THE USE OF CHEMICAL WEAPONS (1984). Document S/16433, Security Council of the United Nations: New York. /

VOGT, R.F., JR., DANNENBERG, A.M., JR., SCHOFIELD, B.H., HYNES, N.A., AND PAPIRMEISTER, B. (1984). Pathogenesis of skin lesions caused by sulfur mustard. Fundam. and Appl. Toxicol. 4, S71-S83.

WADE, J.V., MERSHON, M.M., MITCHELTREE, L.W., AND WOODARD, C.L. (1989). The hairless guinea pig model and vesicant vapor exposures for bioassay purposes. In Proceedings of the 1989 Medical Defense Bioscience Review. August, 1989. pp. 569-575.

WESTROM, D.R. (1987). Animal models for vesicant-induced injury. In Proceedings of the Vesicant Workshop, February, 1987. U.S. Army Medical Research Institute of Chemical Defense, Aberdeen Proving Ground, MD 21010-5425, 91-96.

WILLIAMS, P.L., CARVER, M.P., AND RIVIERE, J.E. (1990) A physiologically relevant pharmacokinetic model of xenobiotic percutaneous absorption utilizing the isolated perfused porcine skin flap (IPPSF). J. Pharm. Sci. 79:305-311.

WILLIAMS, P.L. AND RIVIERE, J.E. (1989). Definition of a physiologic pharmacokinetic model of cutaneous drug distribution using the isolated perfused porcine skin flap. J. Pharm. Sci. 78:(6) 550-555.
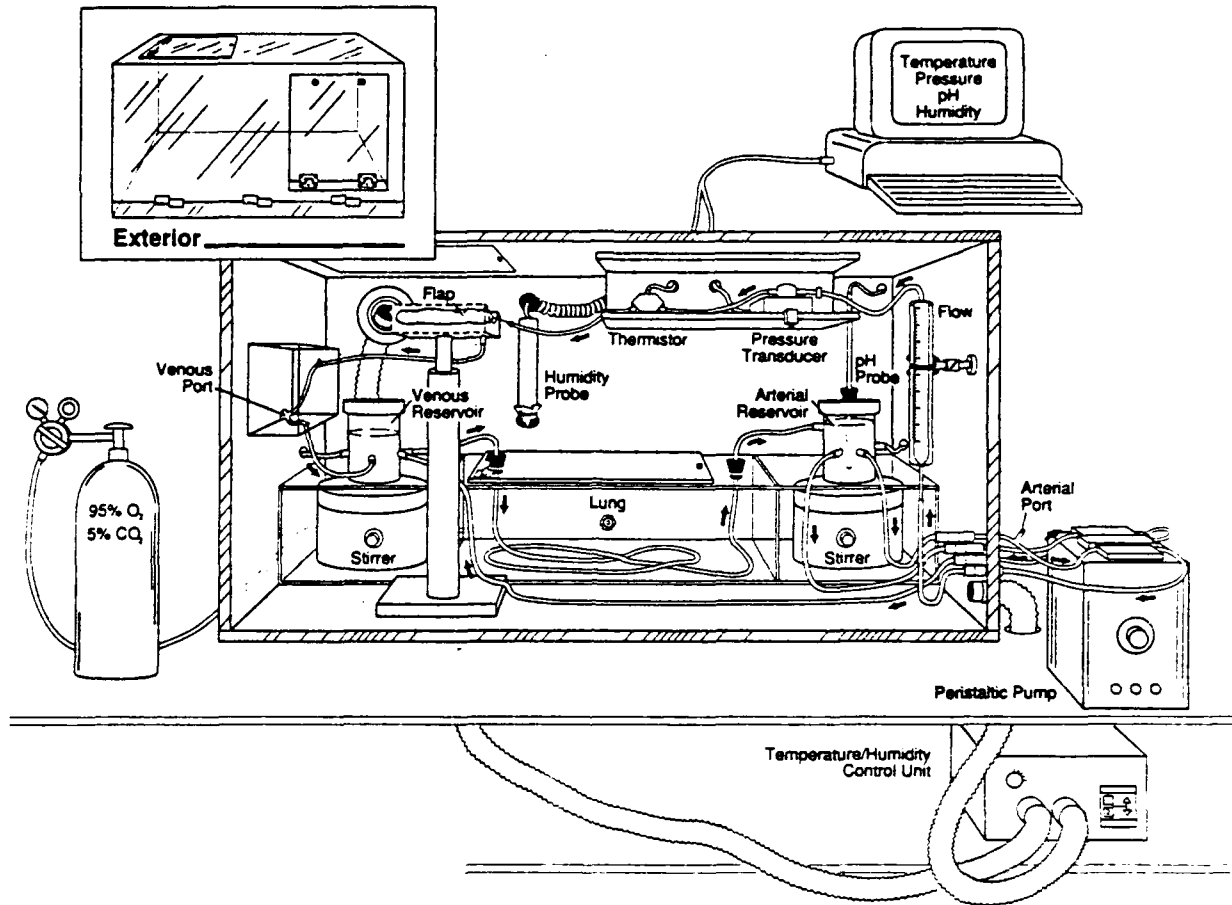
FIGURE 1.   Schematic diagram of the IPPSF chamber.
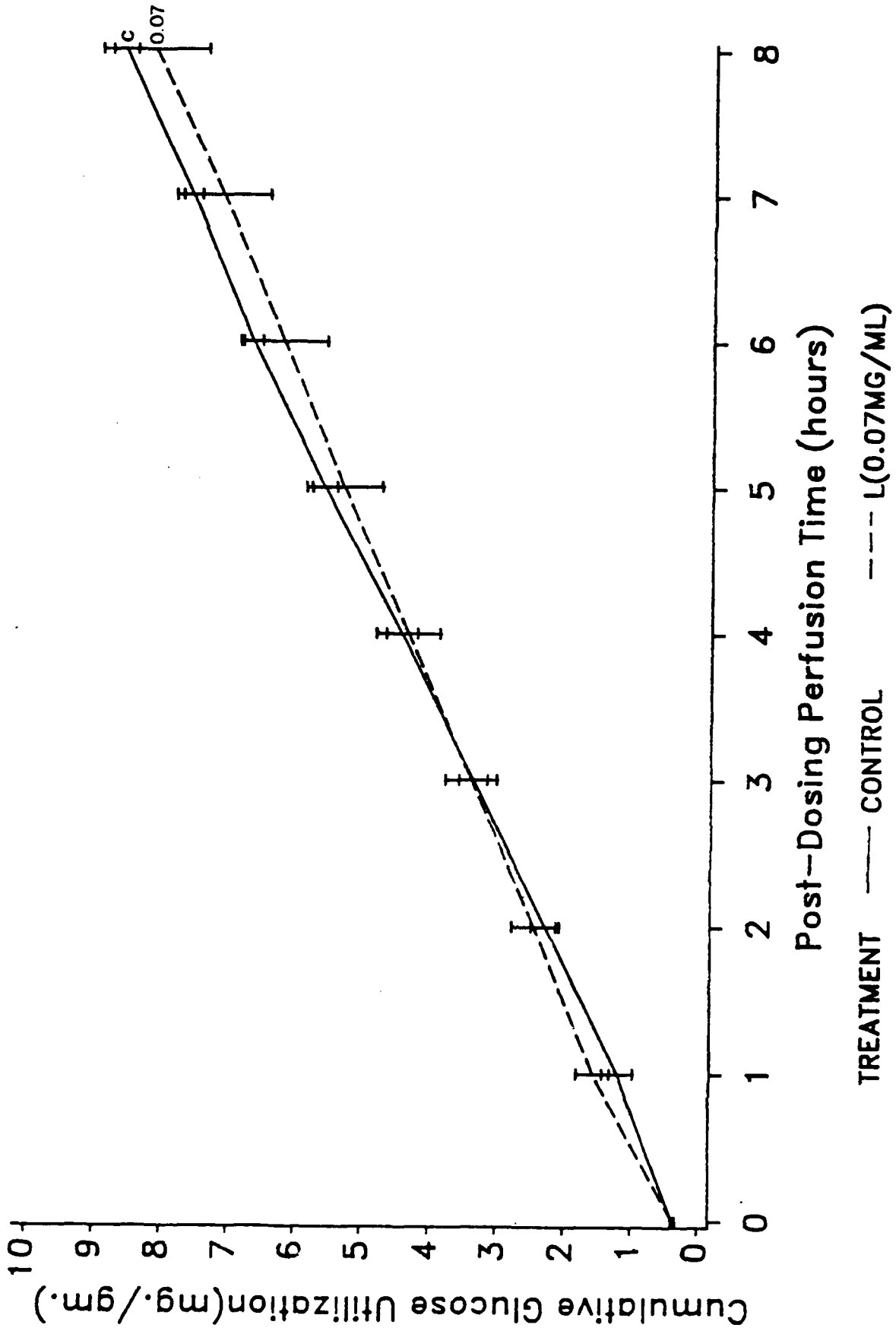
FIGURE 2. Graph Illustrating CGU of 0.07 mg/ml of XL compared to control.
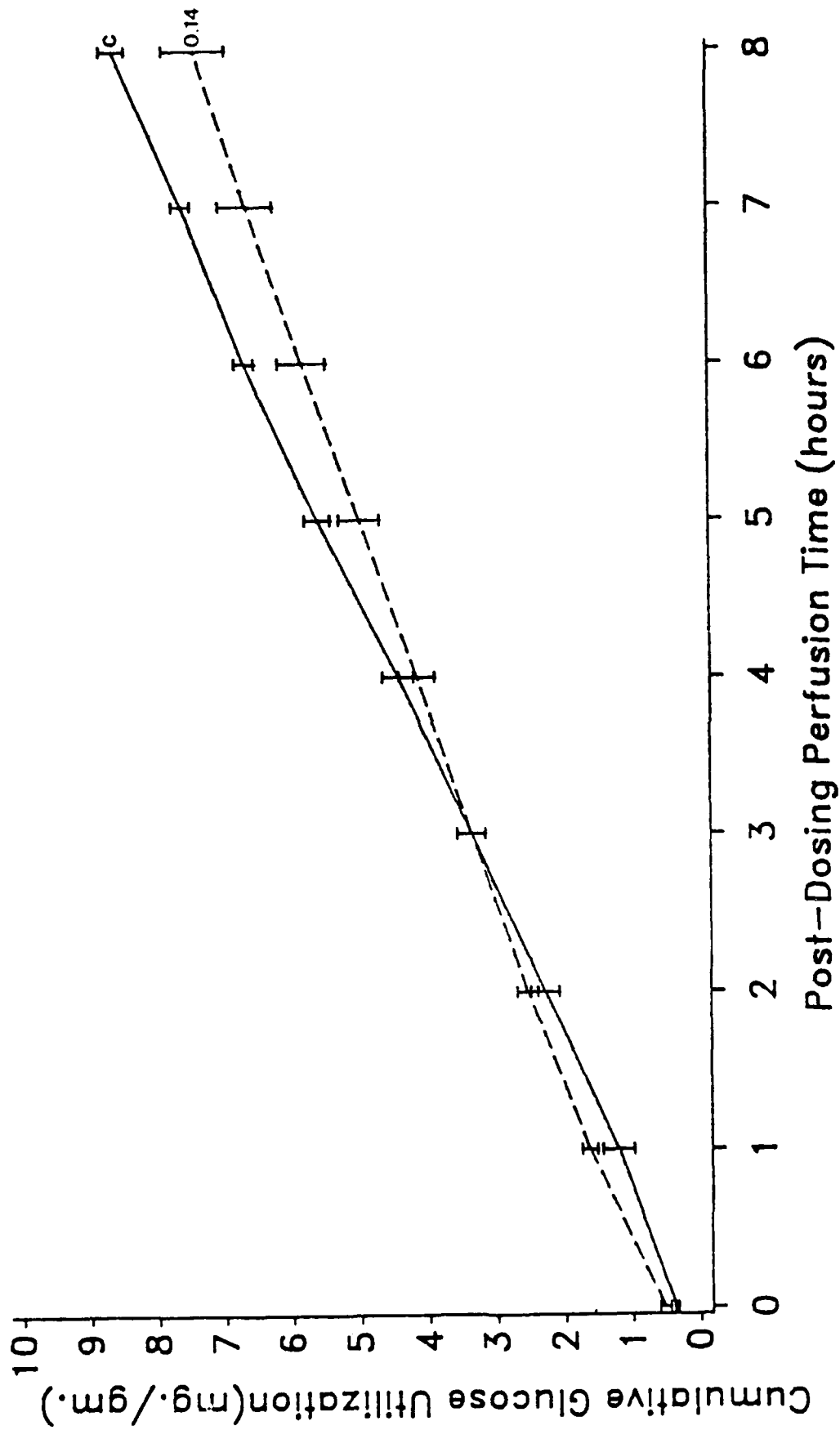
FIGURE 3. Graph illustrating CGU of 0.14 mg/ml of XL compared to control.

TREATMENT ——— CONTROL ———— L(0.14MG/ML)
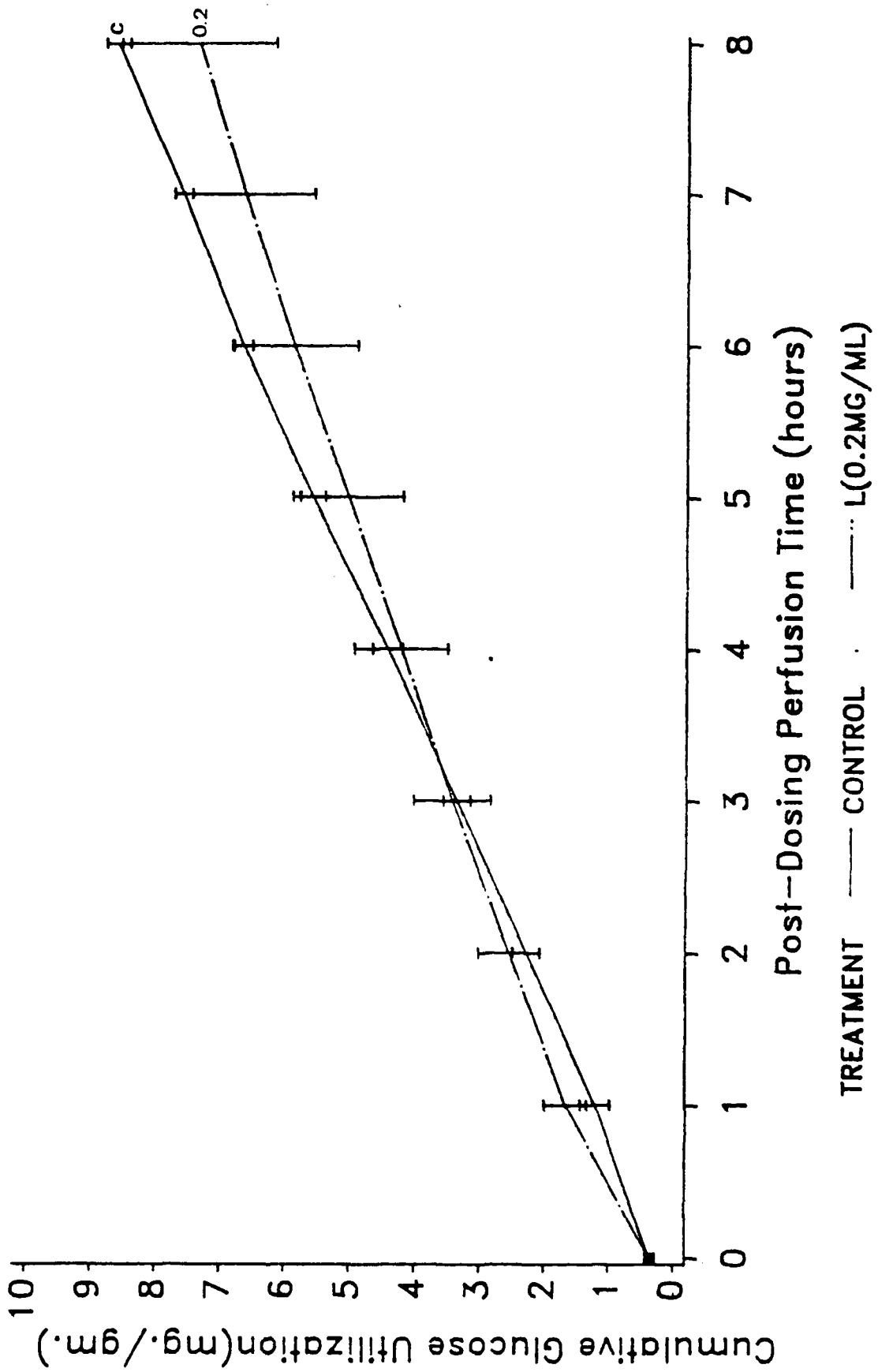
FIGURE 4. Graph illustrating CGU of 0.2 mg/ml of XL compared to control.

Post-Dosing Perfusion Time (hours)

Cumulative Glucose Utilization(mg./gm.)

TREATMENT ——— CONTROL ——·— L(0.2MG/ML)

FIGURE 5. Graph illustrating CGU of 1.25 mg/ml of XL compared to control

Post-Dosing Perfusion Time (hours)

Cumulative Glucose Utilization(mg./gm.)
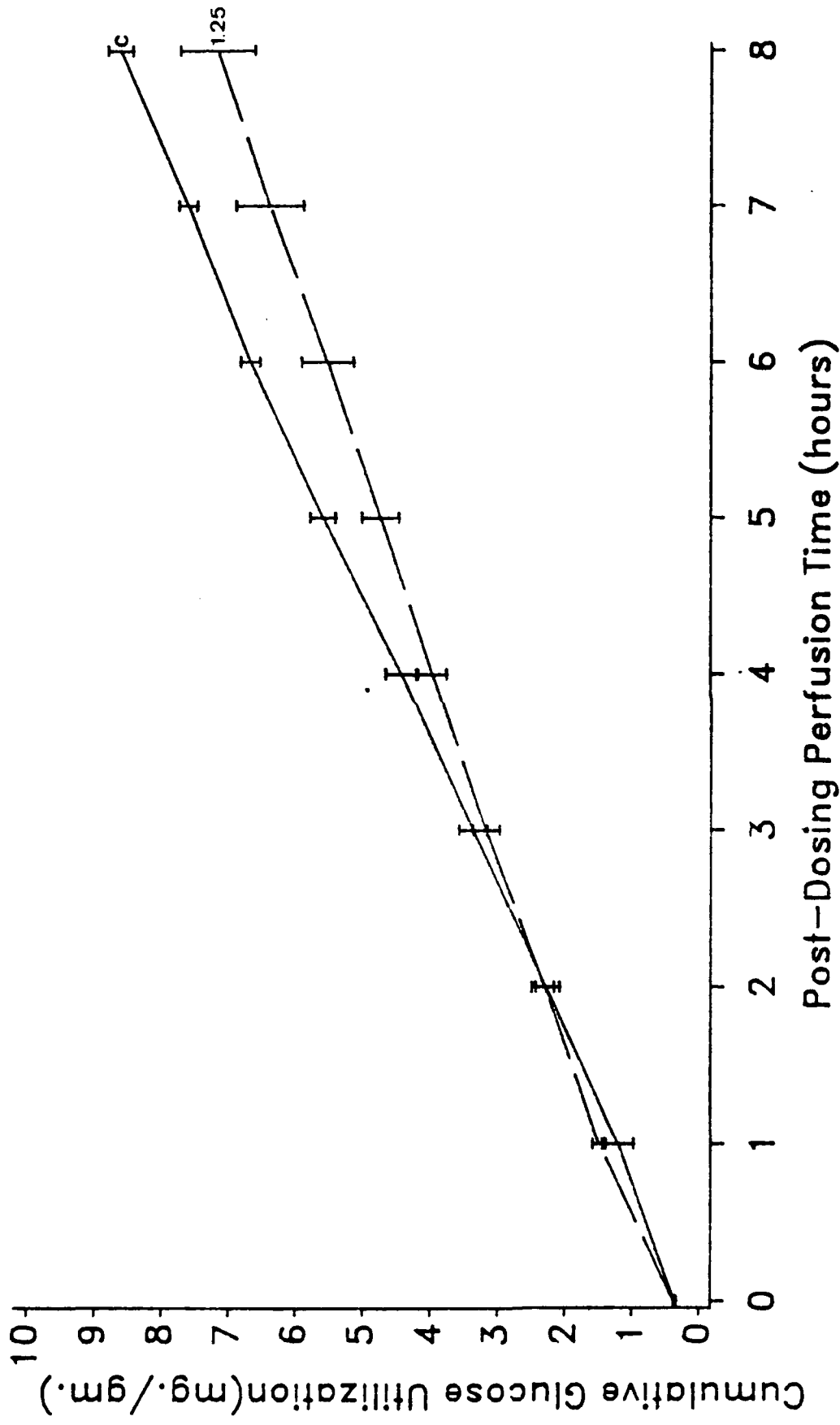
TREATMENT — CONTROL —— L(1.25MG/ML)
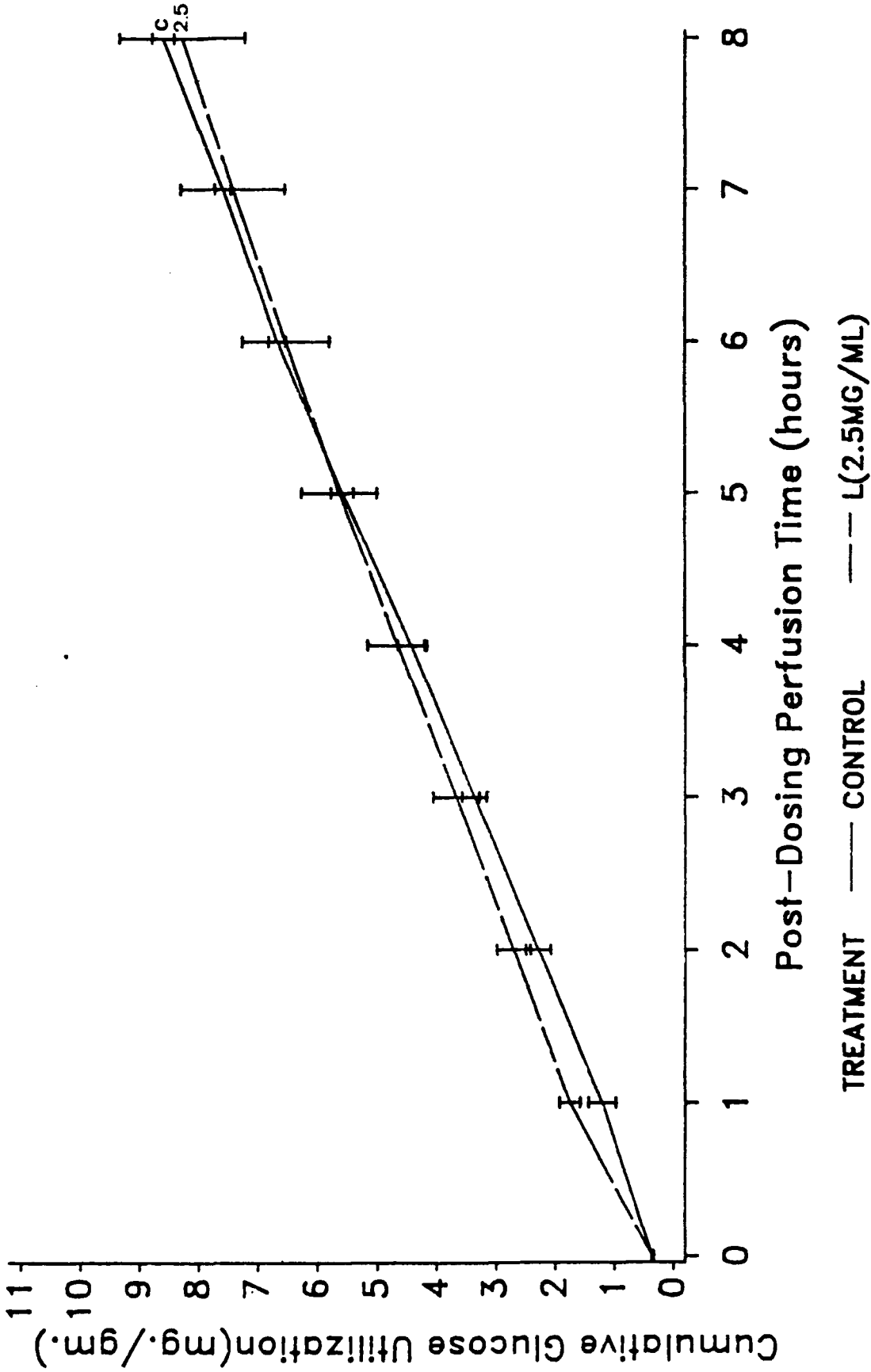
FIGURE 6. Graph Illustrating CGU of 2.5 mg/ml of XL compared to control.

TREATMENT —— CONTROL —— L(2.5MG/ML)

Post-Dosing Perfusion Time (hours)

Cumulative Glucose Utilization(mg./gm.)

51
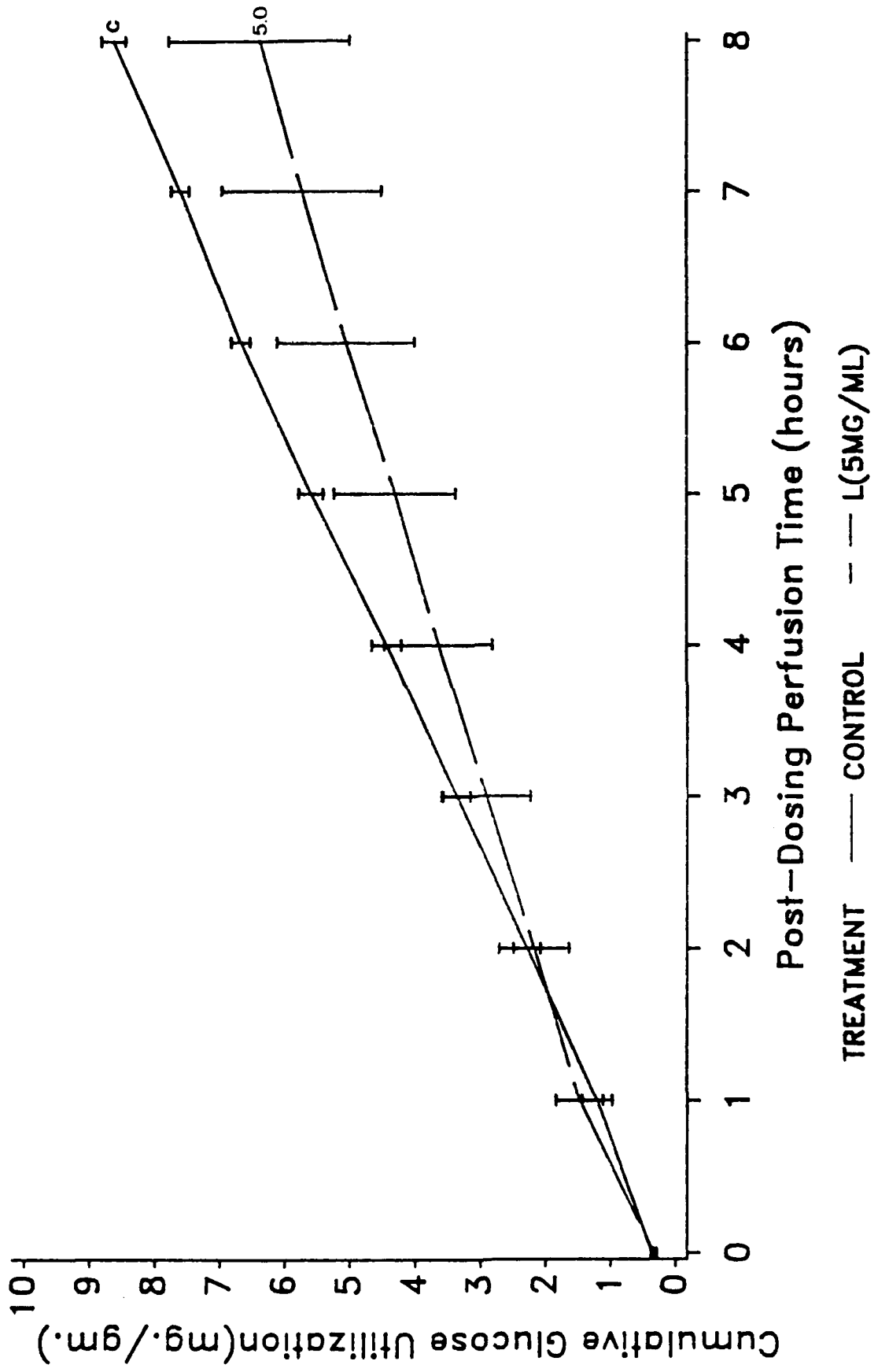
FIGURE 7. Graph illustrating CGU of 5.0 mg/ml of XL compared to control.

TREATMENT —— CONTROL — — L(5MG/ML)

52
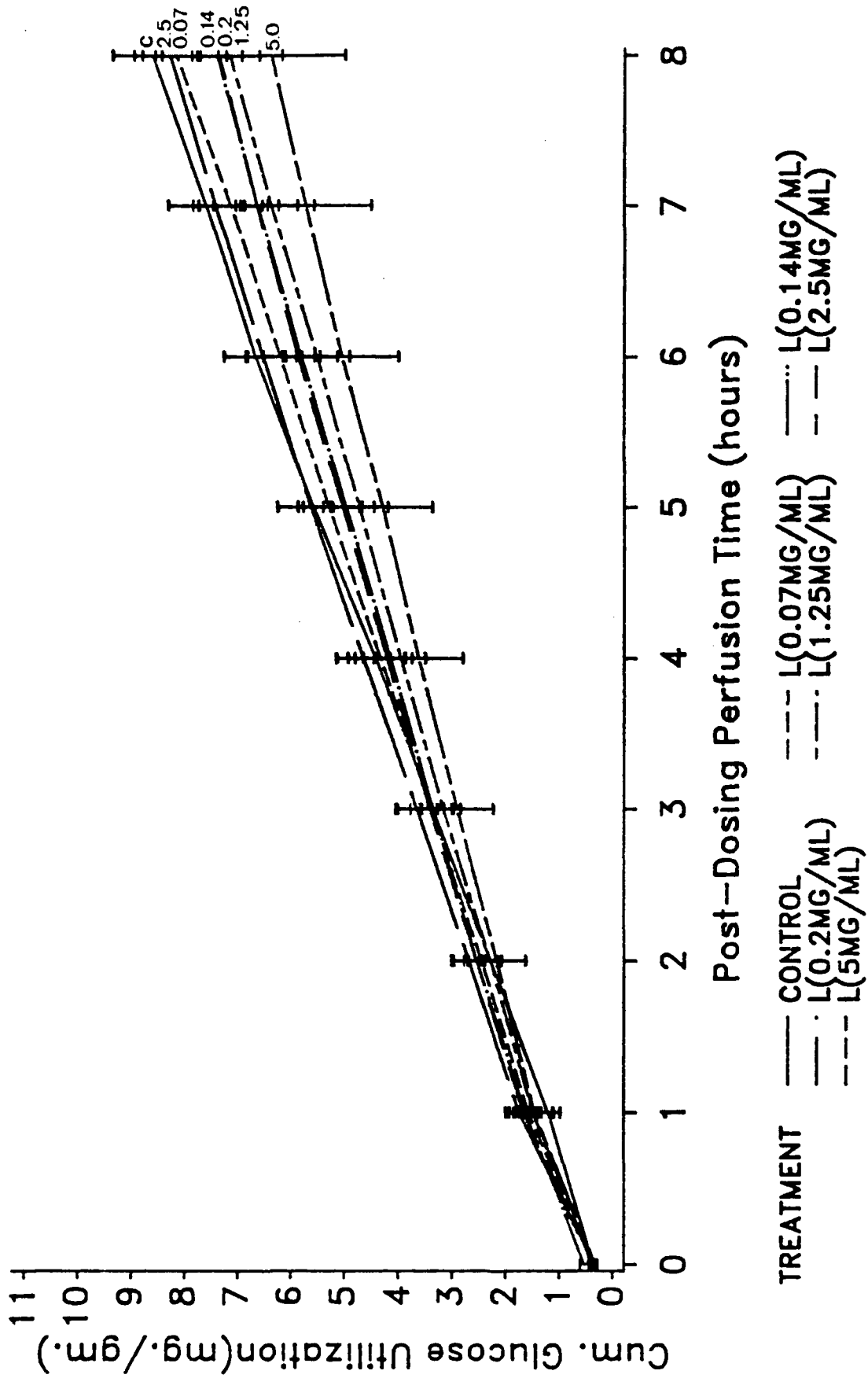
FIGURE 8. Graph Illustrating CGU of all concentrations of XL compared to control.

53
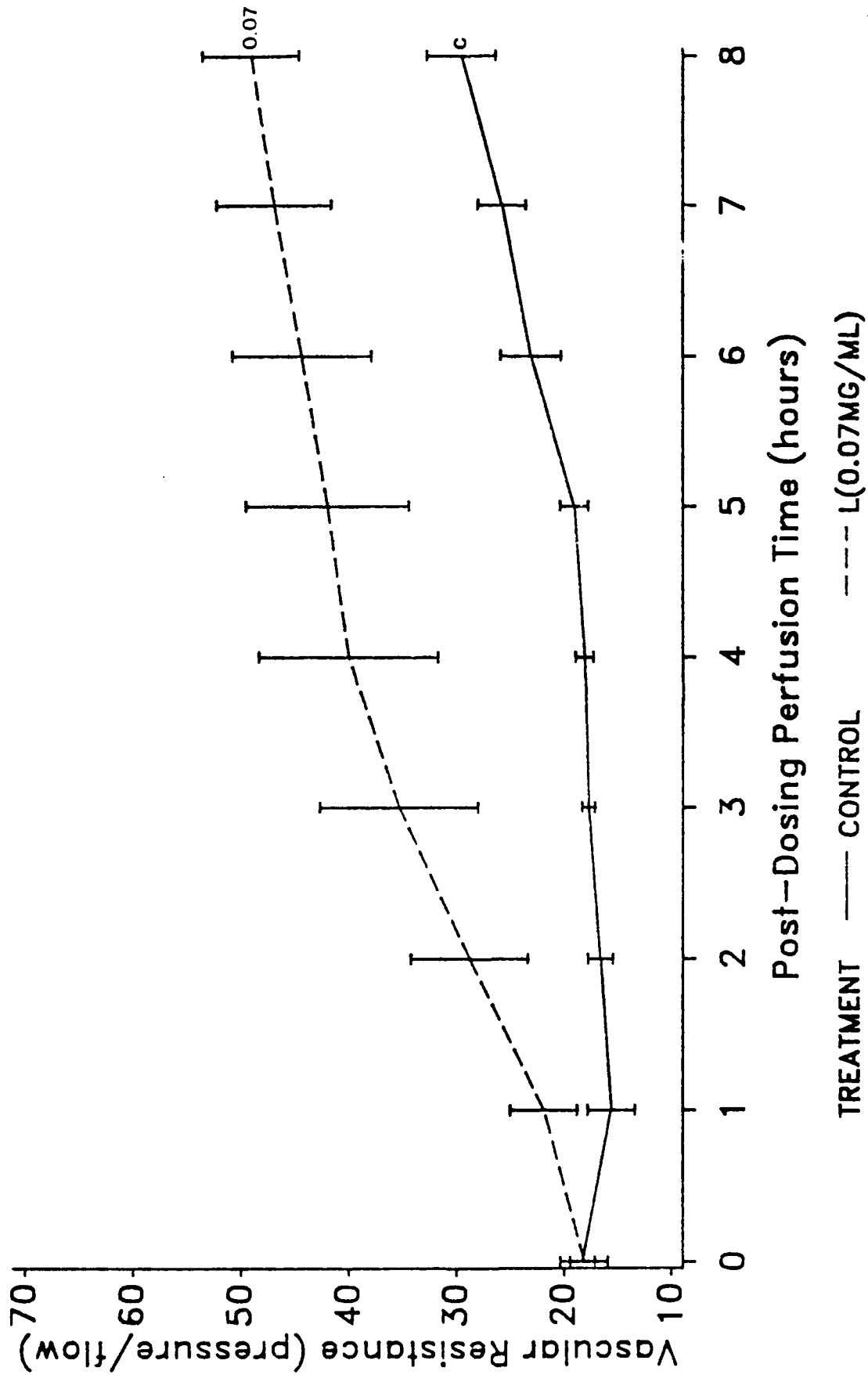
FIGURE 9. Graph illustrating VR of 0.07 mg/ml of XL compared to control.

54
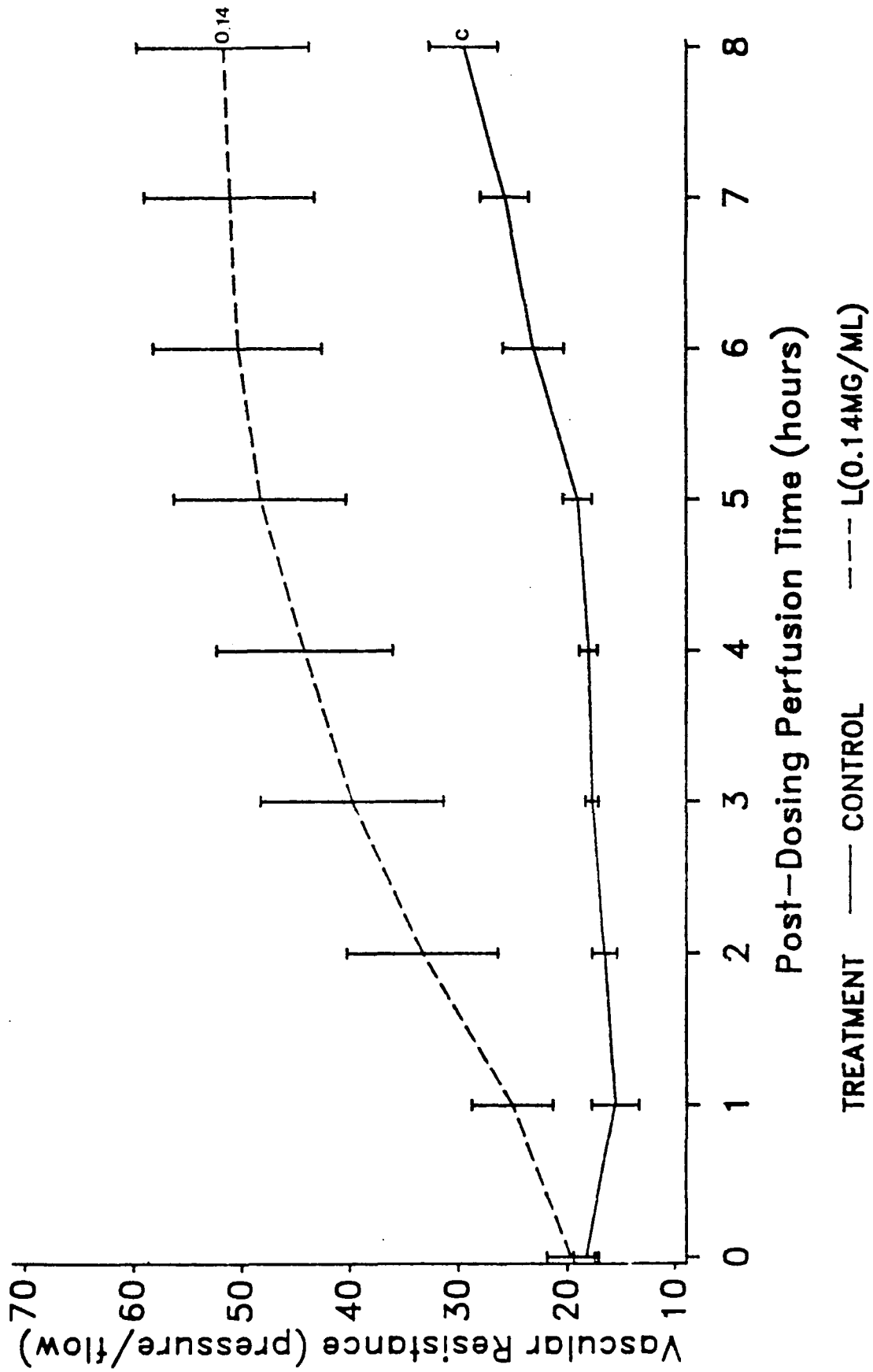
FIGURE 10. Graph Illustrating VR of 0.14 mg/ml of XL compared to control.

TREATMENT —— CONTROL ——— L(0.14MG/ML)

Post-Dosing Perfusion Time (hours)

Vascular Resistance (pressure/flow)

55

FIGURE 11. Graph Illustrating VR of 0.2 mg/ml of XL compared to control
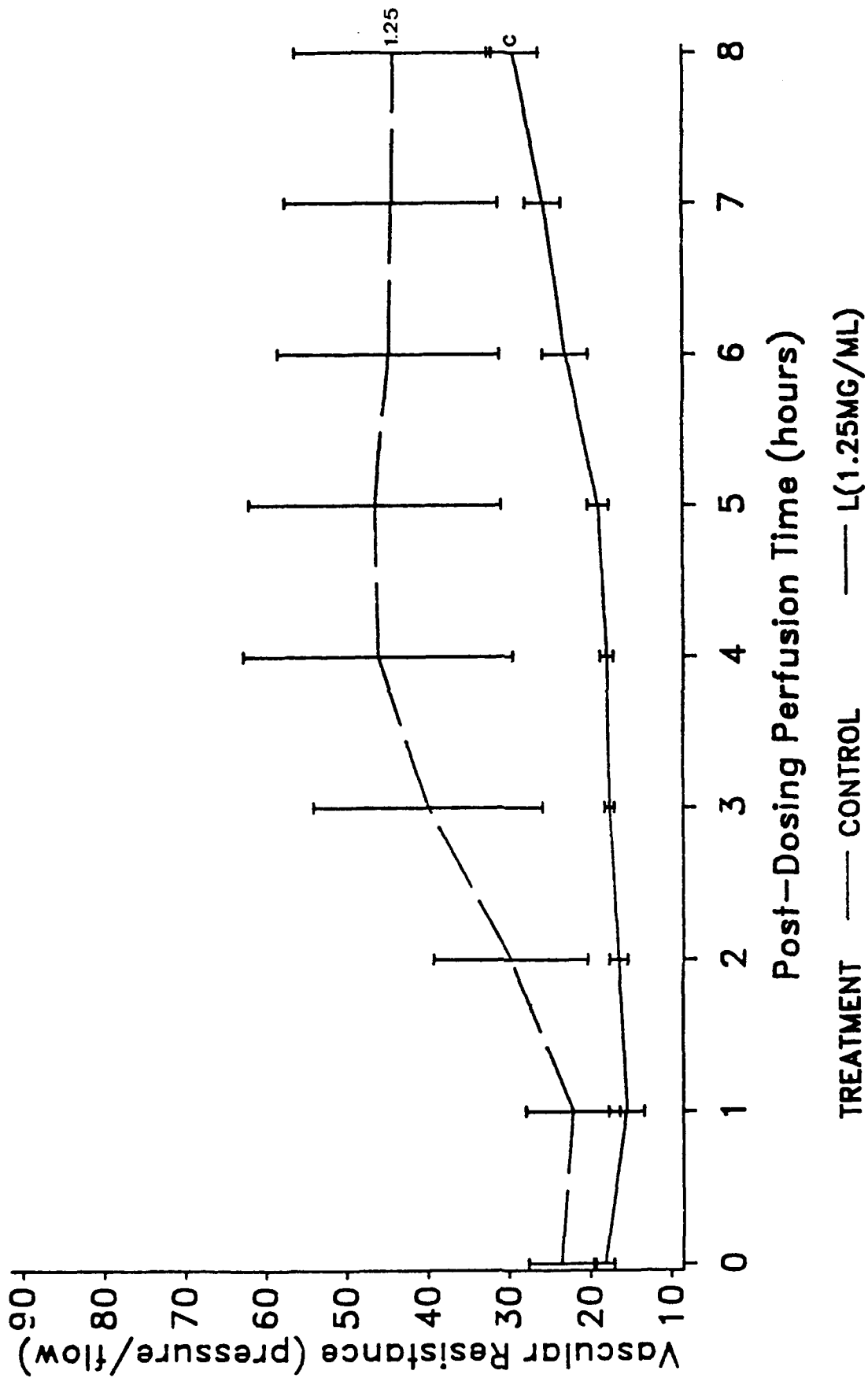
FIGURE 12. Graph Illustrating VR of 1.25 mg/ml of XL compared to control

TREATMENT — CONTROL — L(1.25MG/ML)

Vascular Resistance (pressure/flow)

Post-Dosing Perfusion Time (hours)
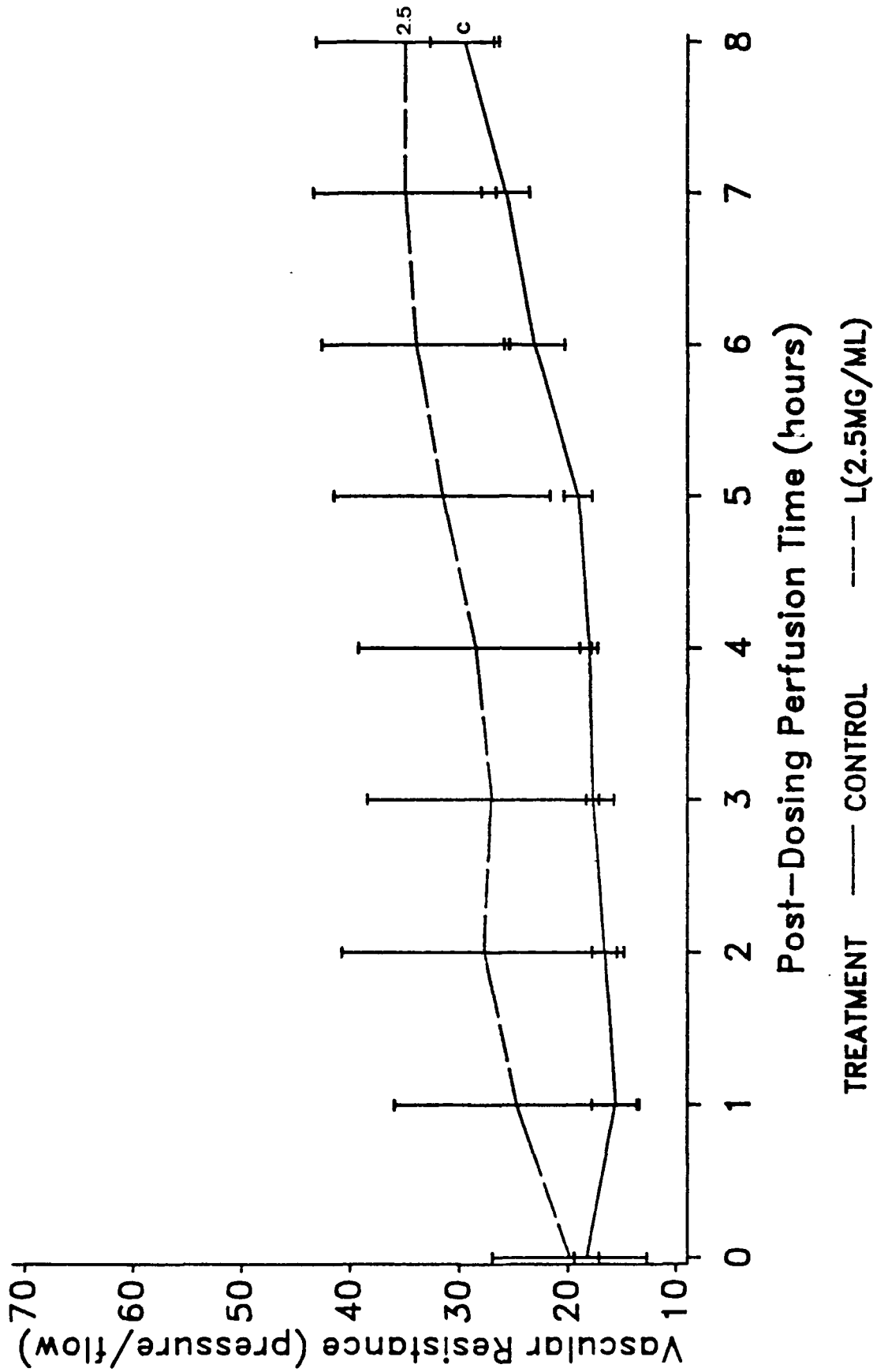
FIGURE 13. Graph illustrating VR of 2.5 mg/ml of XL compared to control.

58
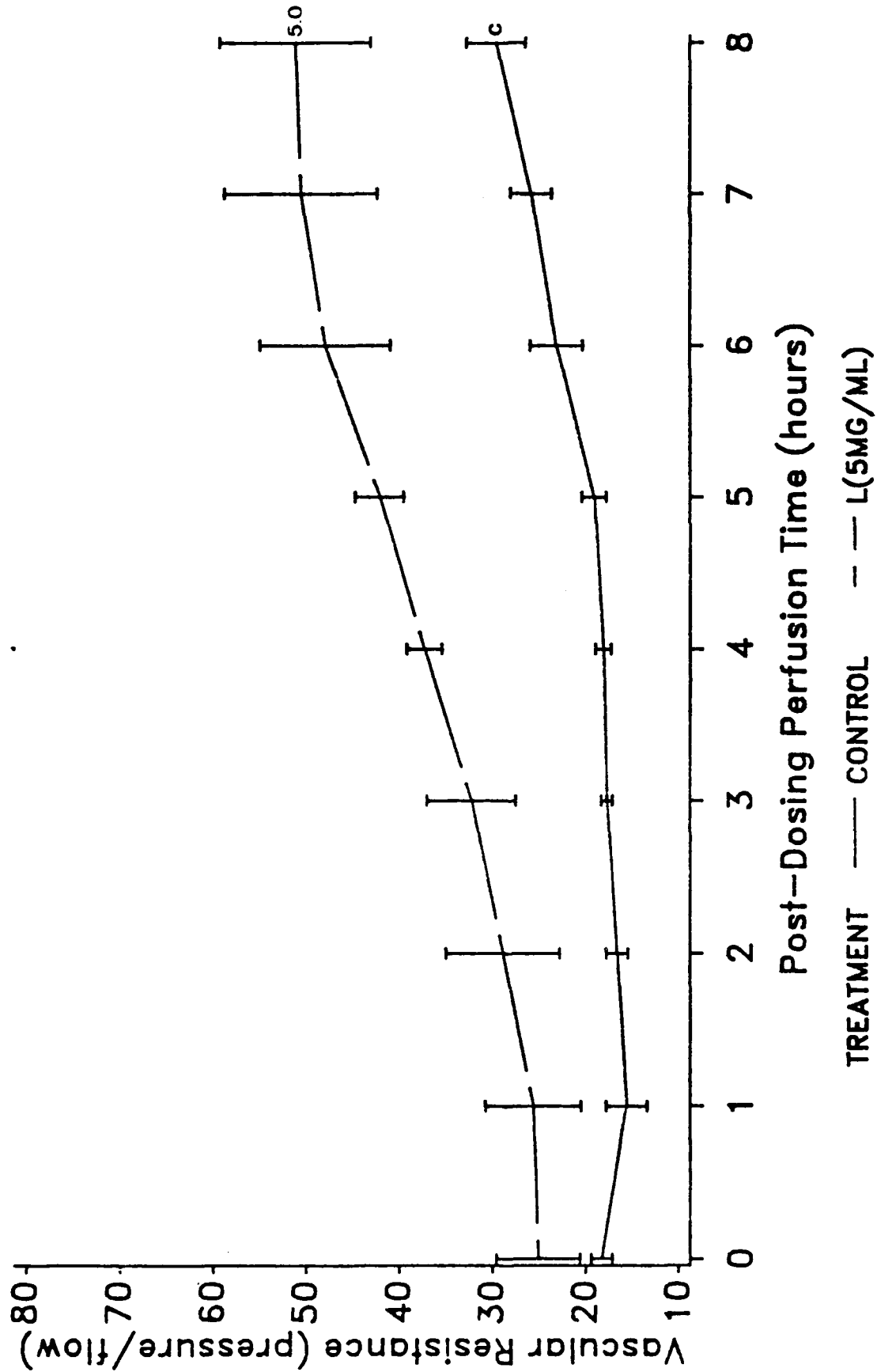
FIGURE 14. Graph Illustrating VR of 5.0 mg/ml of XL compared to control.

TREATMENT —— CONTROL — — L(5MG/ML)

Post–Dosing Perfusion Time (hours)

Vascular Resistance (pressure/flow)
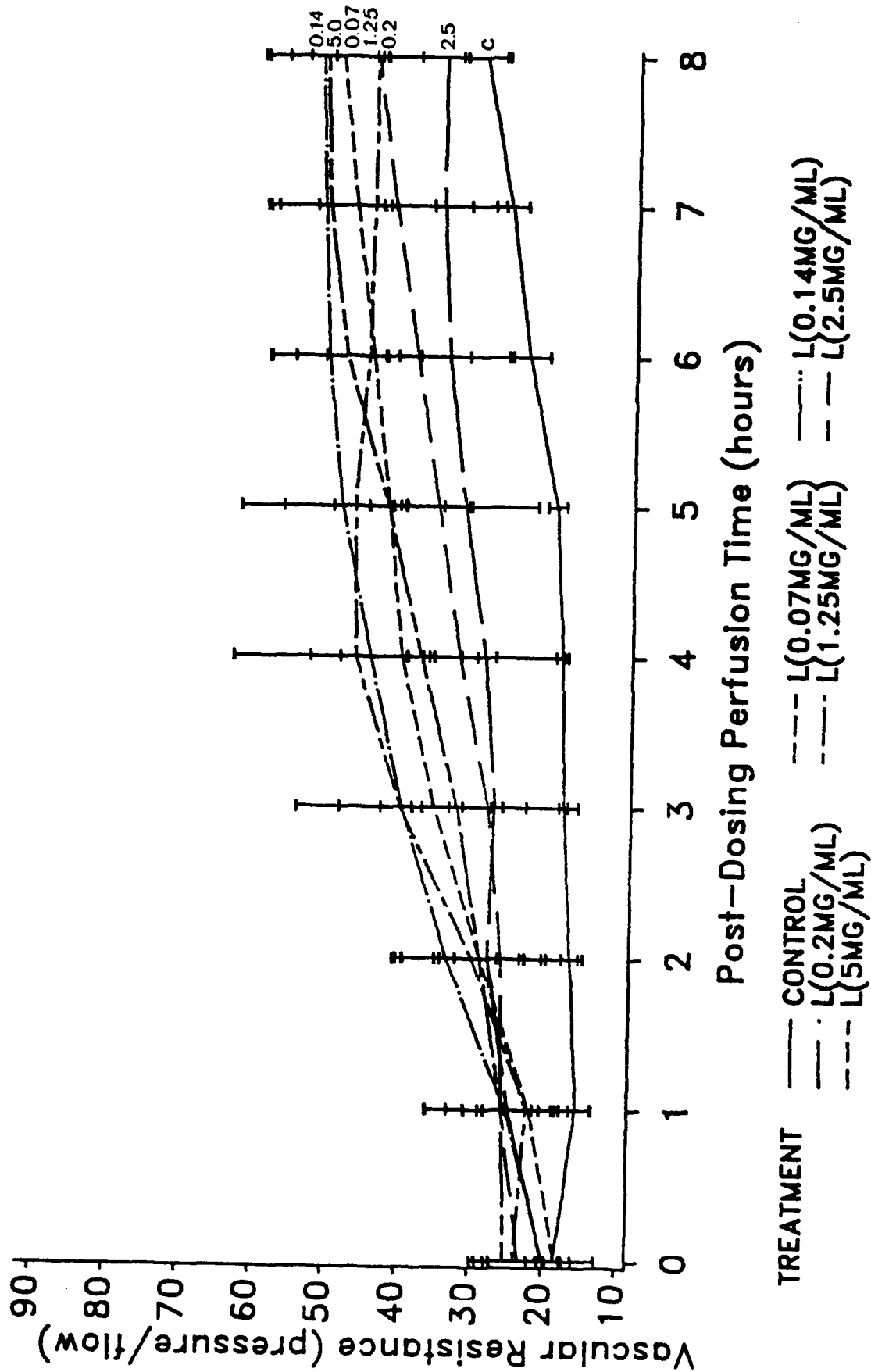
FIGURE 15. Graph Illustrating VR of all concentrations of XL compared to control.

60
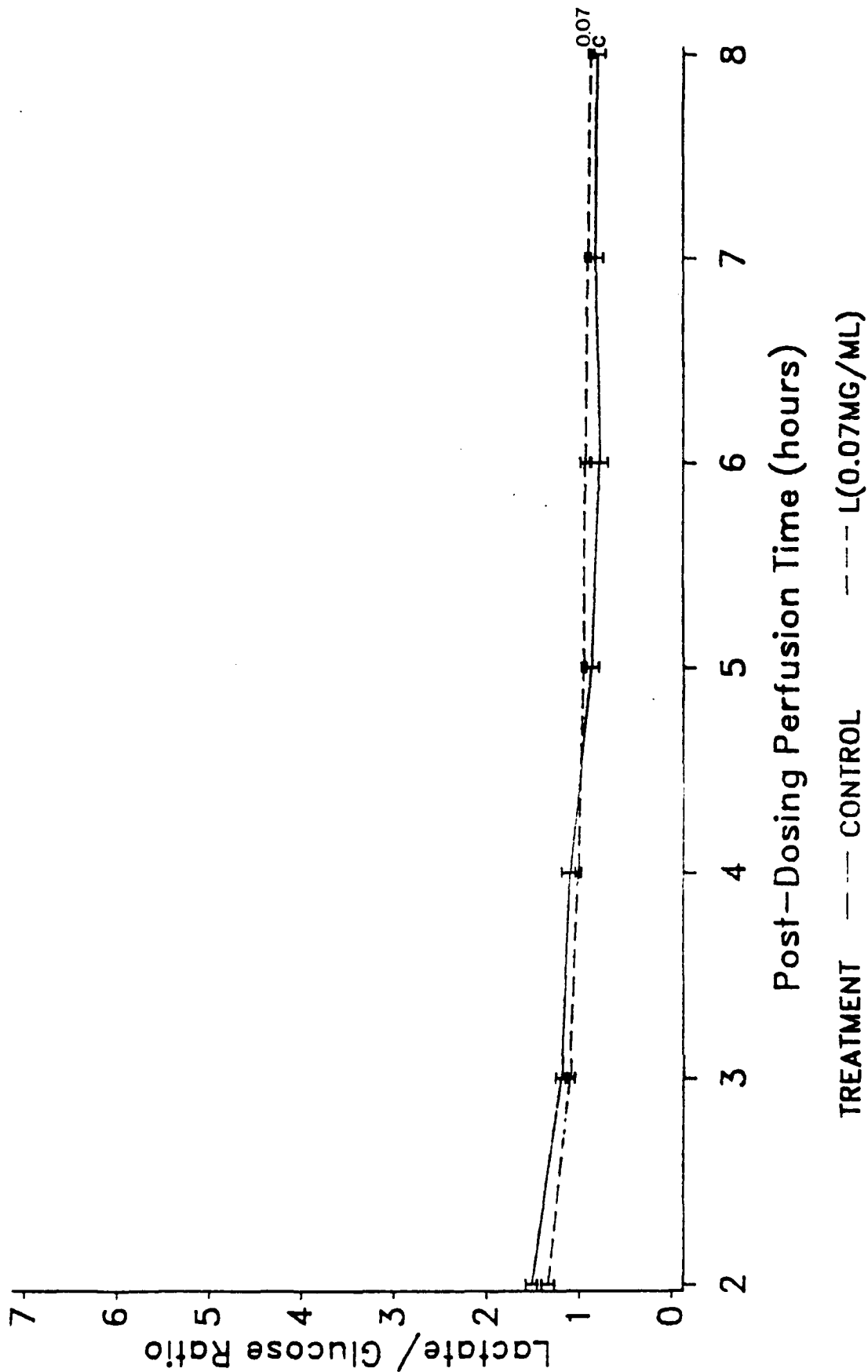
FIGURE 16. Graph illustrating L/GU of 0.07mg/ml of XL compared to control.
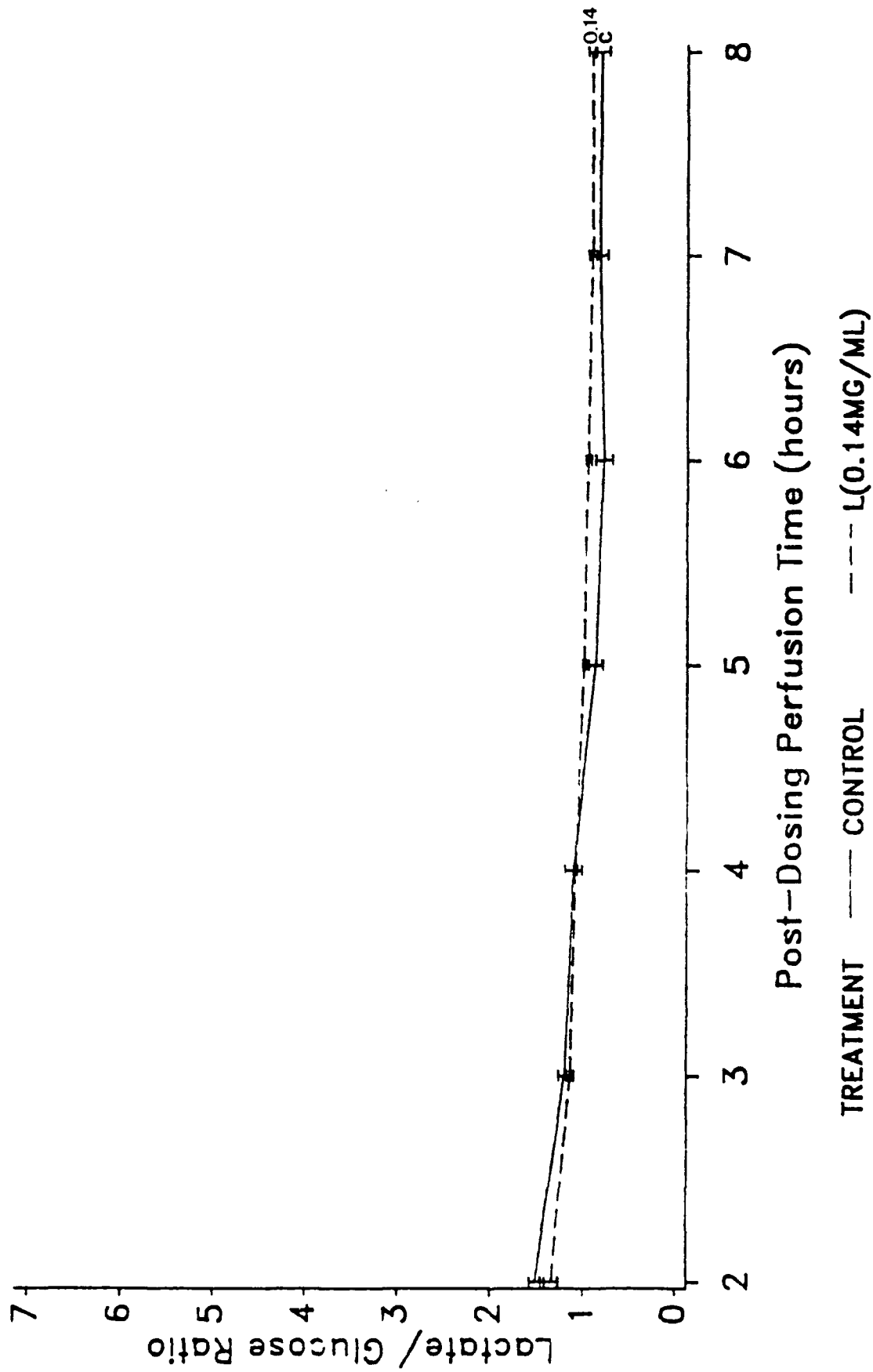
FIGURE 17. Graph illustrating L/GU of 0.14 mg/ml of XL compared to control.

TREATMENT ⎯⎯ CONTROL ⎯ ⎯ L(0.14MG/ML)

Post-Dosing Perfusion Time (hours)

Lactate/Glucose Ratio
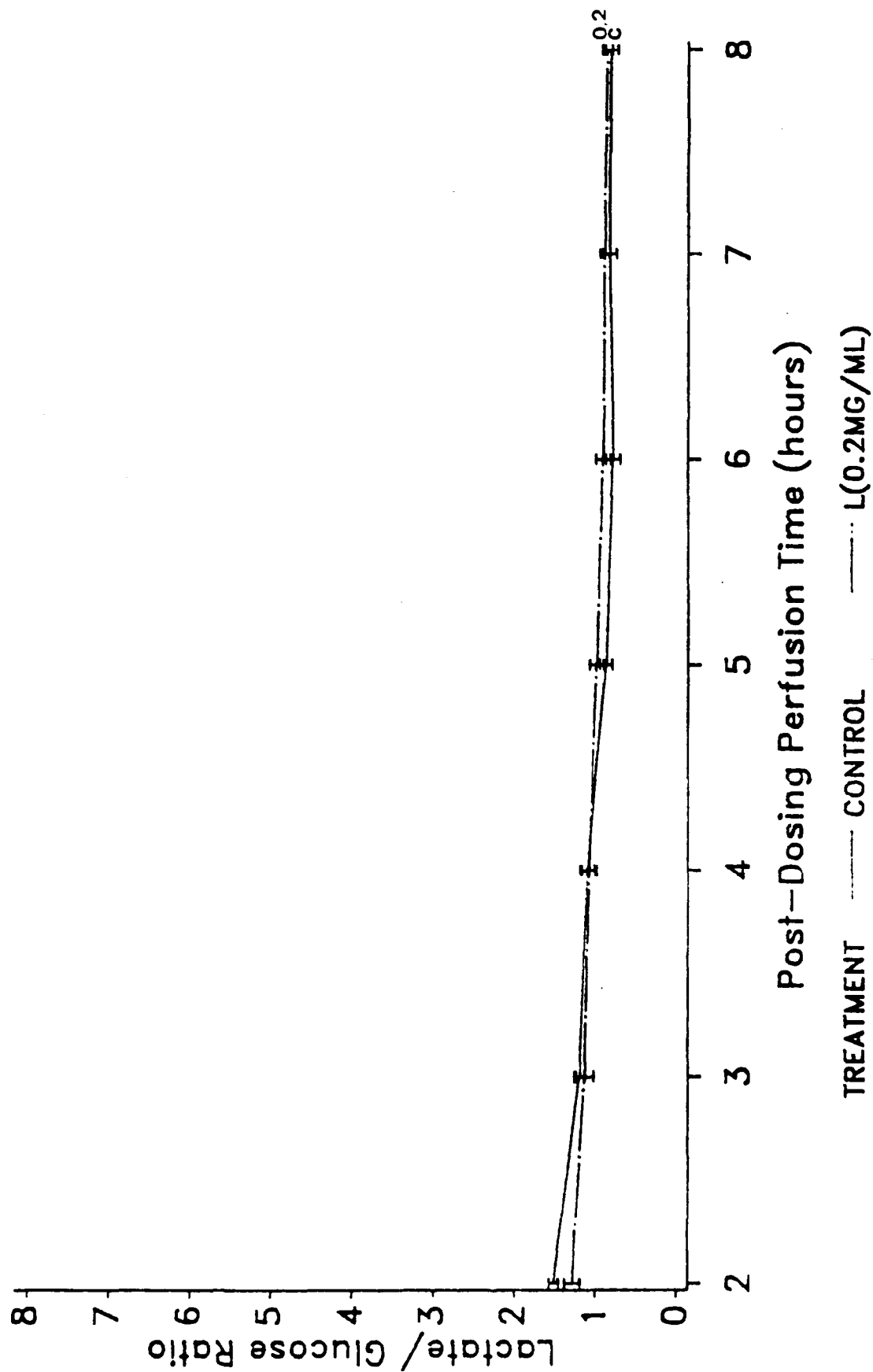
FIGURE 18. Graph illustrating L/GU of 0.2 mg/ml of XL compared to control.
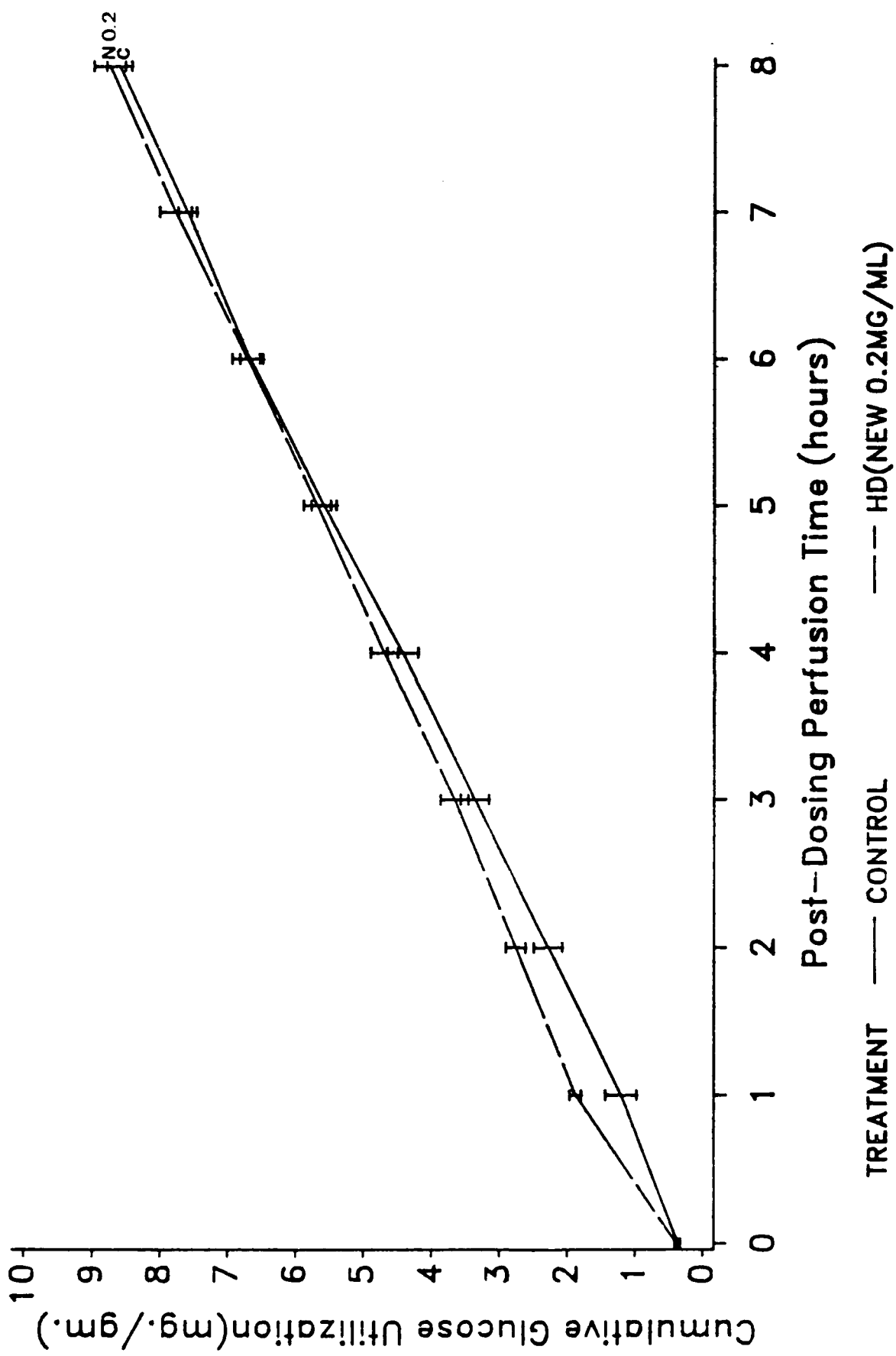
TREATMENT ——— CONTROL ——— L(0.2MG/ML)

63

FIGURE 19. Graph illustrating L/GU of 1.25 mg/ml of XL compared to control.
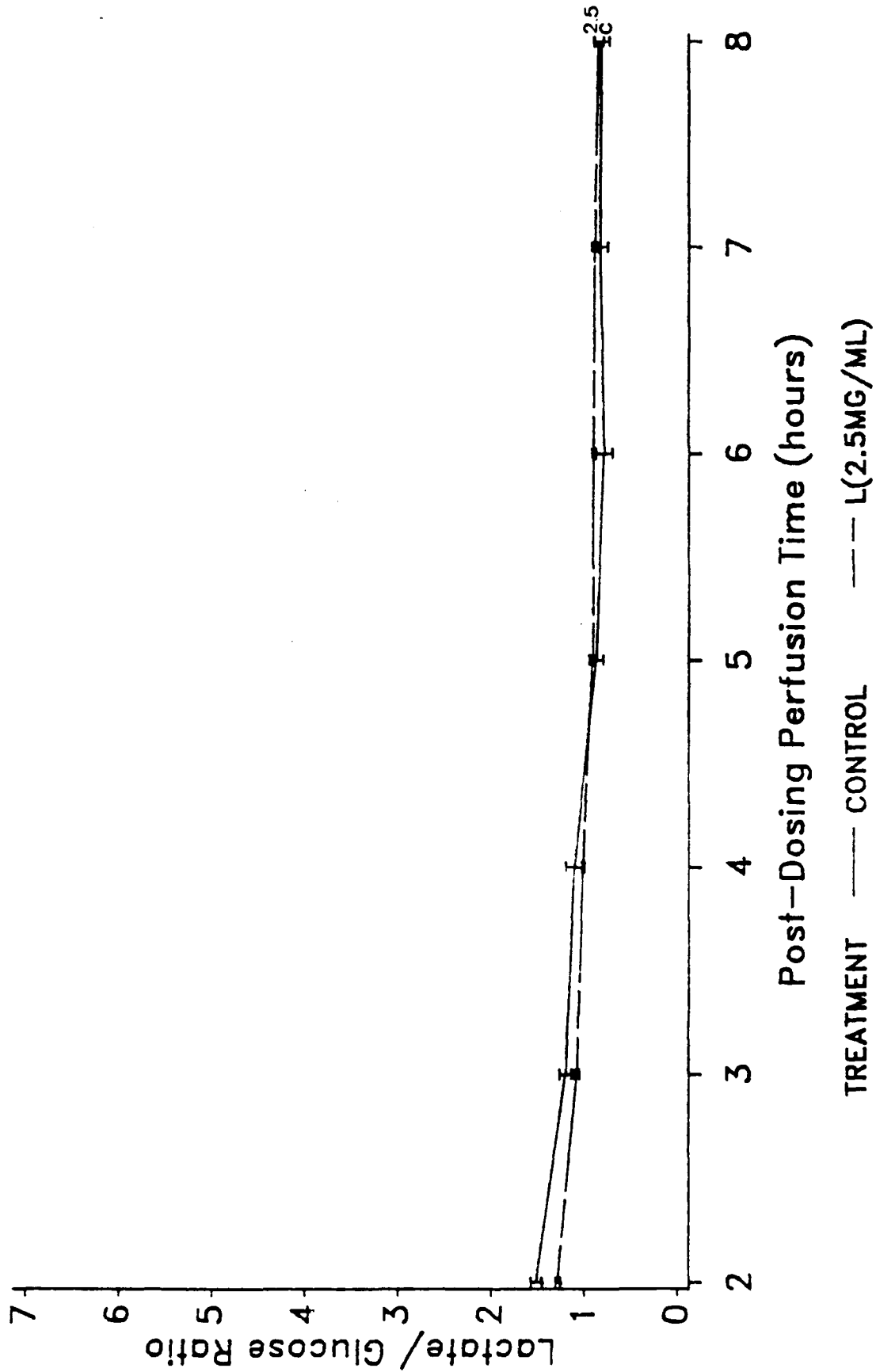
FIGURE 20. Graph illustrating L/GU of 2.5 mg/ml of XL compared to control.

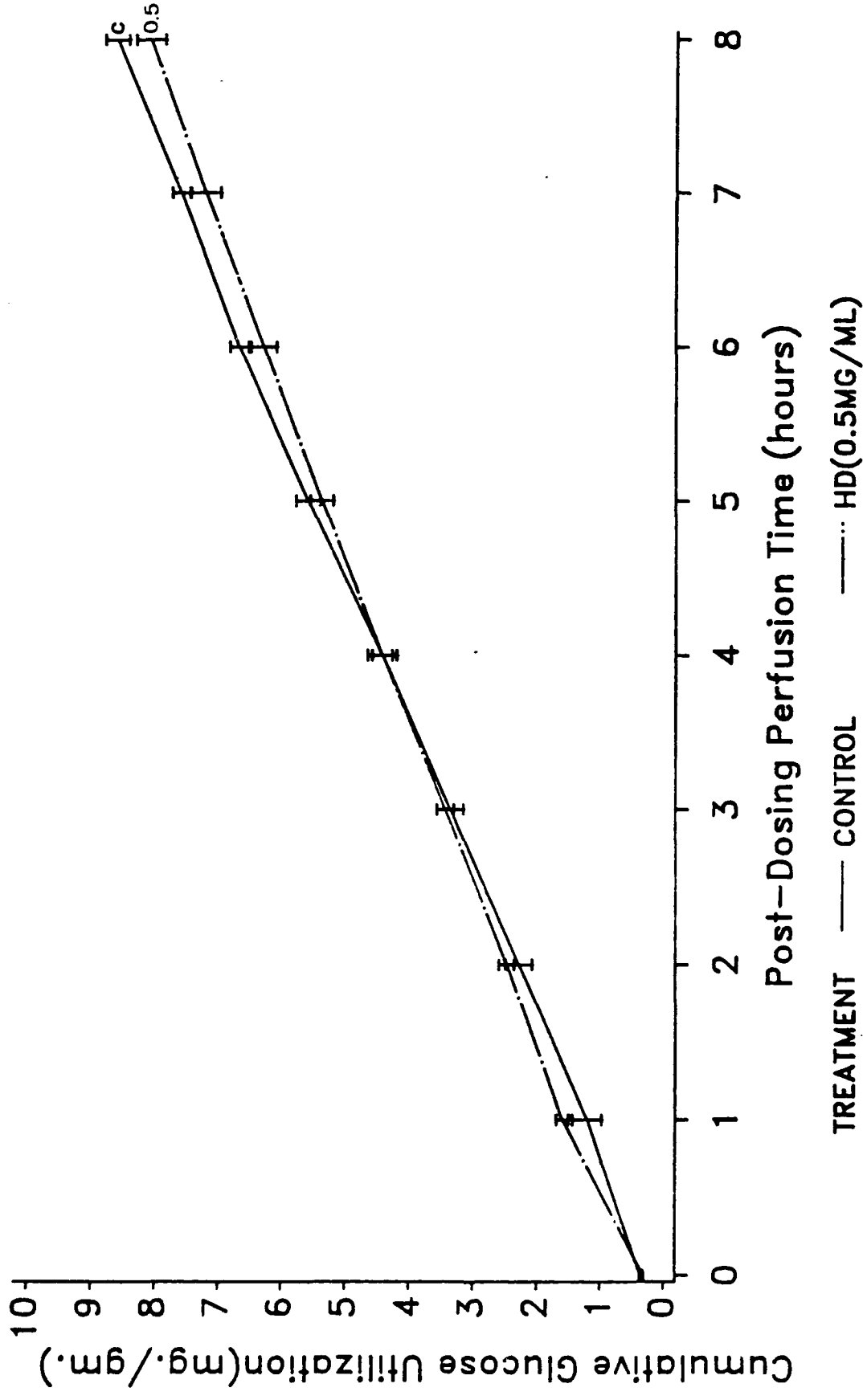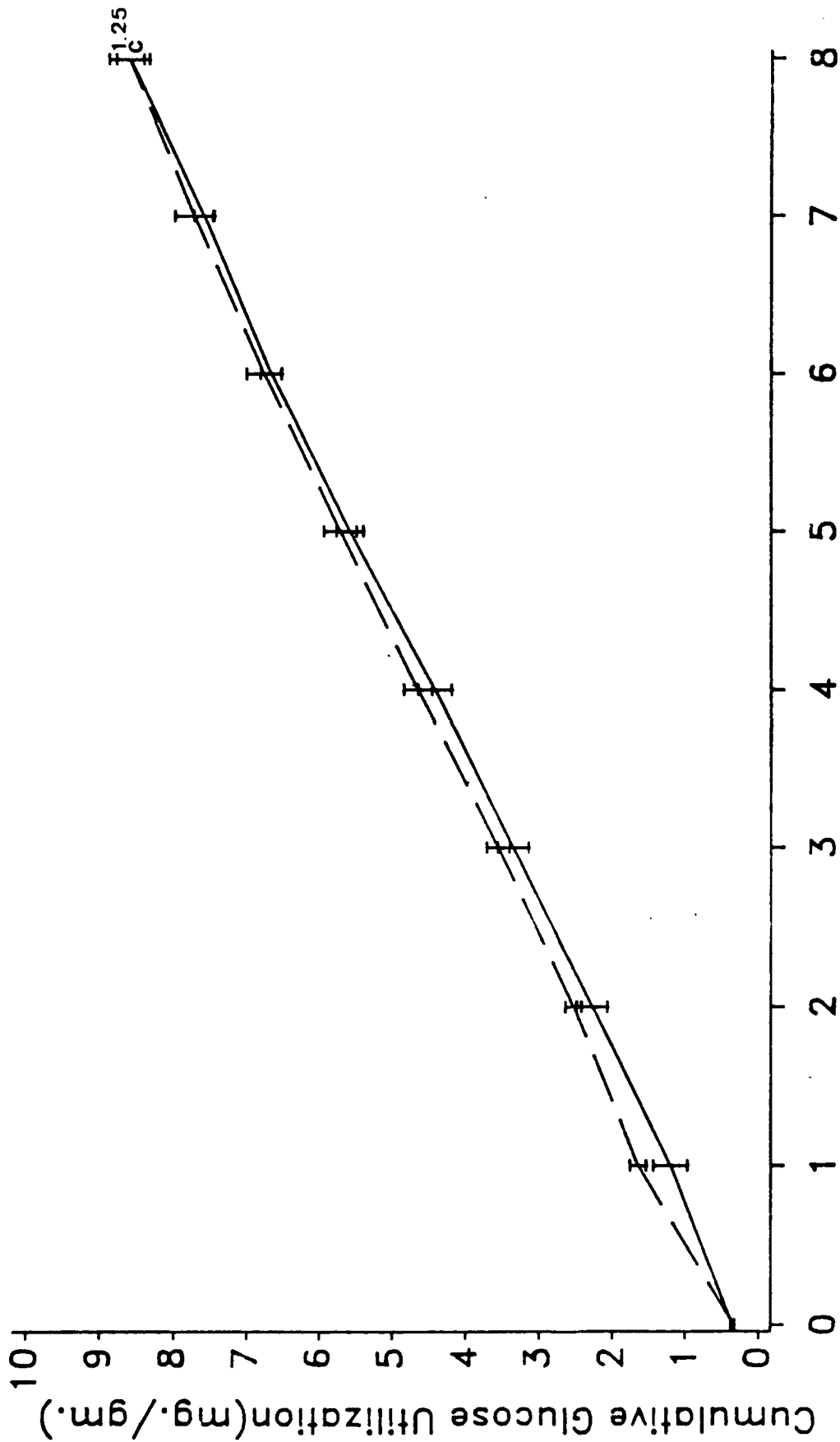FIGURE 21. Graph illustrating L/GU of 5.0 mg/ml of XL compared to control.

Lactate/Glucose Ratio
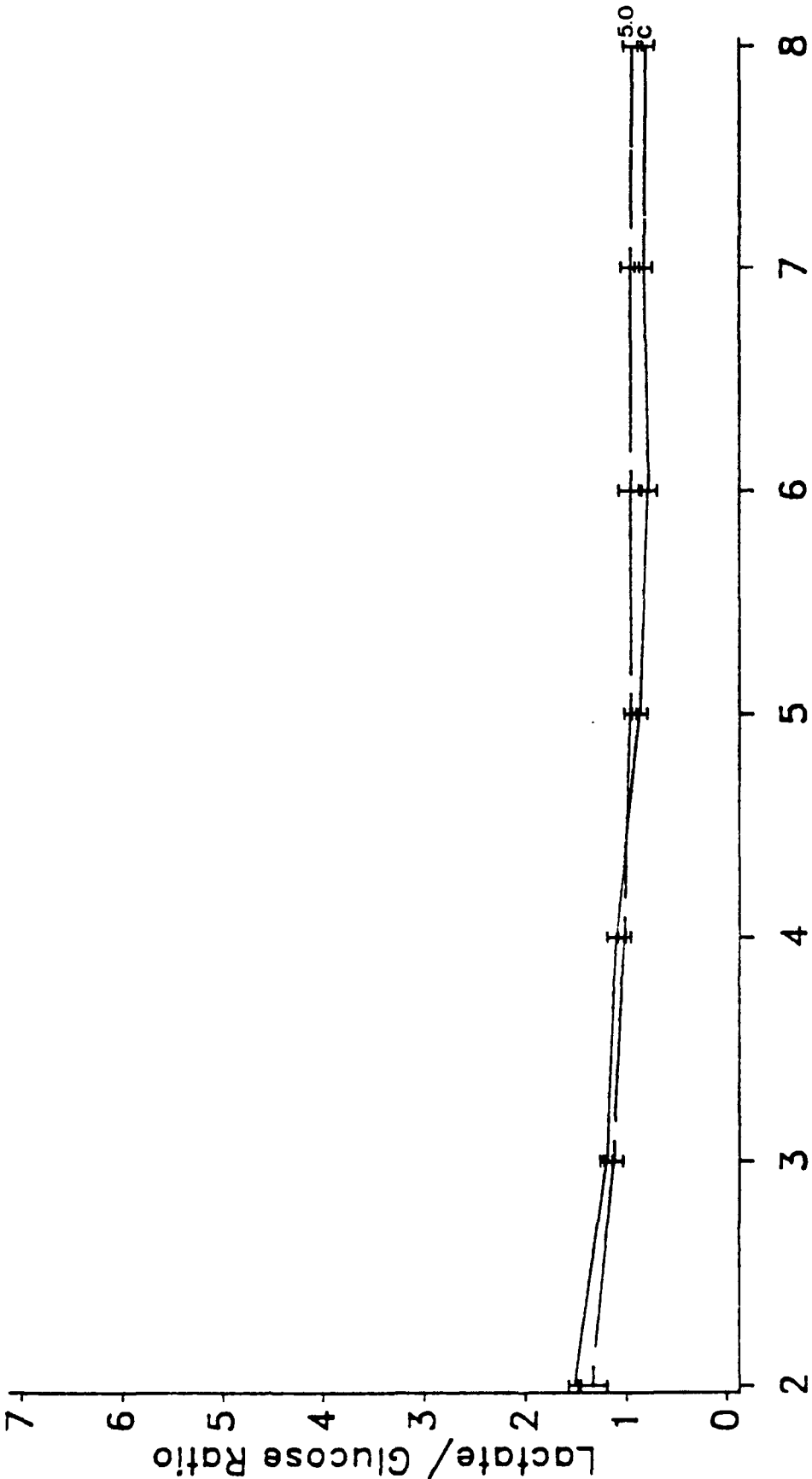
Post-Dosing Perfusion Time (hours)

TREATMENT ——— CONTROL – – L(5MG/ML)
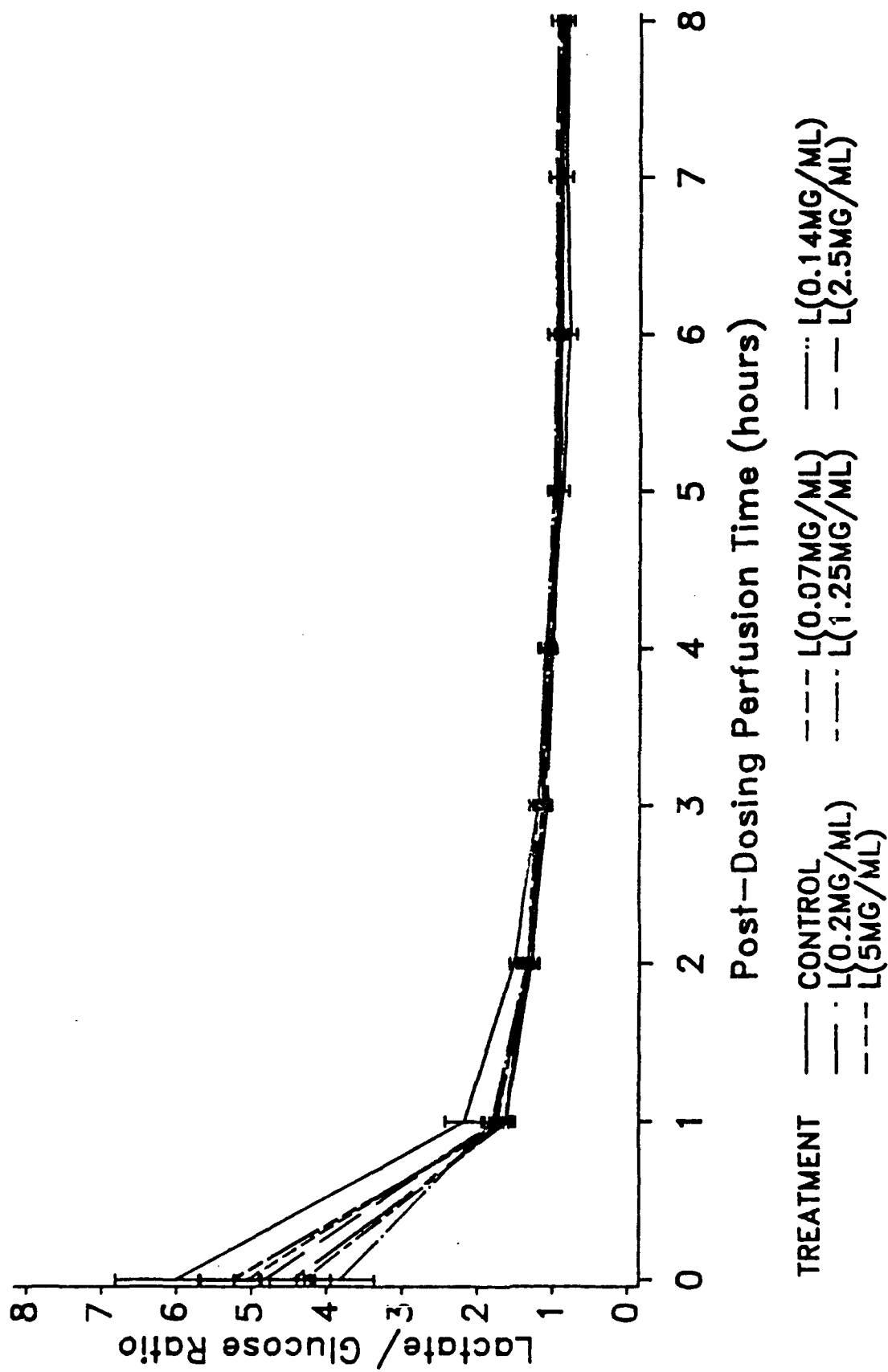
FIGURE 22. Graph illustrating L/GU ratio of all concentrations of XL compared to control.

67
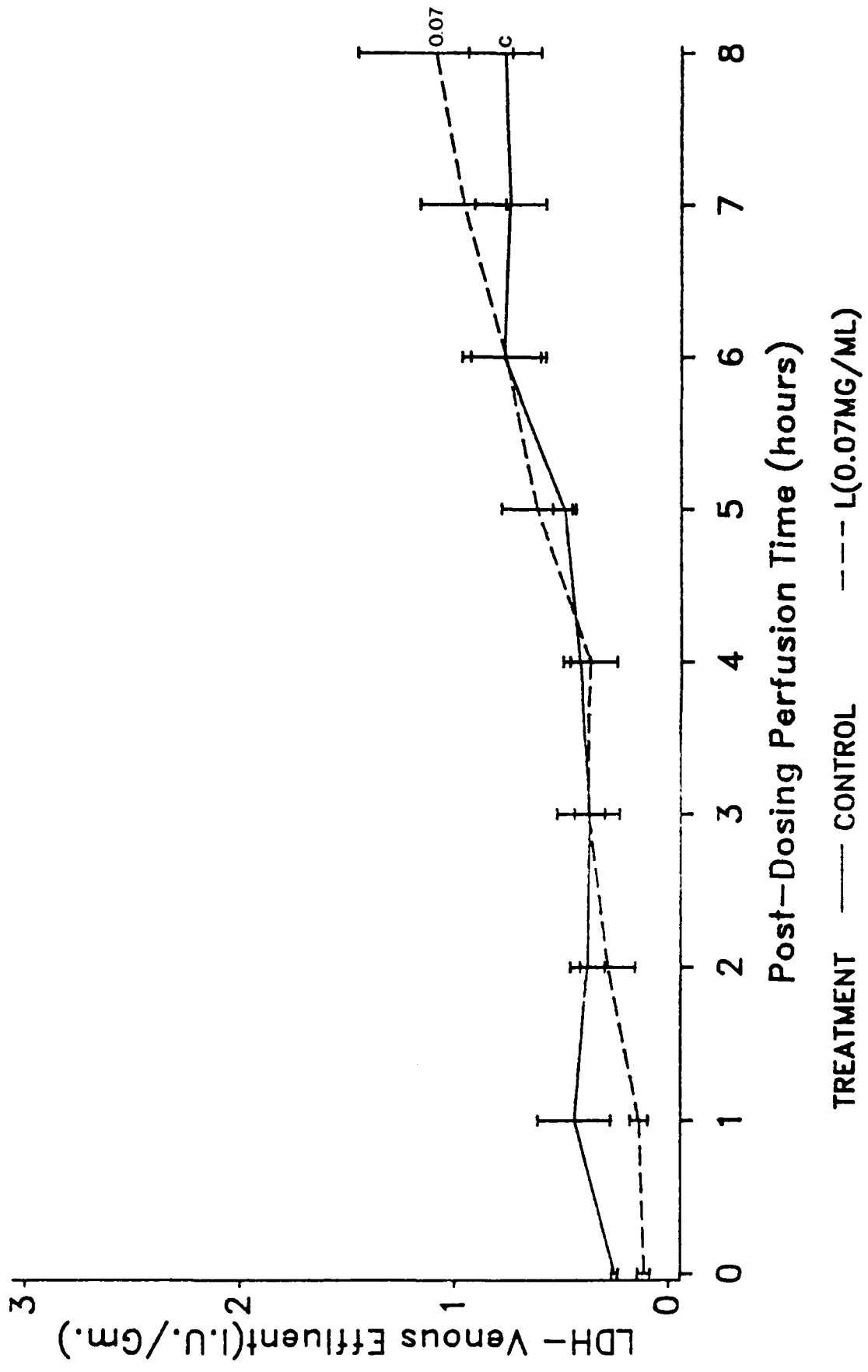
FIGURE 23. Graph illustrating LDH release of 0.07 mg/ml XL compared to control.

TREATMENT ——— CONTROL ——— L(0.07MG/ML)
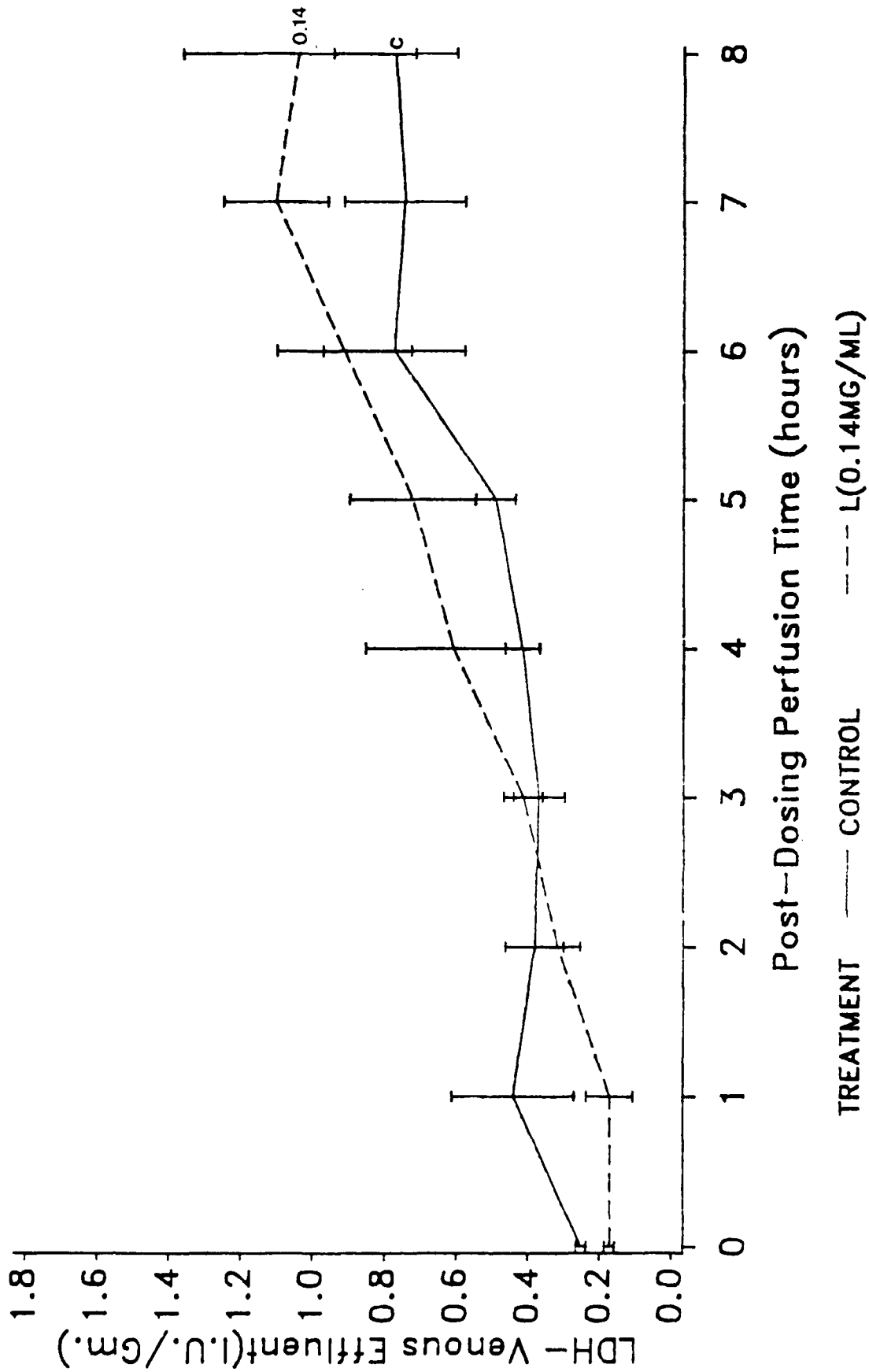
FIGURE 24. Graph illustrating LDH release of 0.14 mg/ml of XL compared to control.

TREATMENT — CONTROL - - - L(0.14MG/ML)
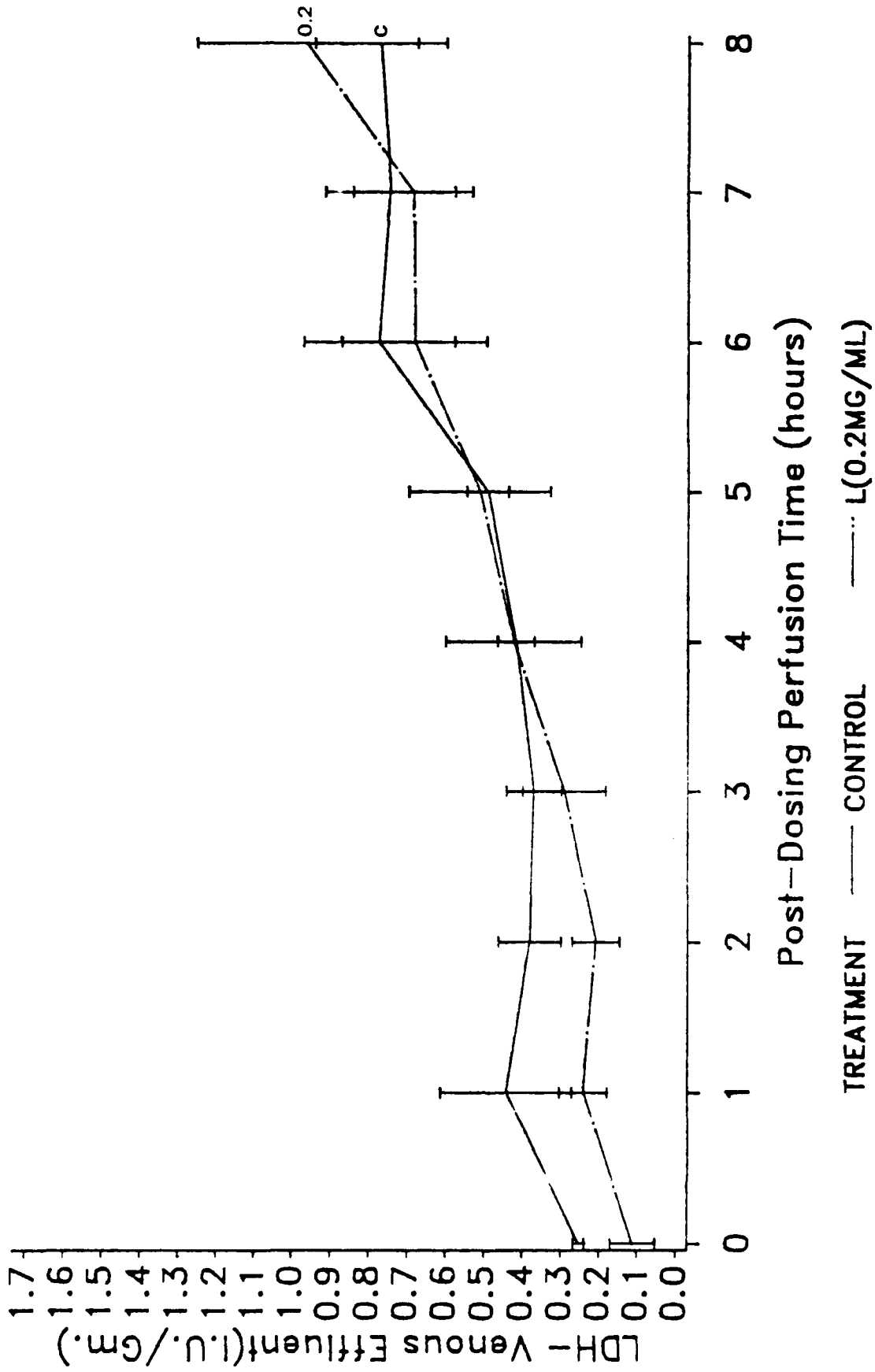
FIGURE 25. Graph illustrating LDH release of 0.2 mg/ml of XL compared to control.

FIGURE 26. Graph illustrating LDH release of 1.25 mg/ml of XL compared to control.
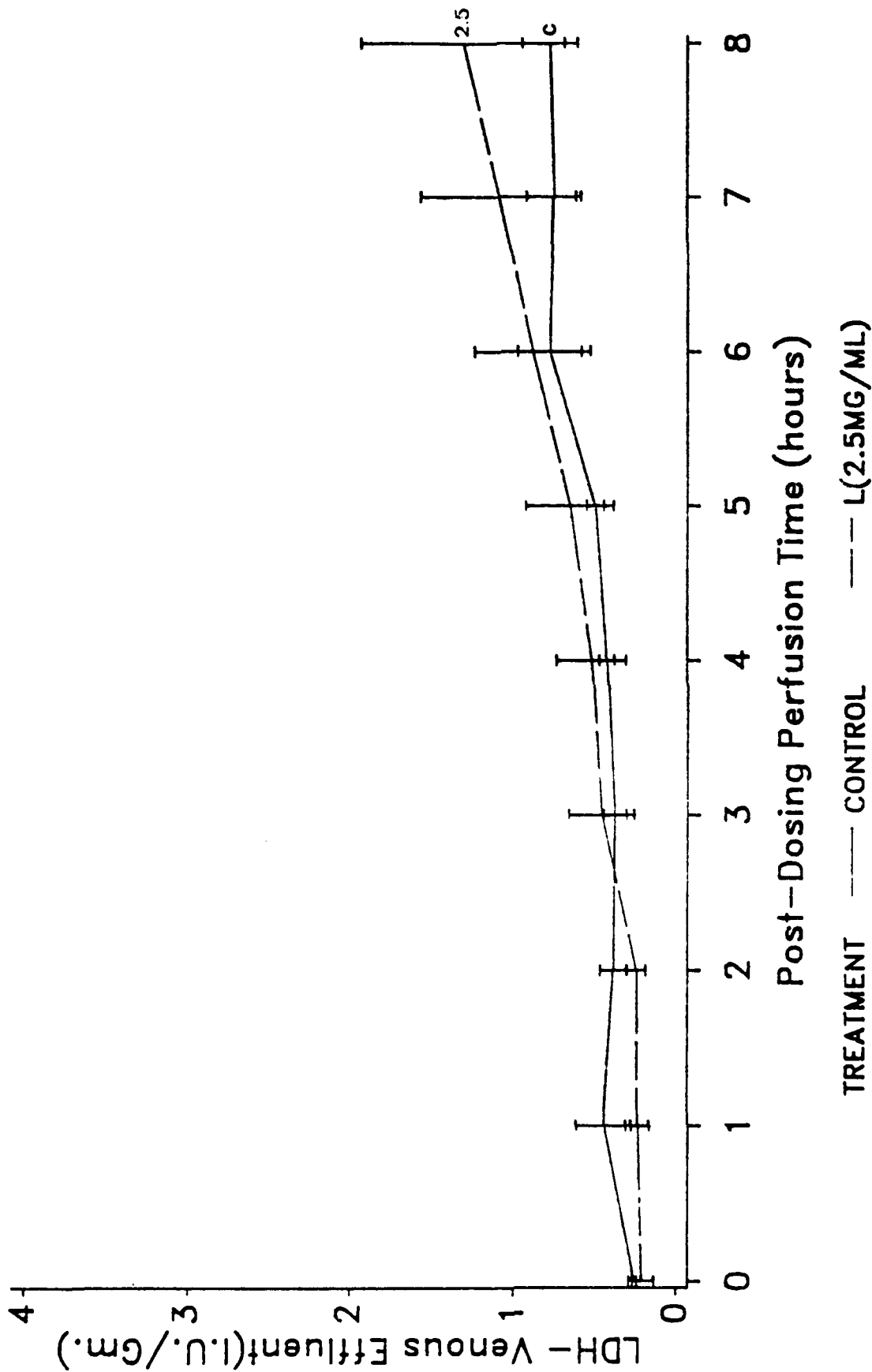
FIGURE 27. Graph illustrating LDH release of 2.5 mg/ml of XL compared to control.

TREATMENT — CONTROL ---- L(2.5MG/ML)

Post-Dosing Perfusion Time (hours)

LDH-Venous Effluent(I.U./Gm.)
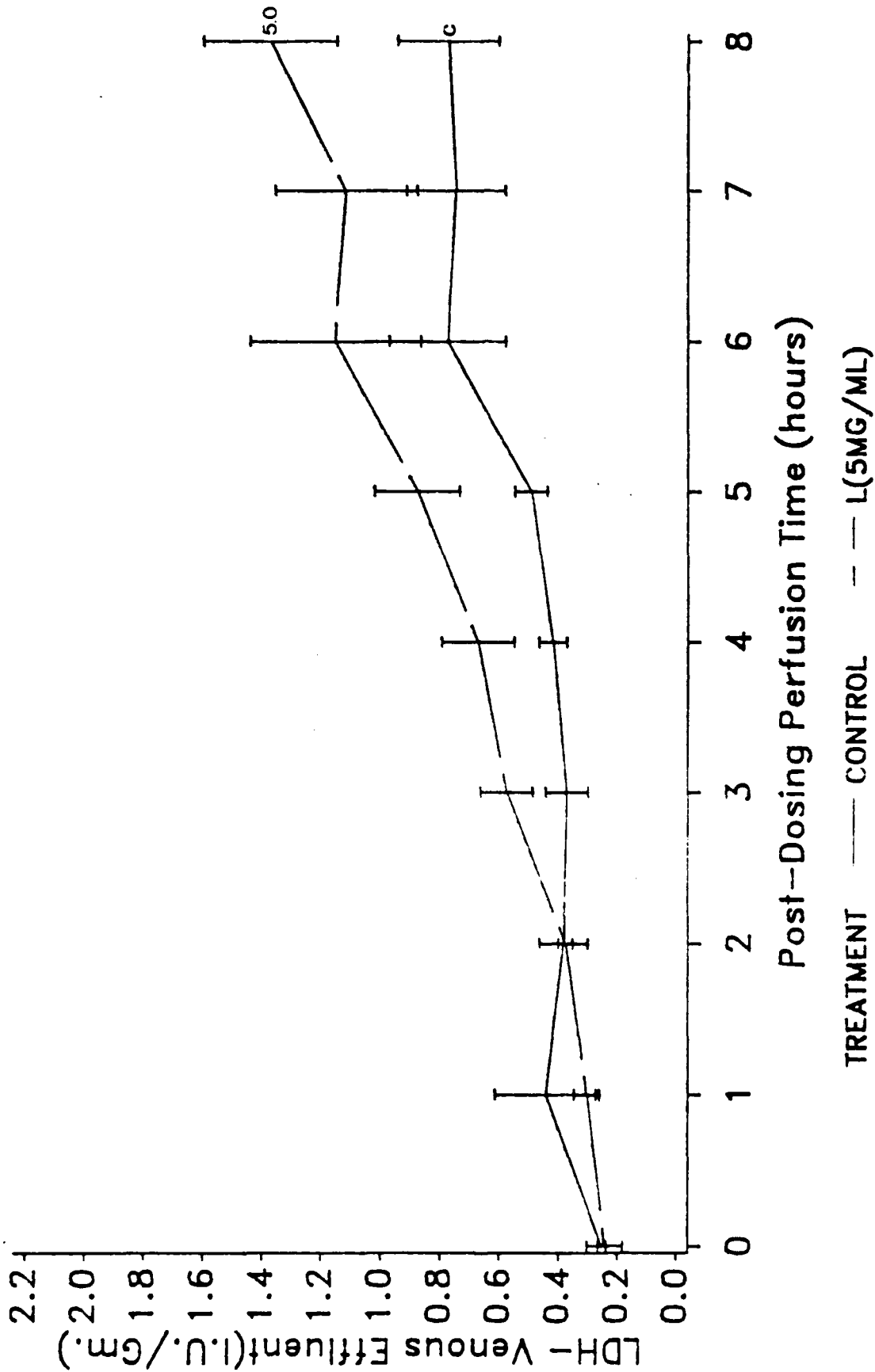
FIGURE 28. Graph illustrating LDH release of 5.0 mg/ml of XL compared to control.

TREATMENT ——— CONTROL — — L(5MG/ML)

Post–Dosing Perfusion Time (hours)

LDH– Venous Effluent(I.U./Gm.)

73
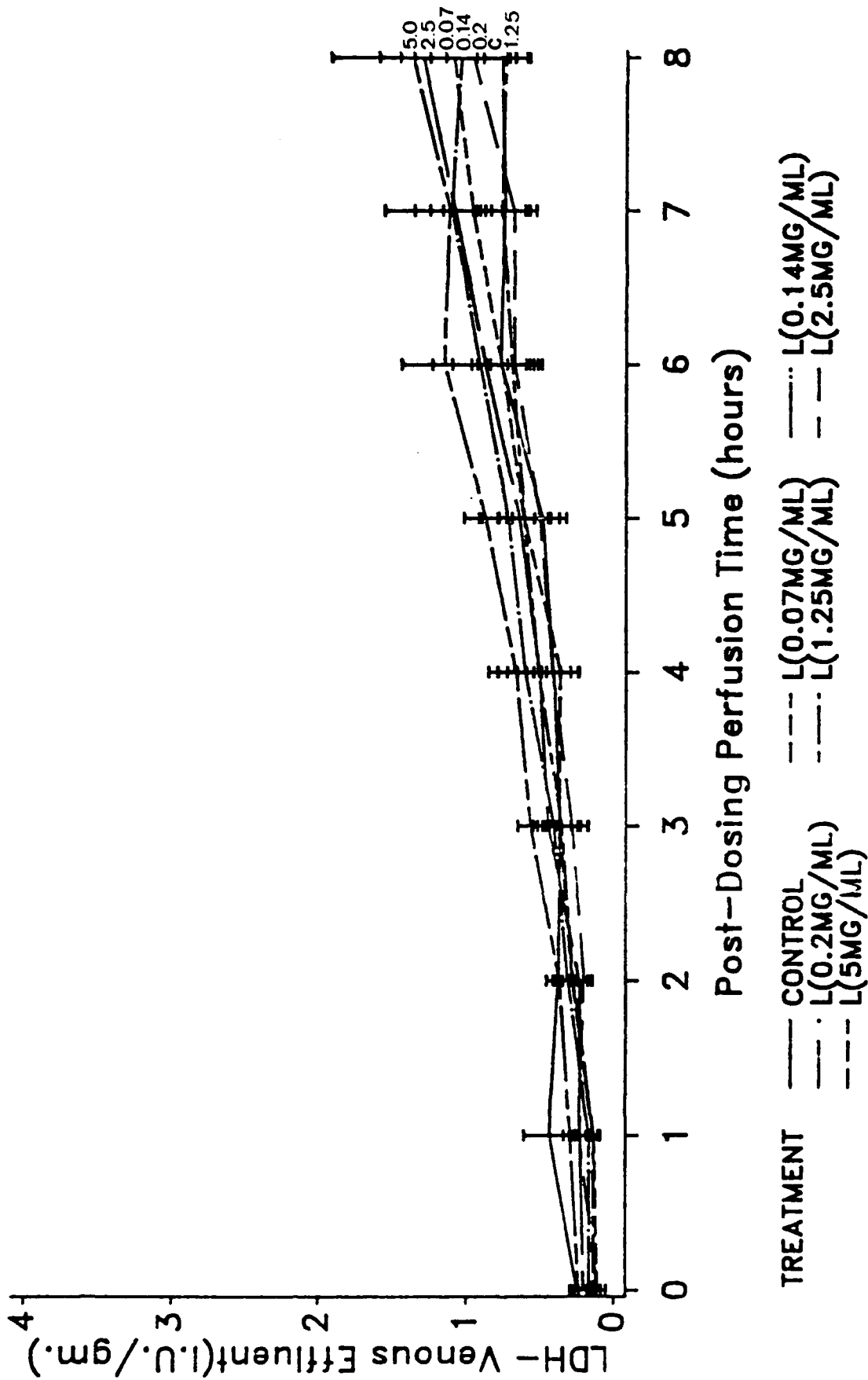
FIGURE 29. Graph illustrating LDH release of all concentrations of XL compared to control.

74
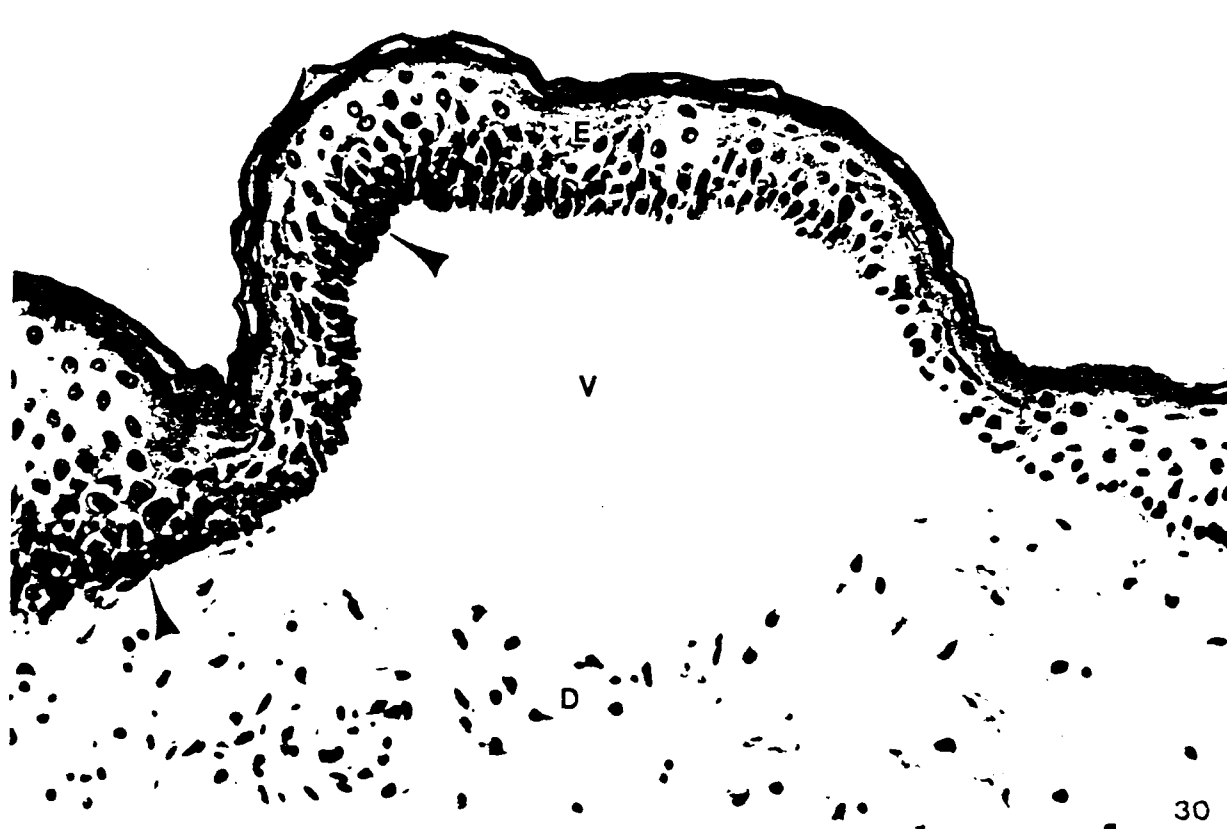
FIGURE 30. IPPSF treated with 5.0 mg/ml of XL. Note the large subepidermal vesicle (V),

separation of the epidermis (E) from the dermis (D). Pyknotic cells (arrows)

were noted. (X360)

FIGURE 31. Intercellular edema (I) was present in the stratum basale and spinosum layers of 2.5 mg/ml of XL. (X730)
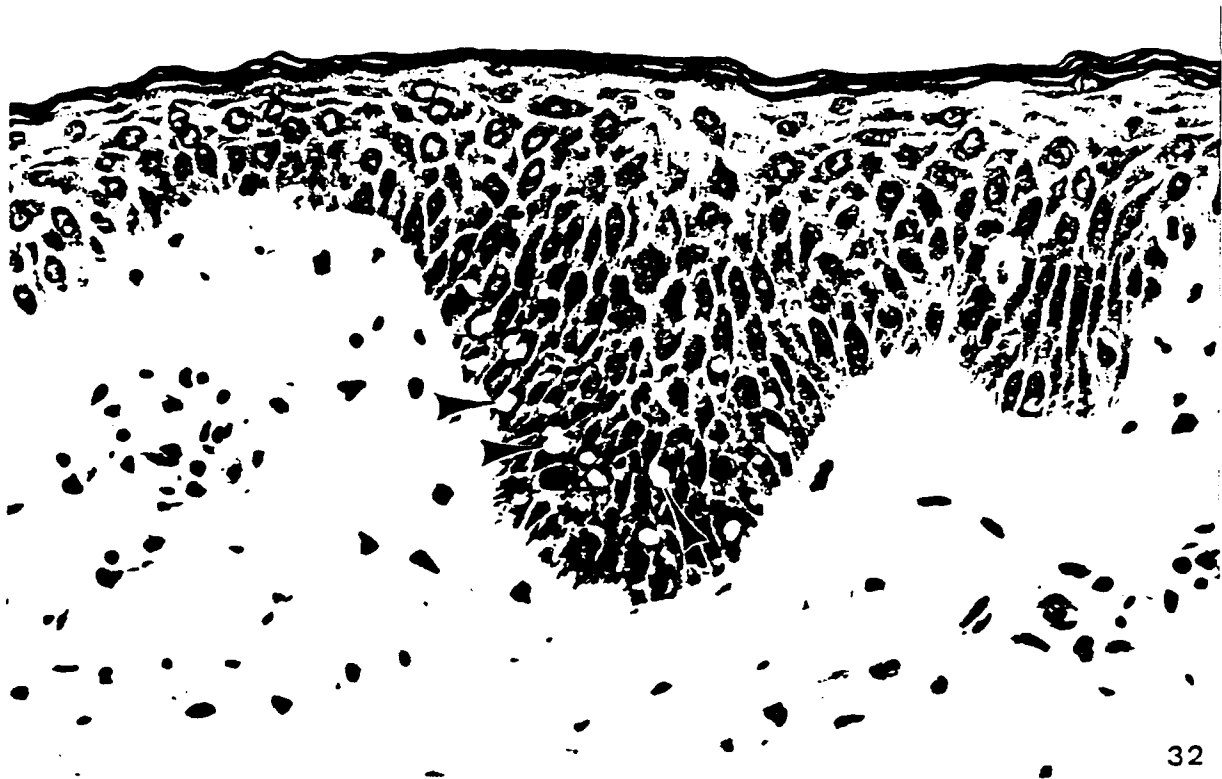
FIGURE 32. Intracellular edema (arrows) was present in the stratum basale and spinosum

layers of 1.25 mg/ml of XL. (X440)
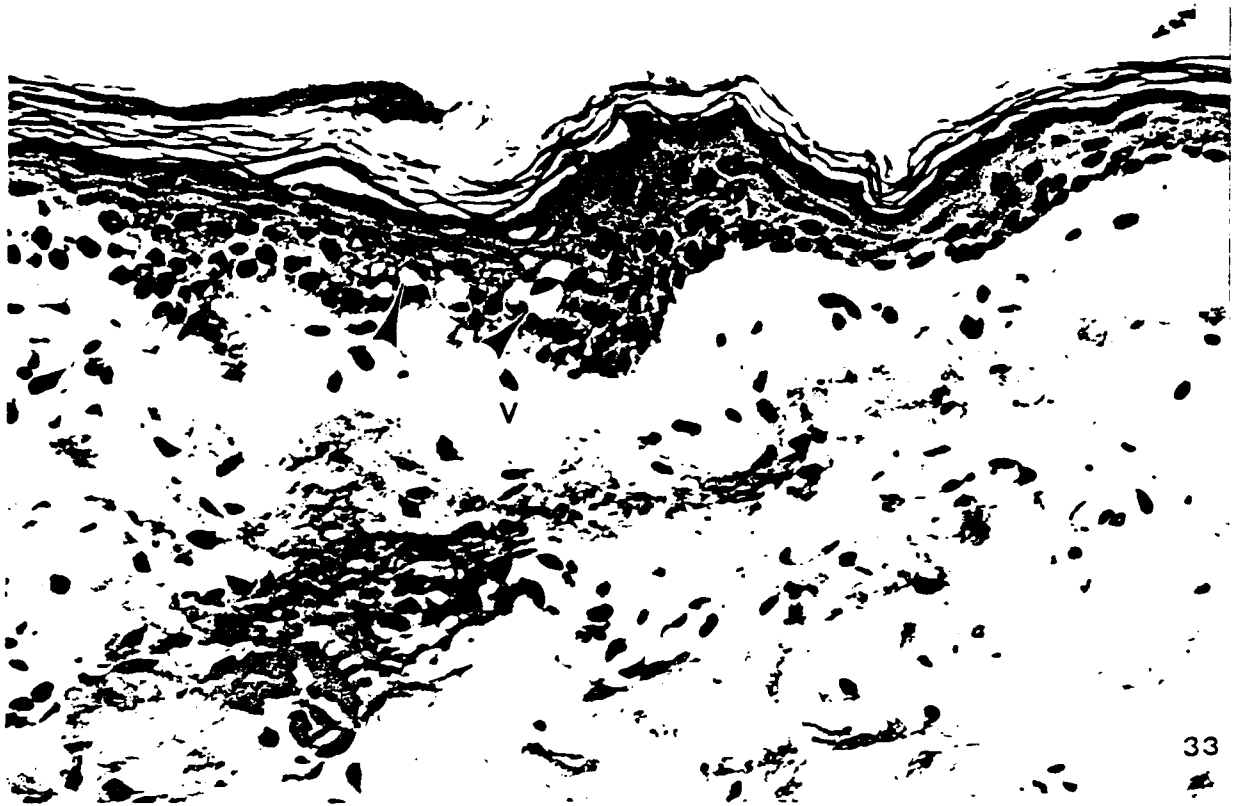
FIGURE 33. Microvesicles (V) seen with 0.2 mg/ml of XL and hydropic degeneration of the epidermis (arrows). (X440)
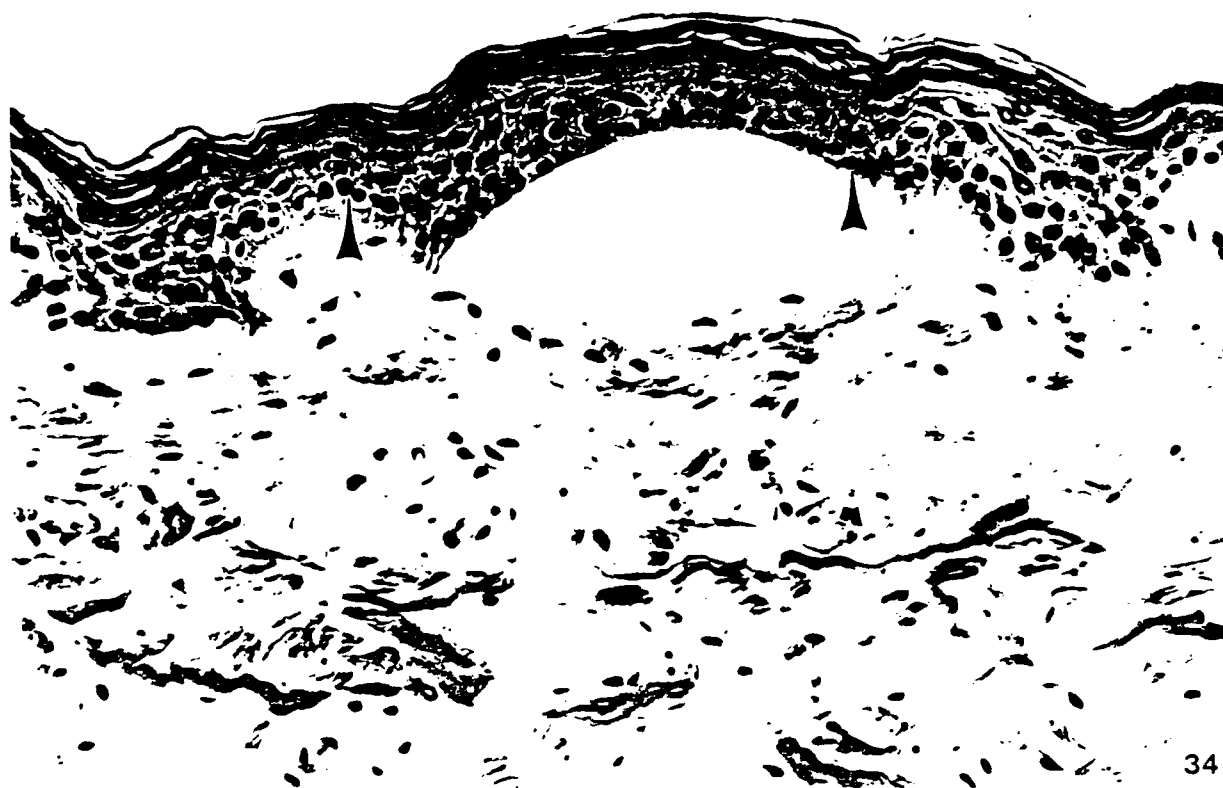
FIGURE 34. This 0.14 mg/ml of XL developed well-organized microvesicles and pyknotic

stratum basale cells (arrows). (X360)

FIGURE 35. Treatment with 0.07 mg/ml of XL resulted in microvesicle formation (V). (X360)

FIGURE 36. TEM of a 5.0 mg/ml of XL flap. Note the separation of the epidermal-dermal junction (arrows). (X6,600)

FIGURE 37. Glycogen accumulation (G) and intracellular lamellar membranes (L) were noted in some stratum basale cells after treatment with 5.0 mg/ml of XL. (X22,880)

FIGURE 38. XL treatment with 2.5 mg/ml resulted in the formation of intracellular clefts (small arrow), chromatin clumping around nucleoli (large arrow), lipid (L), and mitochondrial swelling (M). (X9,680)

FIGURE 39. Electron micrograph demonstrating focal disruption of the basal cells from the basal lamina (arrow) and blebbing of the nuclear envelope (B) at 2.5 mg/ml of XL. (X6,600)
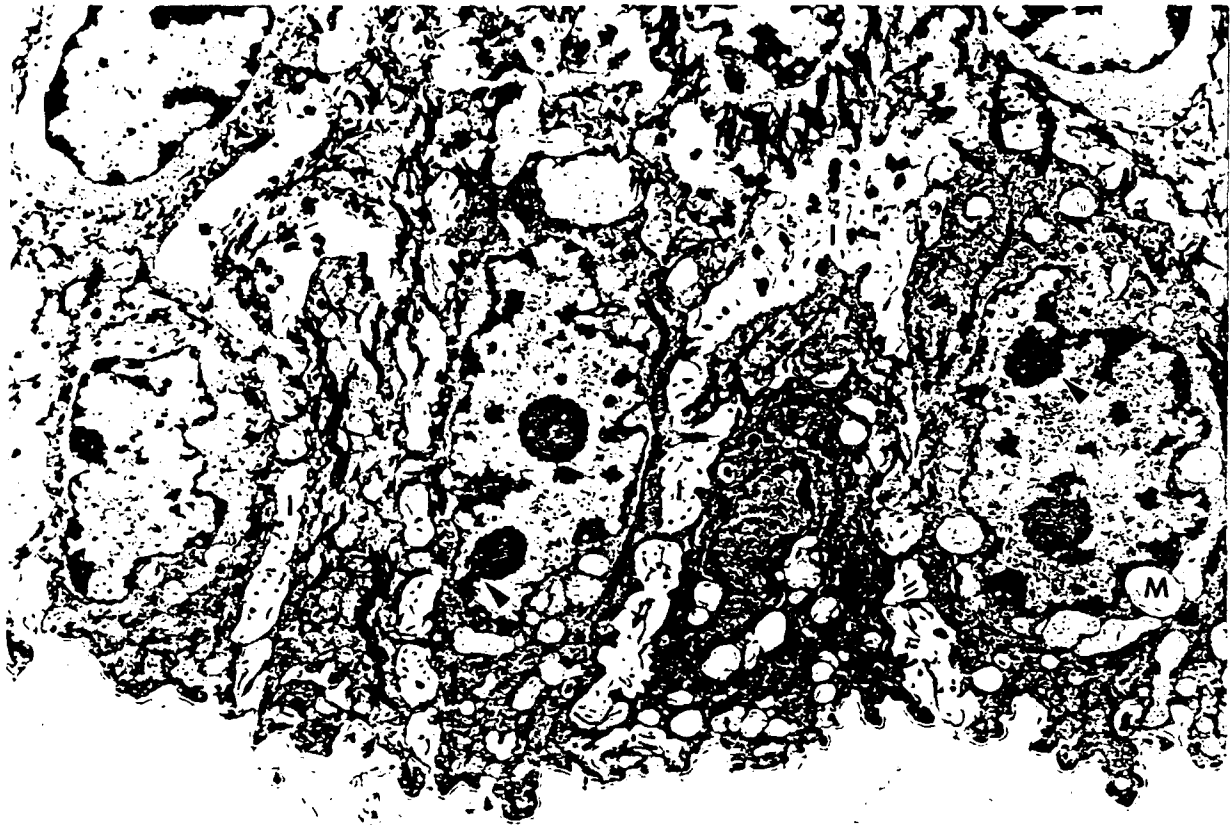
FIGURE 40. The 1.25 mg/ml of XL dose resulted in intercellular edema (I), nucleolar margination (arrows), and swollen mitochondria (M). (X6,600)
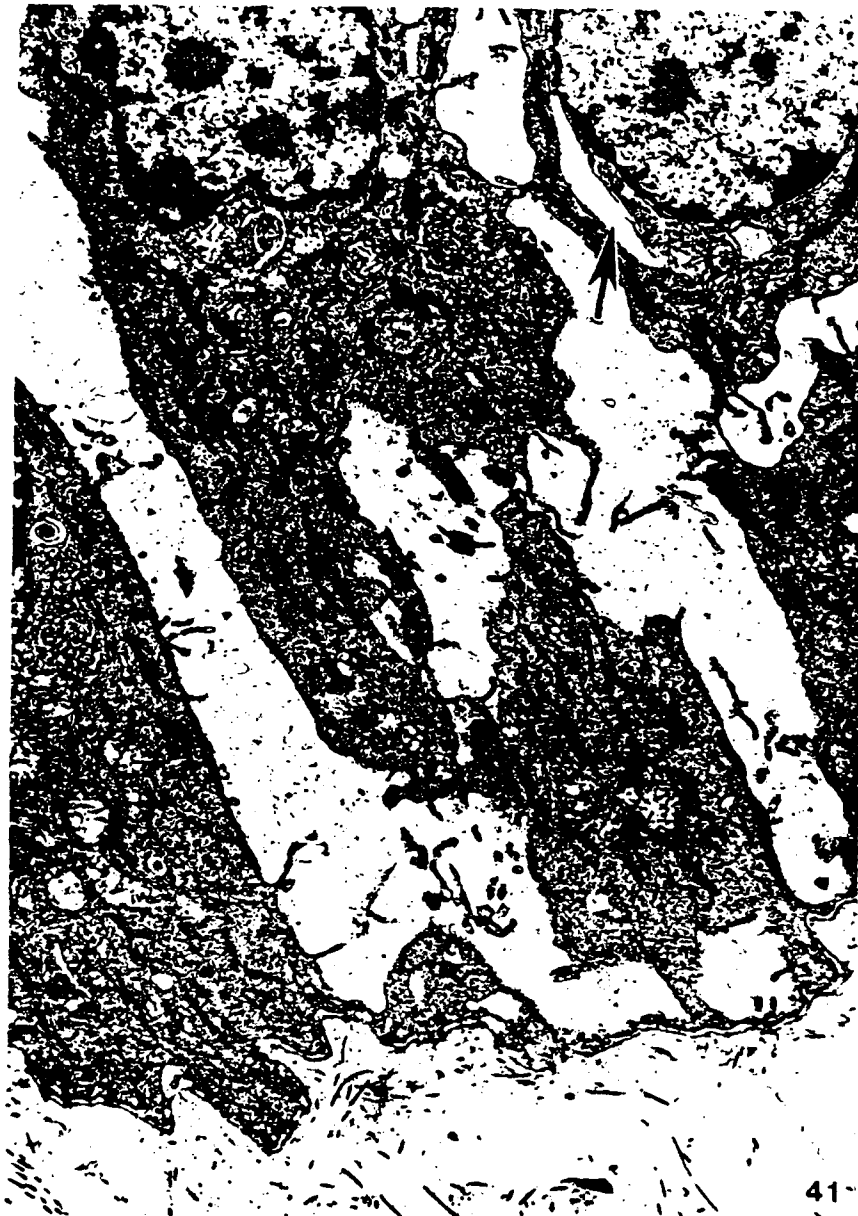
FIGURE 41. Focal disruption of basal cells and intracellular clefts (arrow) were noted in the 1.25 mg/ml of XL. (X9,680)
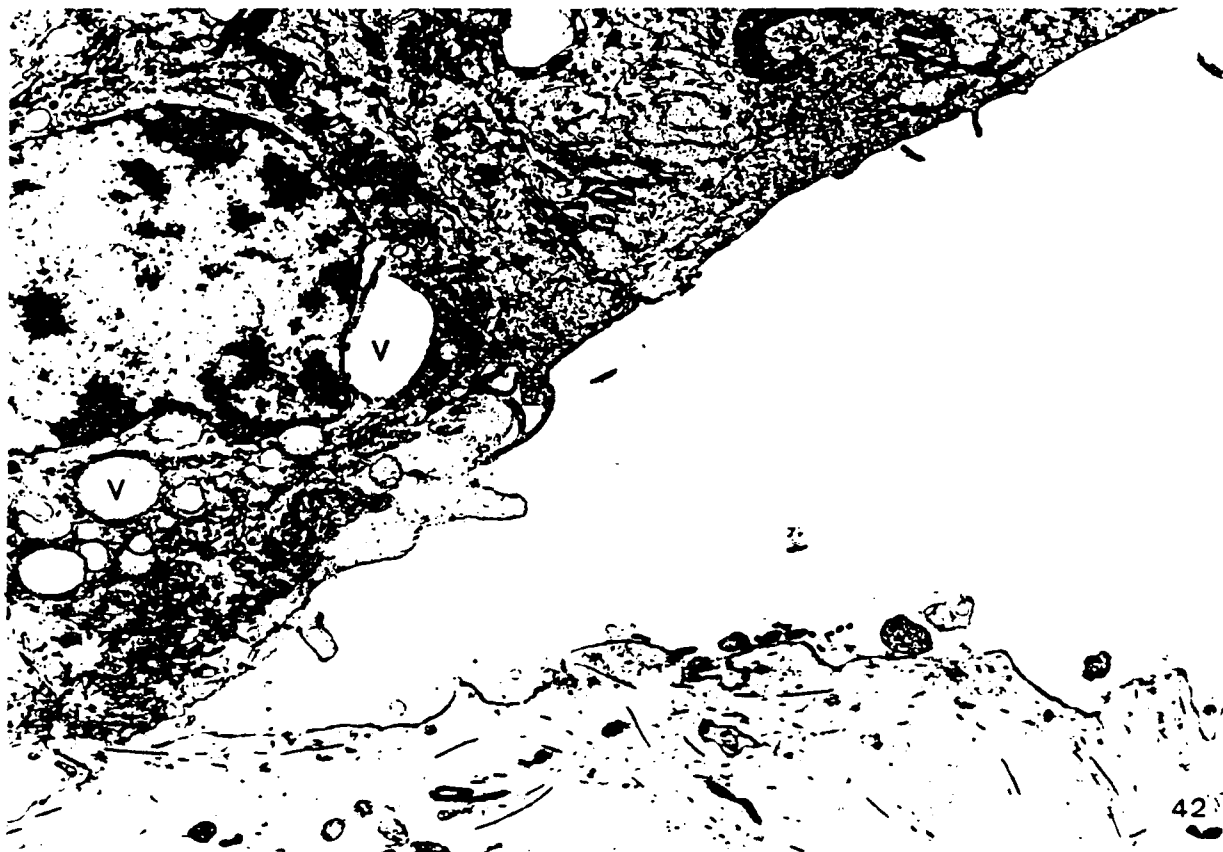
FIGURE 42. The 0.2 mg/ml of XL dose resulted in separation of the epidermal-dermal

junction and large intracellular vacuoles (V). (X9,680)

FIGURE 43. TEM of a 0.2 mg/ml of XL flap showing swollen

mitochondria (M) and lamellar remnants of basal

cell membranes (L). (X9,680)

FIGURE 44. Intercellular edema (I) was prominent in the 0.14 mg/ml of XL, along with

intracellular clefts (arrow). (X3,520)
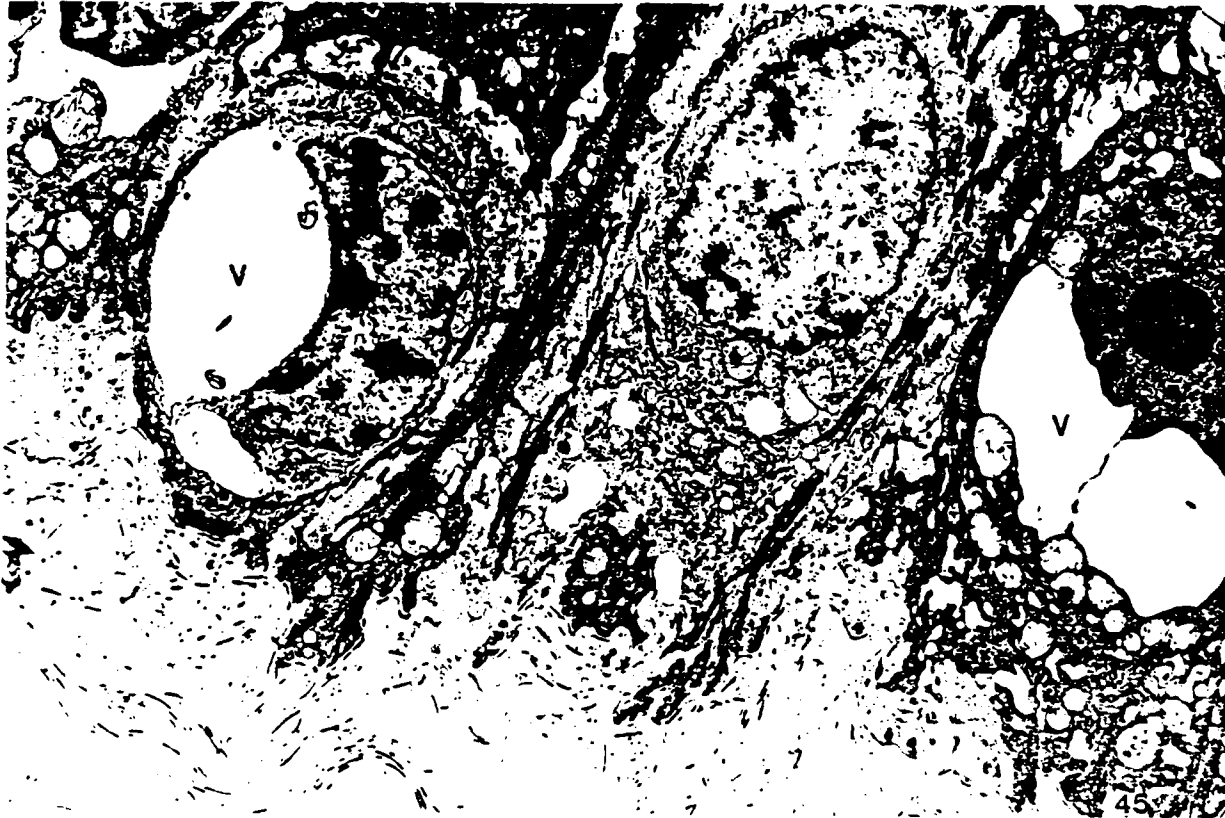
FIGURE 45. Paranuclear vacuoles (V) were noted in some of the basal cells treated with 0.14 mg/ml of XL. (X6,600)

FIGURE 46. The lowest concentration (0.07 mg/ml XL) caused focal degeneration of basal cells, nucleolar chromatin clumping (arrows), and blebbing of the nuclear envelope (B). (X9,680)
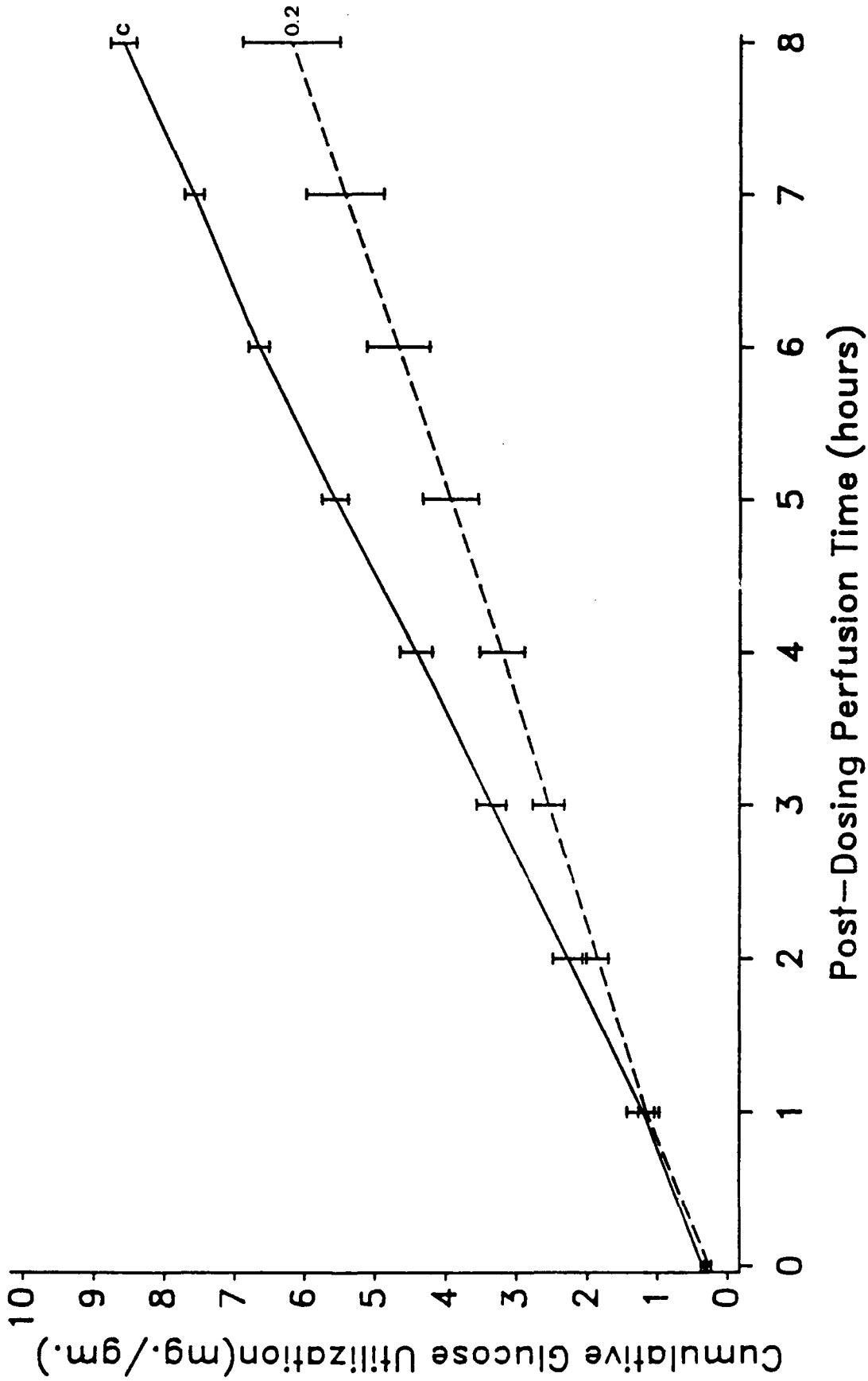
FIGURE 47. Graph Illustrating CGU of 0.2 mg/ml of XHD compared to control.

TREATMENT —— CONTROL - - - HD(0.2MG/ML)

Post−Dosing Perfusion Time (hours)

Cumulative Glucose Utilization(mg./gm.)

FIGURE 48. Graph Illustrating CGU of another group of 0.2 mg/ml of XHD compared to control.

Post-Dosing Perfusion Time (hours)

Cumulative Glucose Utilization(mg./gm.)

TREATMENT —— CONTROL —— HD(NEW 0.2MG/ML)

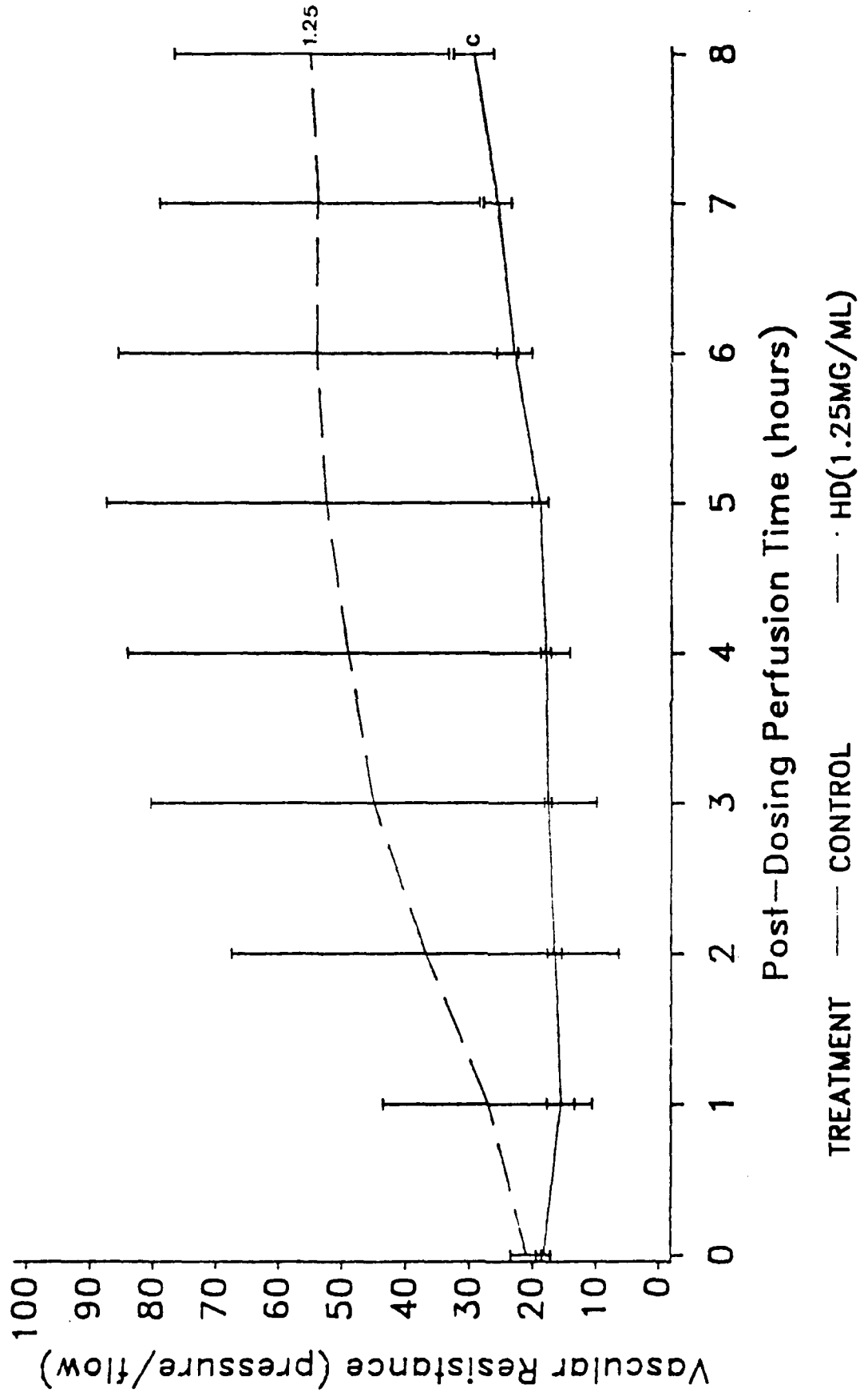FIGURE 49. Graph illustrating CGU of 0.5 mg/ml of XHD compared to control.

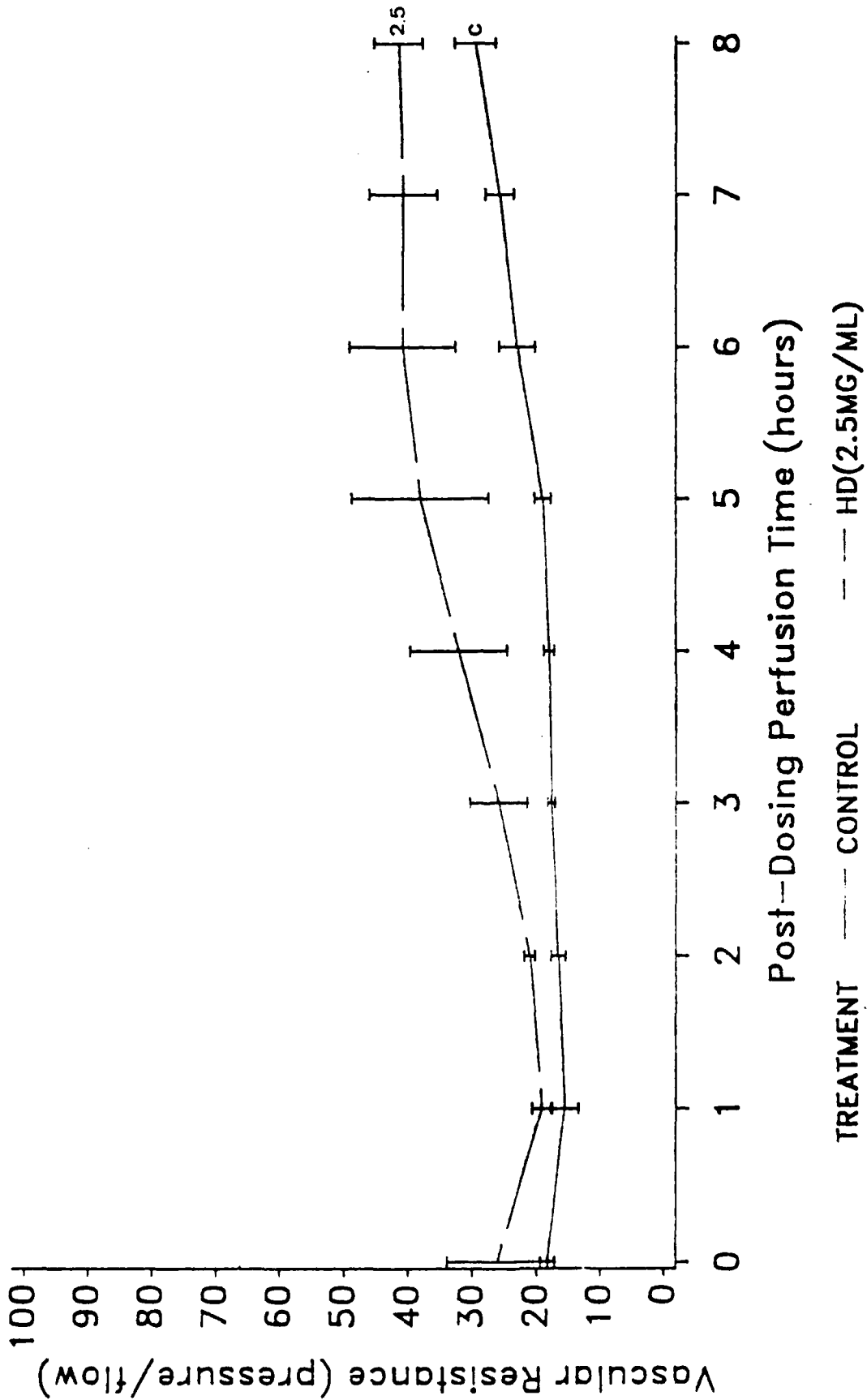FIGURE 50. Graph illustrating CGU of 1.25 mg/ml of XHD compared to control.
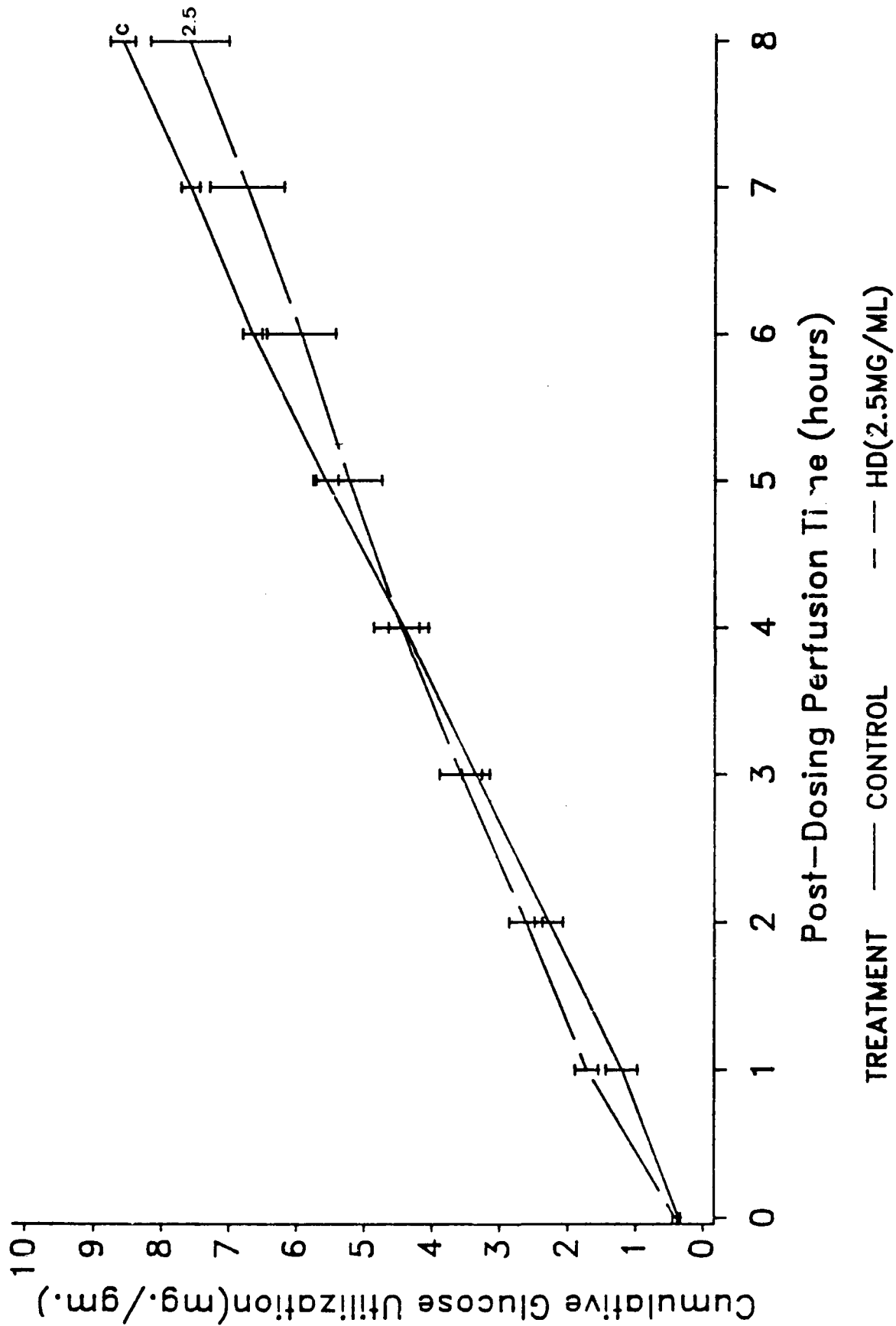
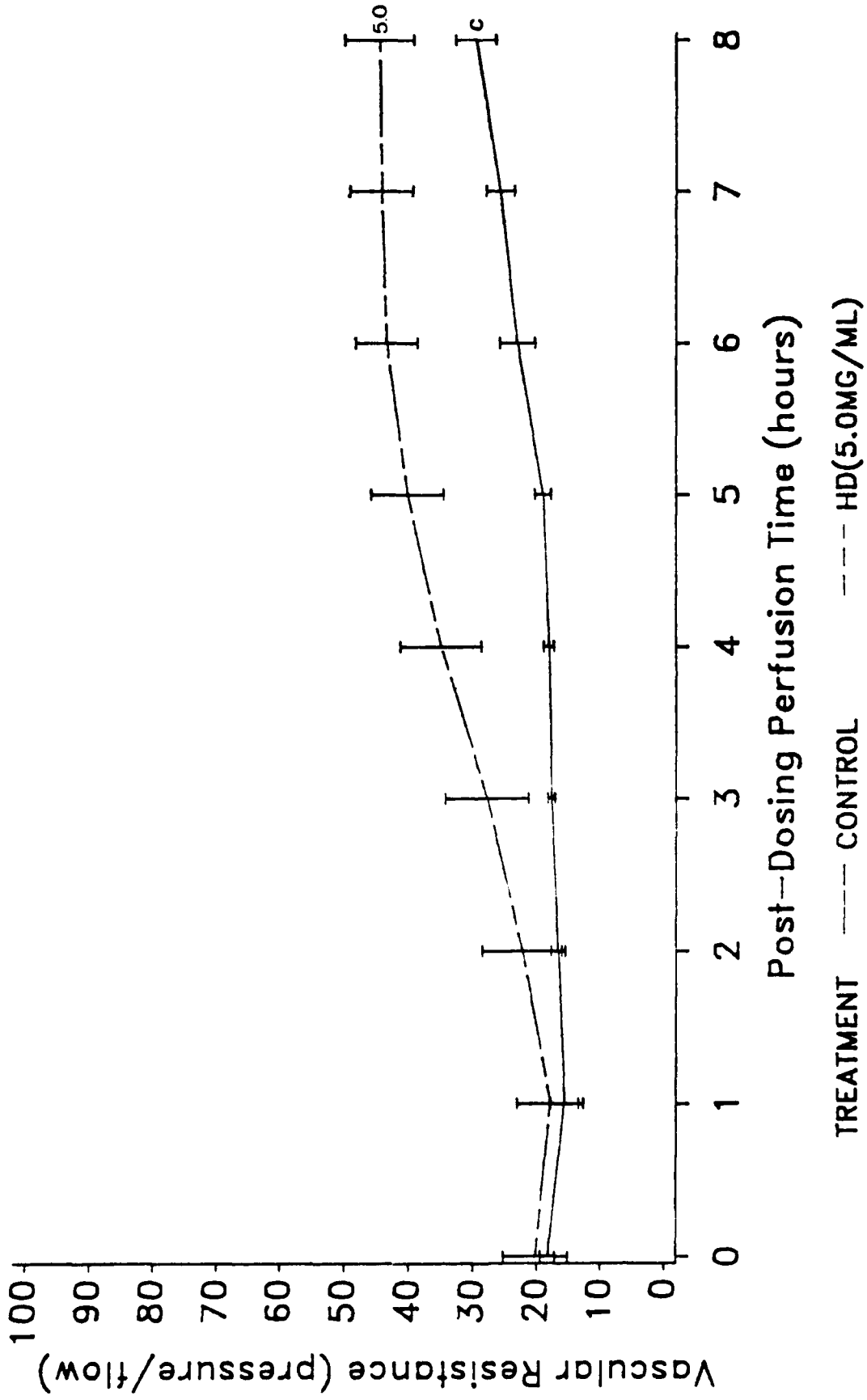FIGURE 51. Graph Illustrating CGU of 2.5 mg/ml of XHD compared to control.

TREATMENT   —— CONTROL   — — HD(2.5MG/ML)

96
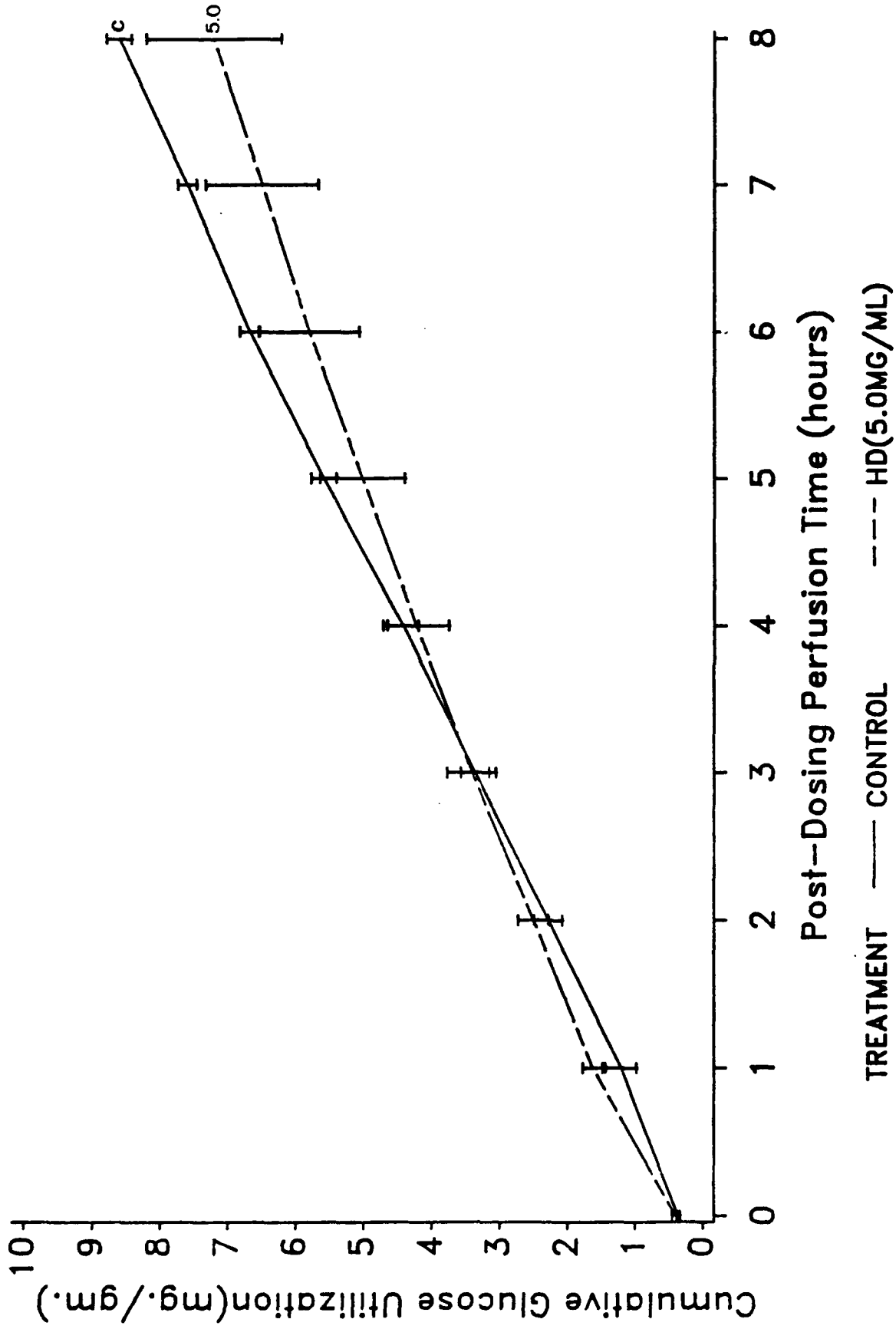
FIGURE 52. Graph illustrating CGU of 5.0 mg/ml of XHD compared to control.
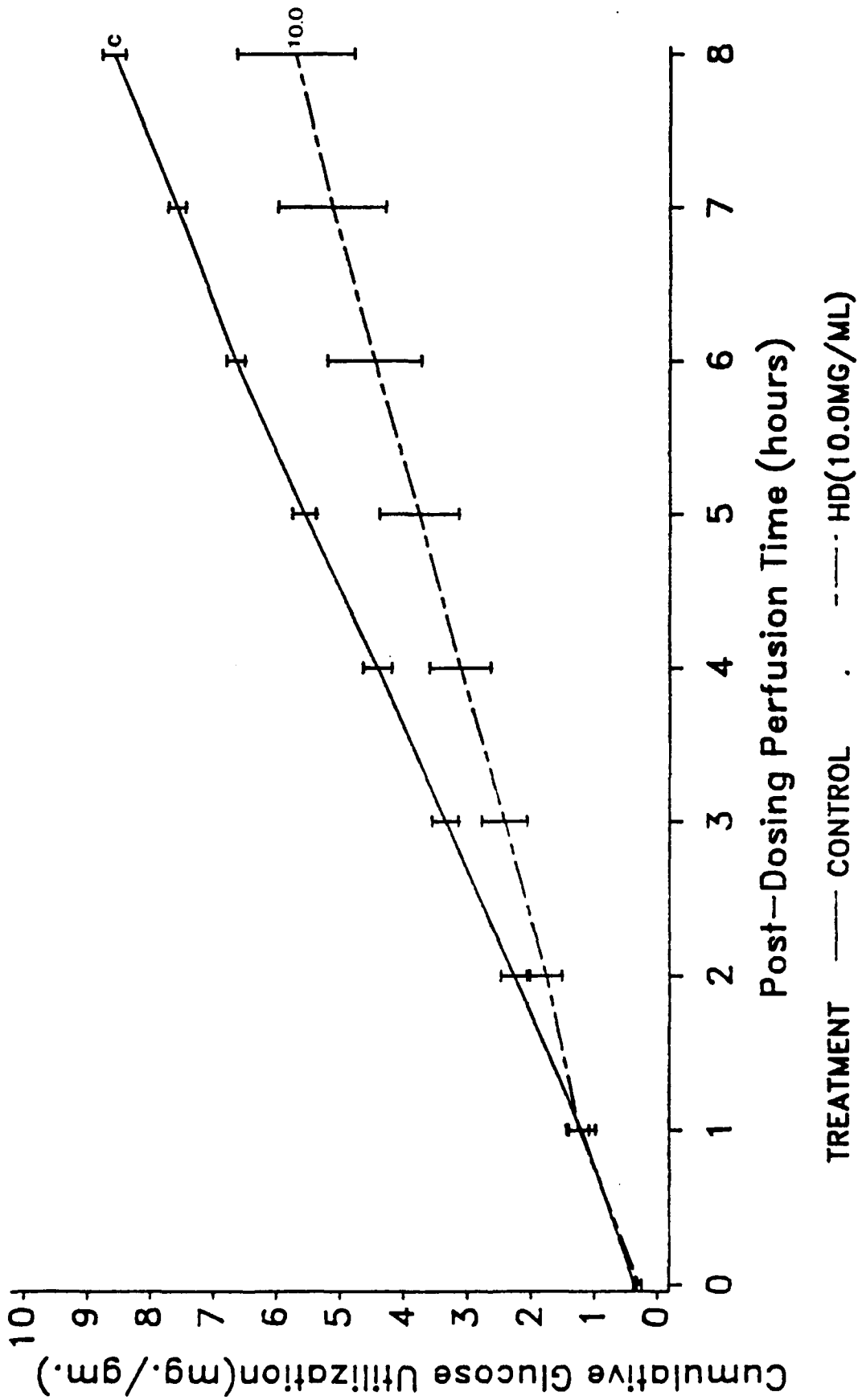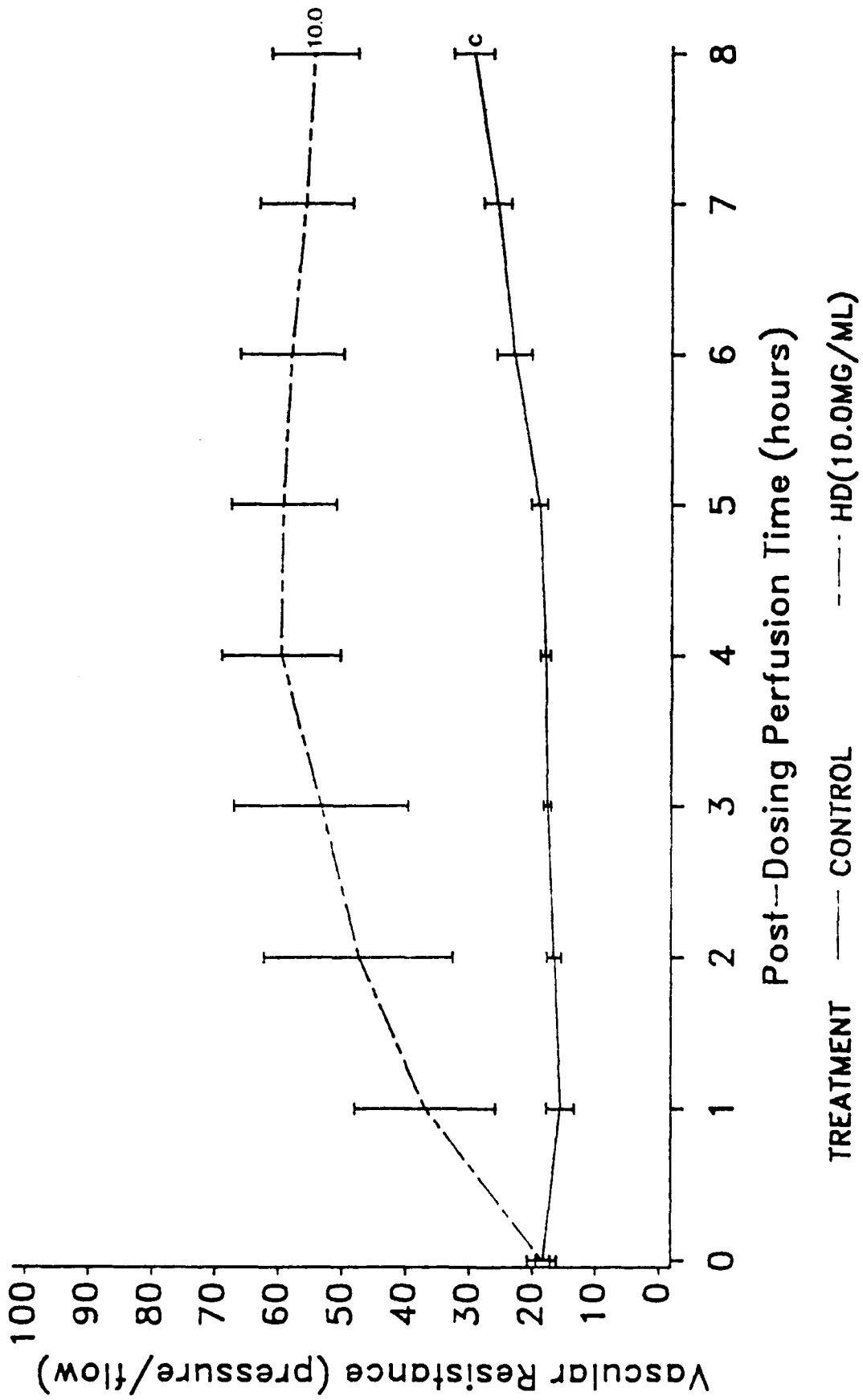
FIGURE 53. Graph illustrating CGU of 10.0 mg/ml of XHD compared to control.
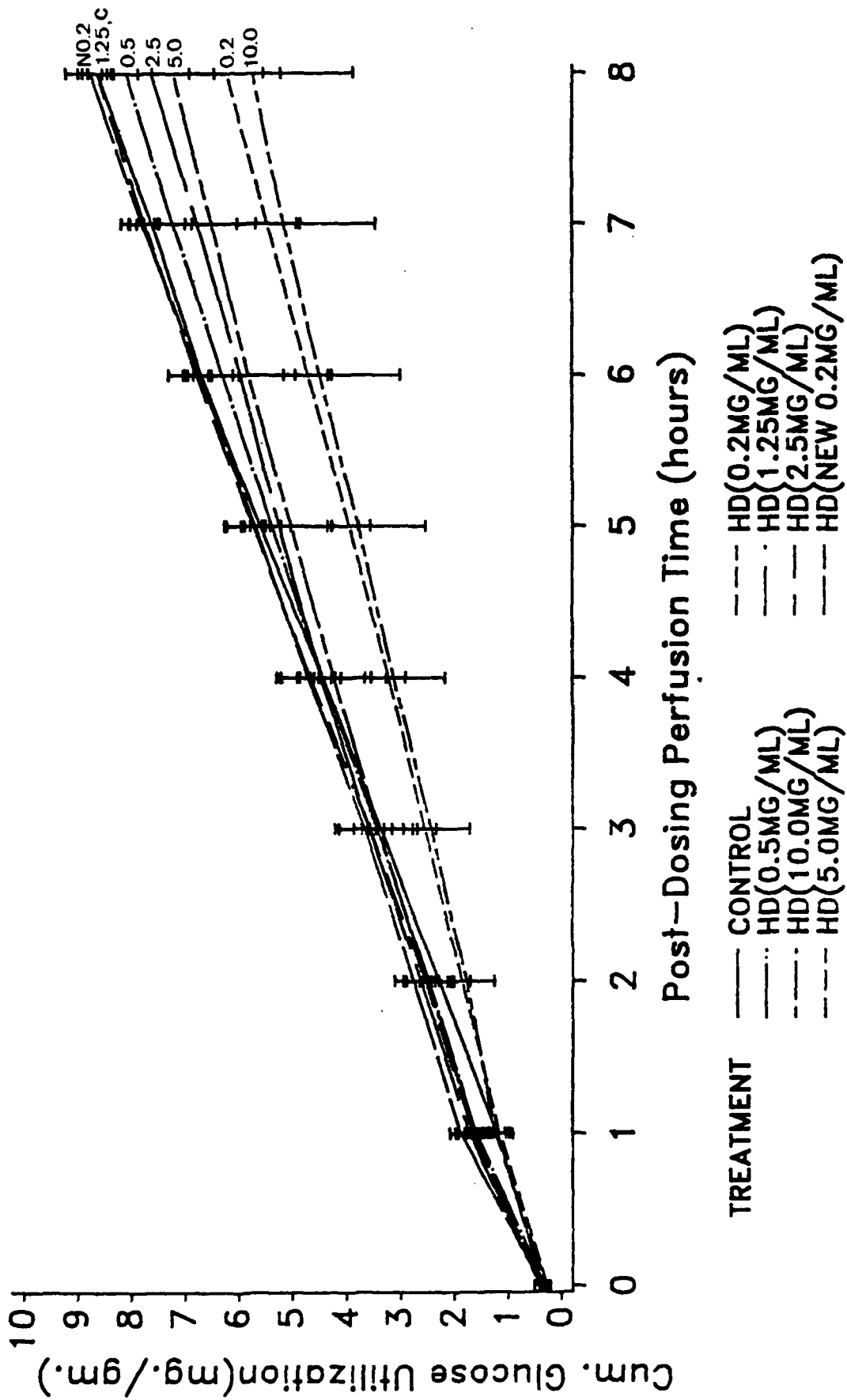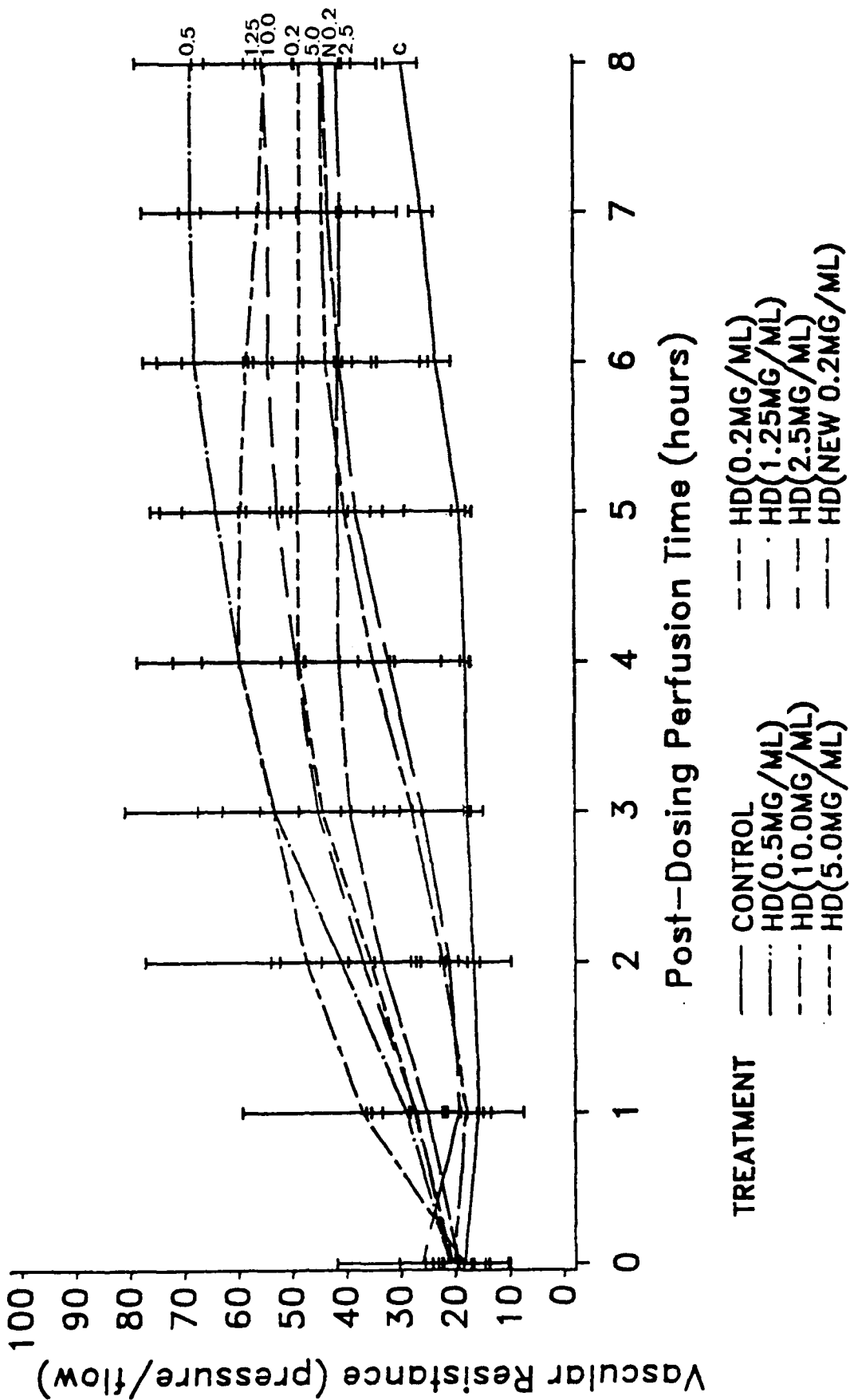
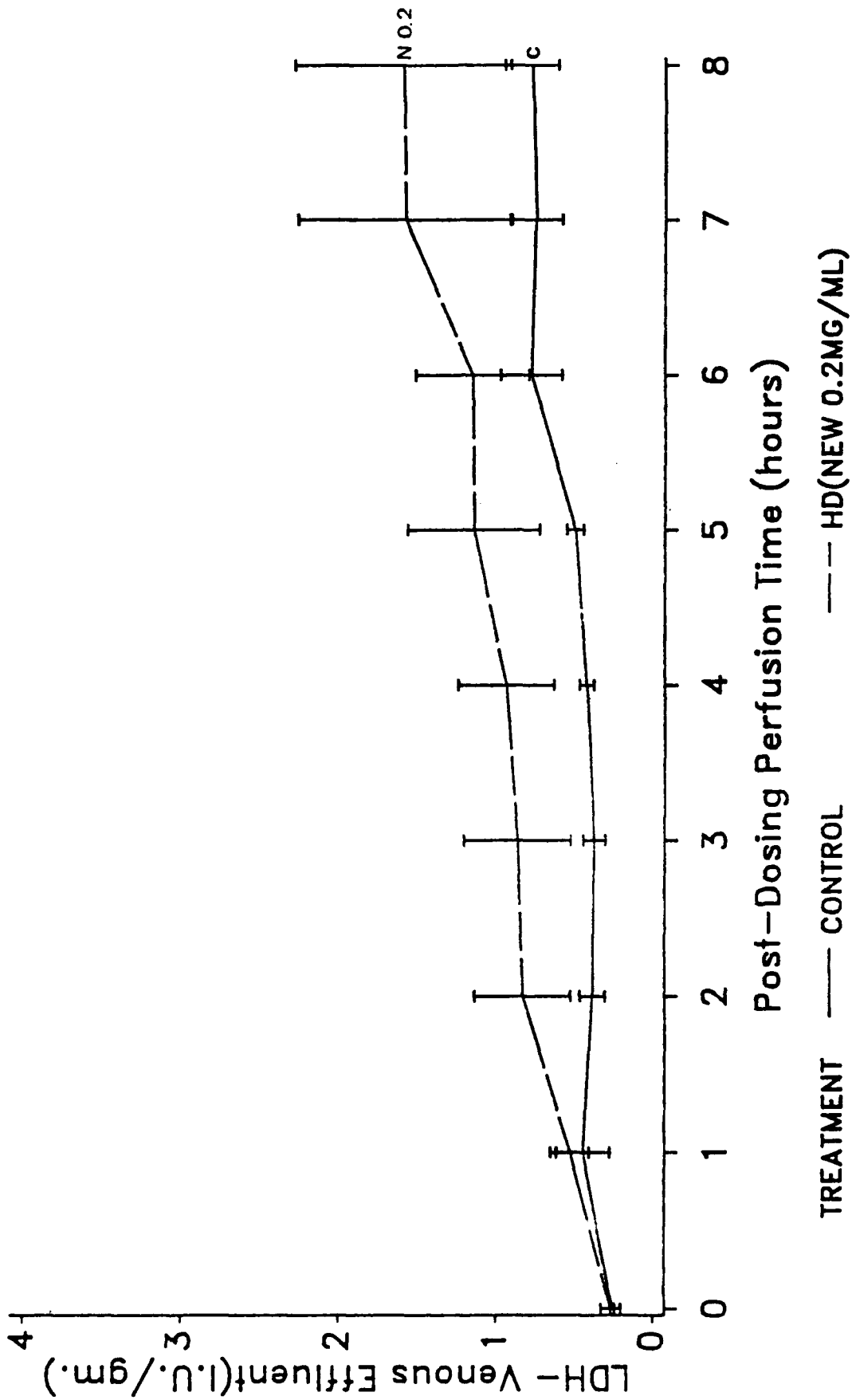FIGURE 54. Graph Illustrating CGU of all concentrations of XHD compared to control.
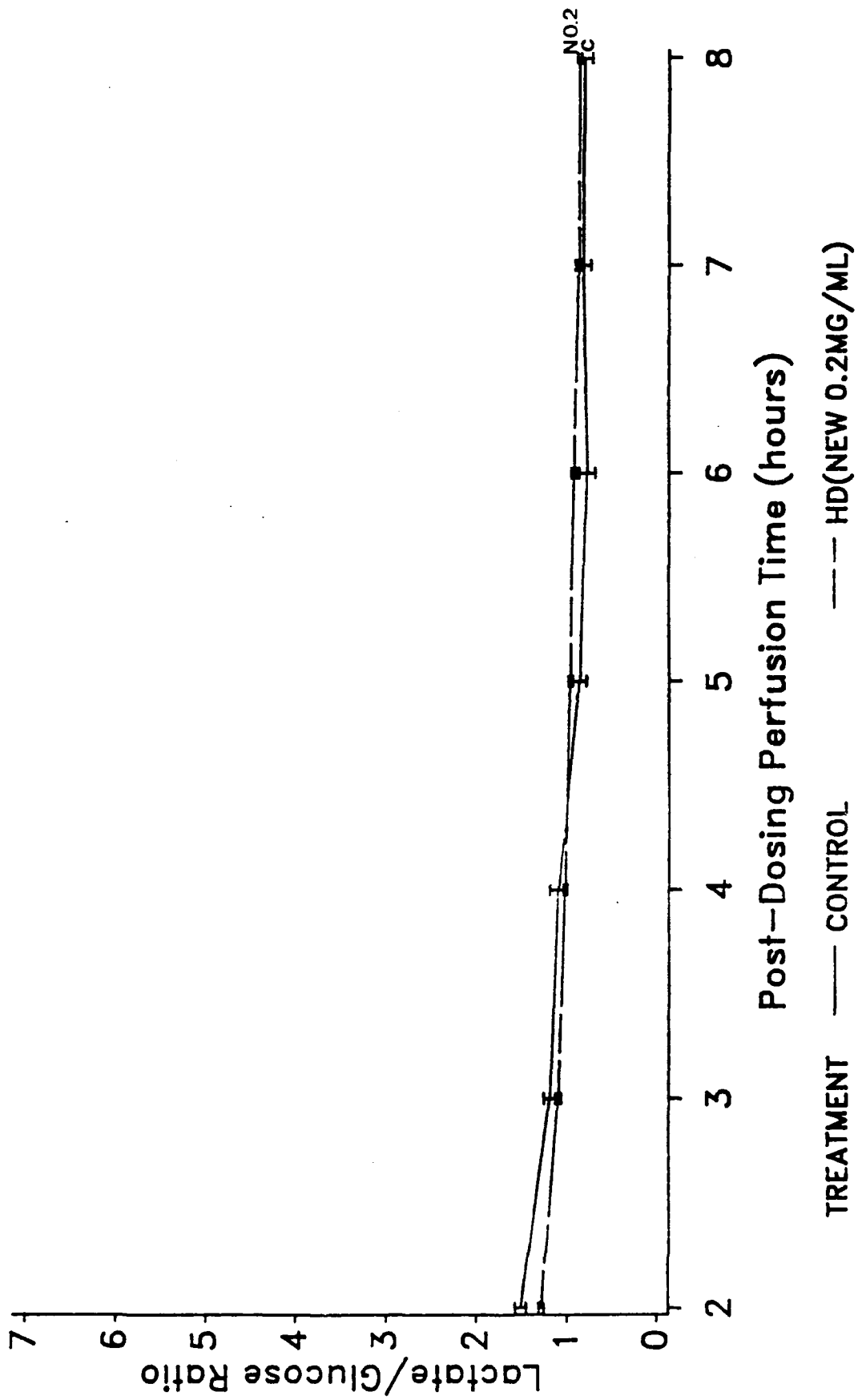
FIGURE 55. Graph illustrating L/GU of the new 0.2 mg/ml of XHD compared to control.
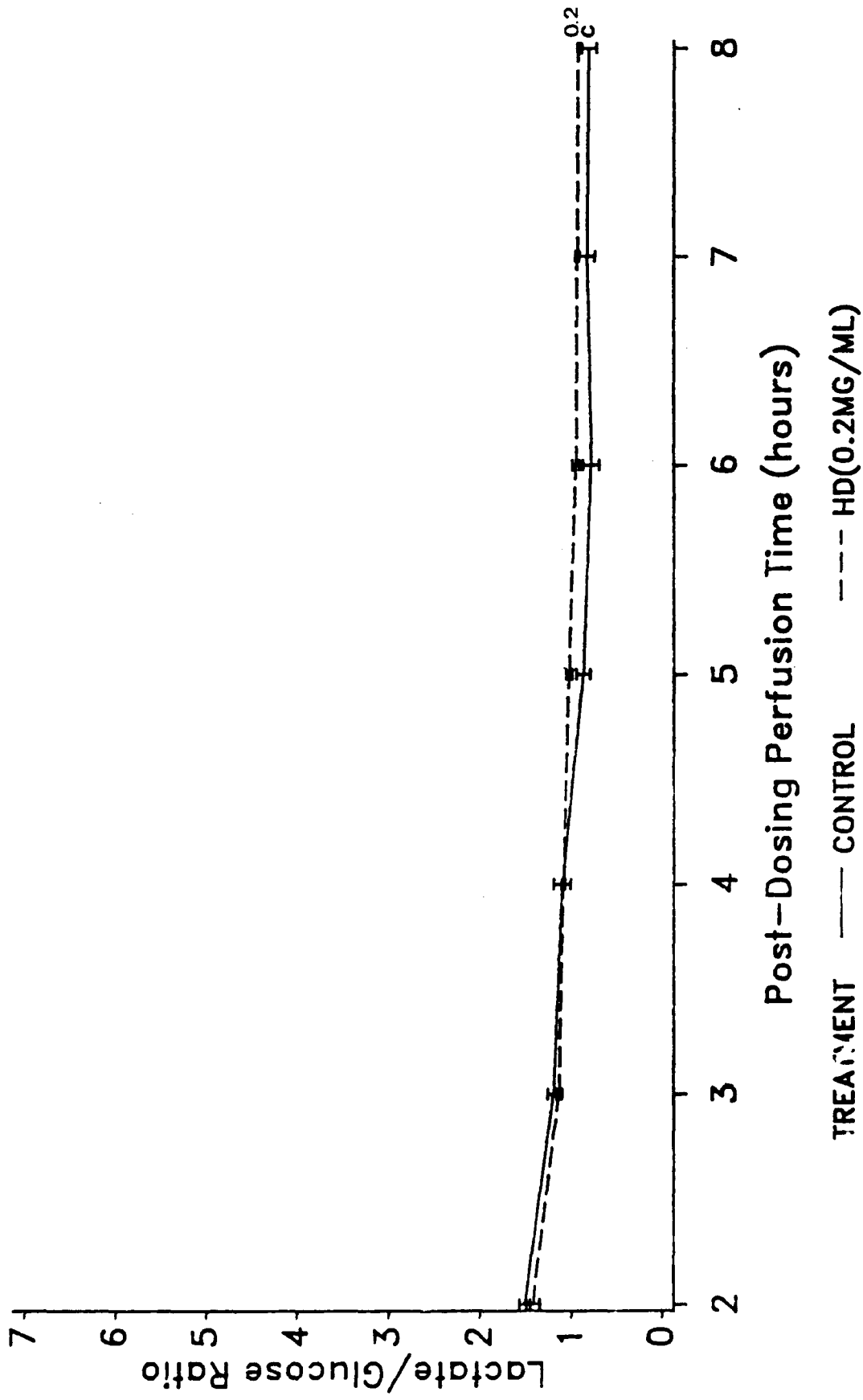
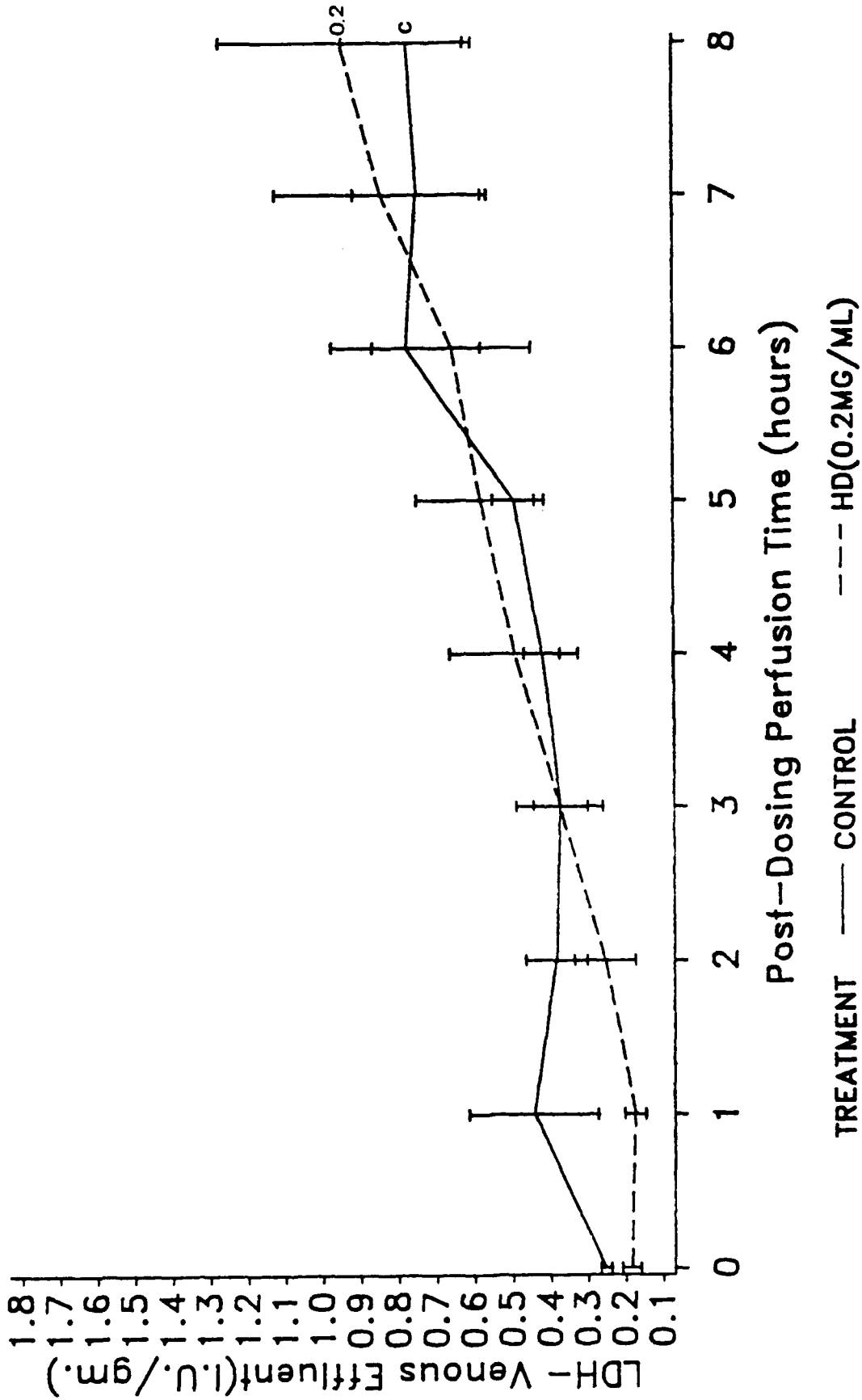FIGURE 56. Graph Illustrating L/GU of 0.2 mg/ml of XHD compared to control.

TREATMENT —— CONTROL —— HD(0.2MG/ML)

Post-Dosing Perfusion Time (hours)
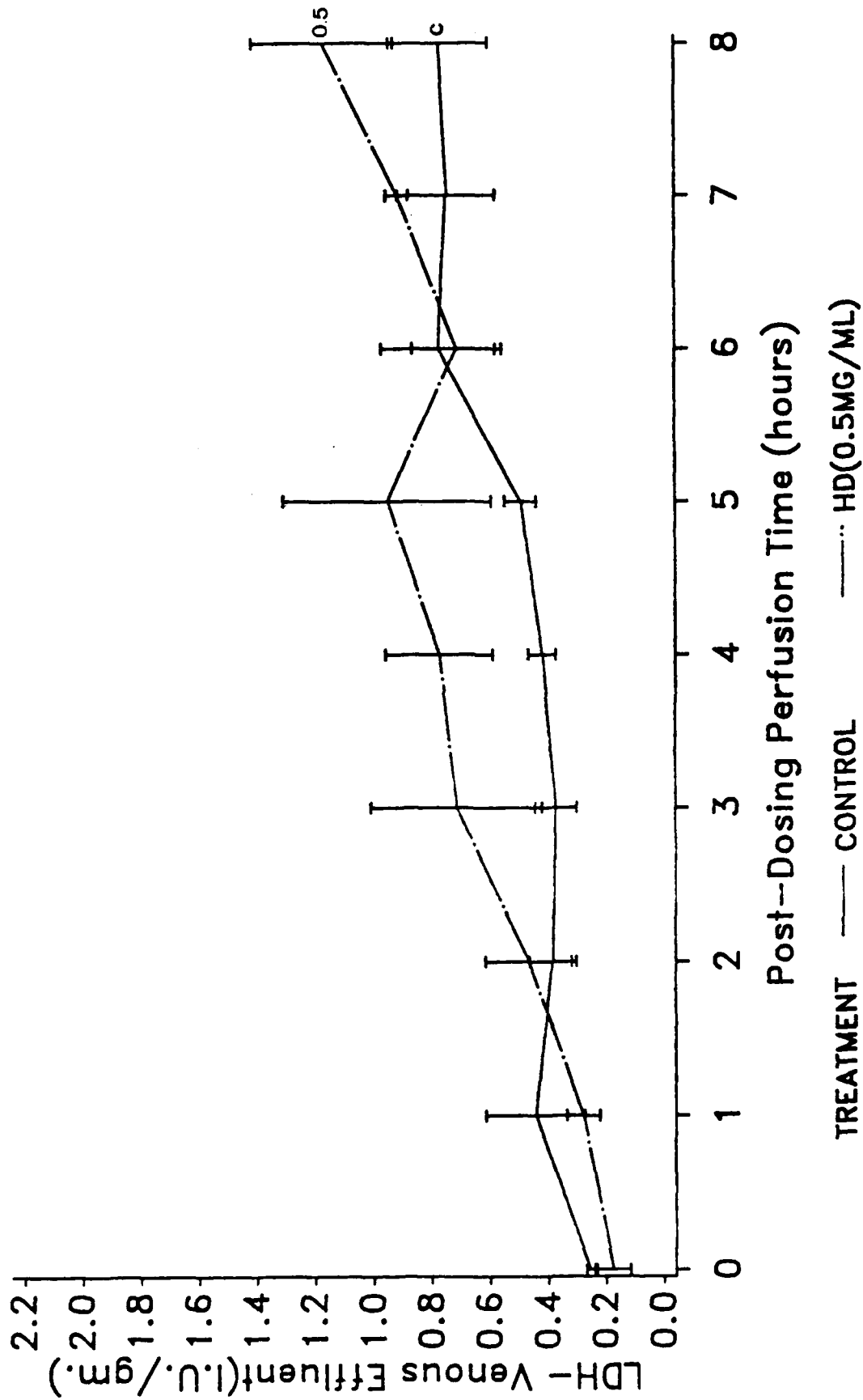
Lactate/Glucose Ratio
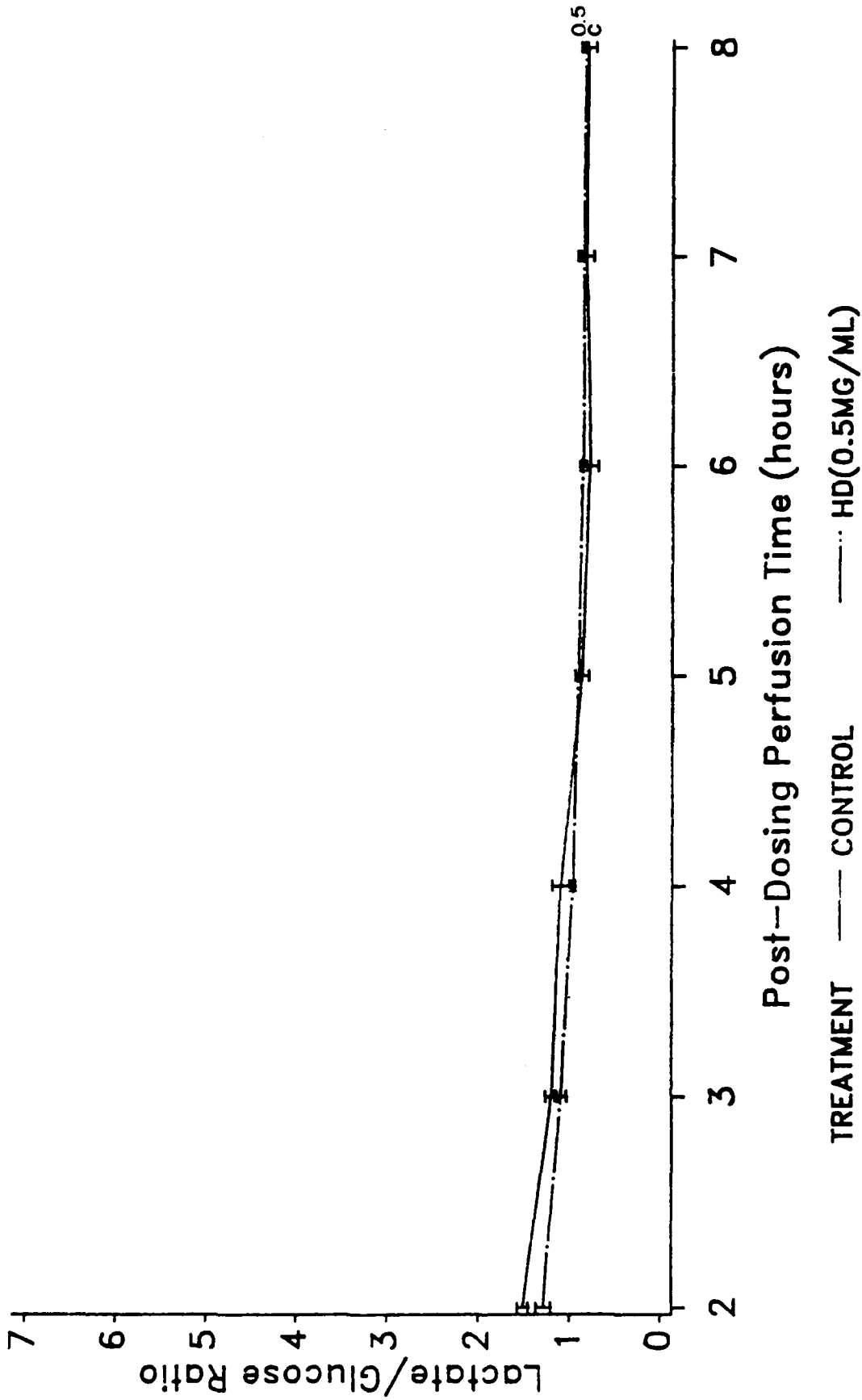
FIGURE 57. Graph Illustrating L/GU of 0.5 mg/ml of XHD compared to control.
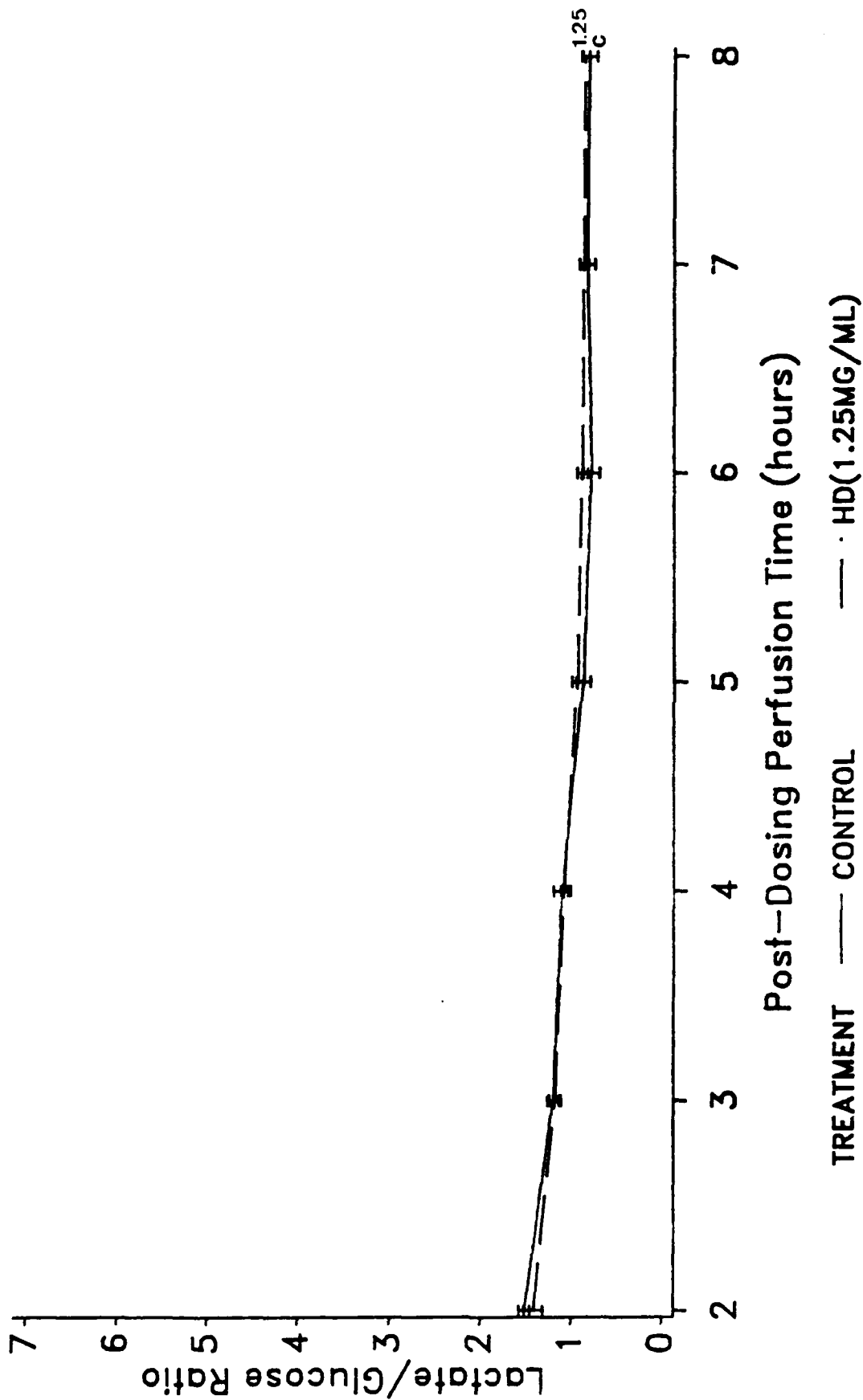
FIGURE 58. Graph Illustrating L/GU of 1.25 mg/ml of XHD compared to control.
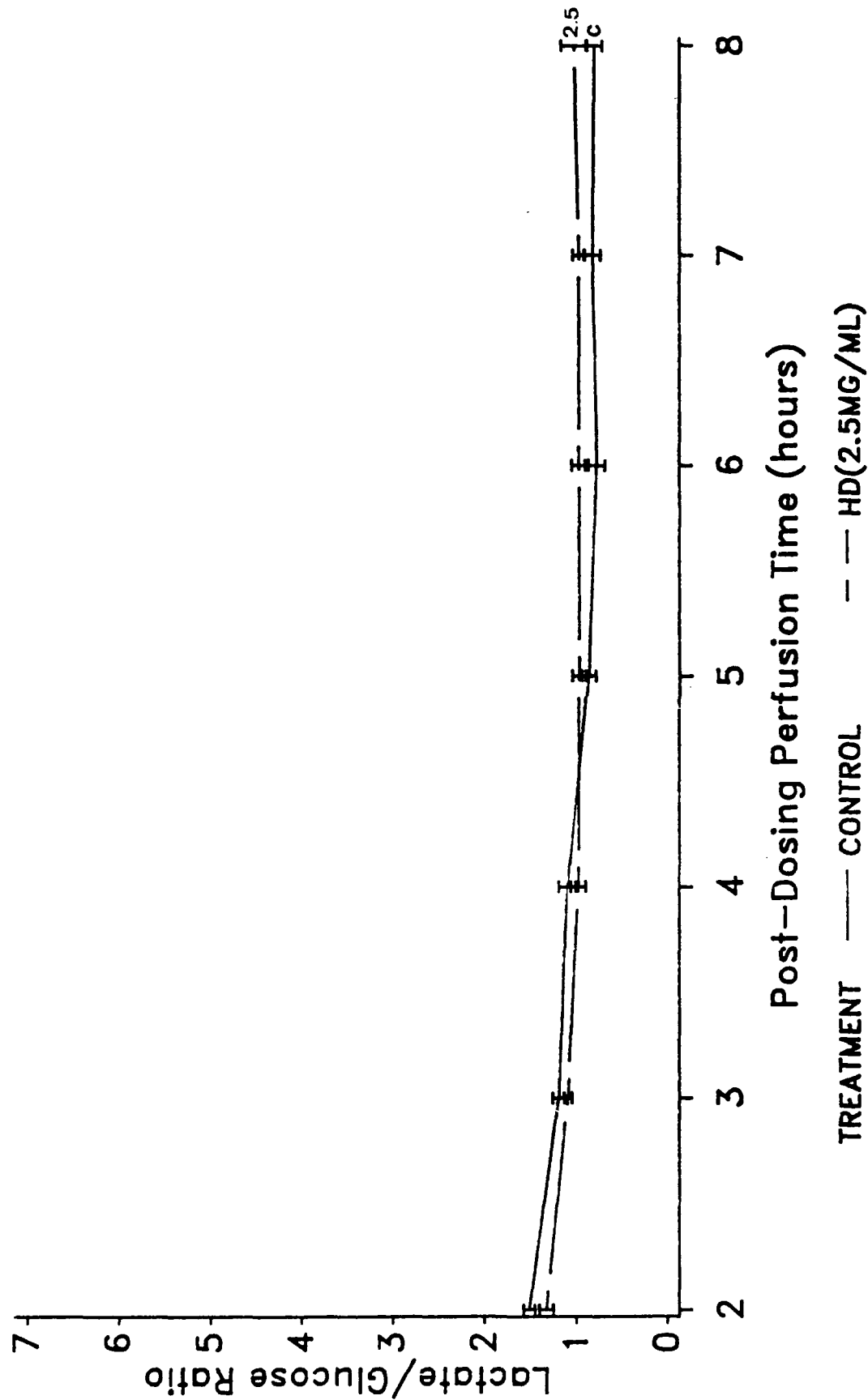
FIGURE 59. Graph illustrating L/GU of 2.5 mg/ml of XHD compared to control.

Lactate/Glucose Ratio

Post-Dosing Perfusion Time (hours)

TREATMENT ——— CONTROL — — — HD(2.5MG/ML)

104
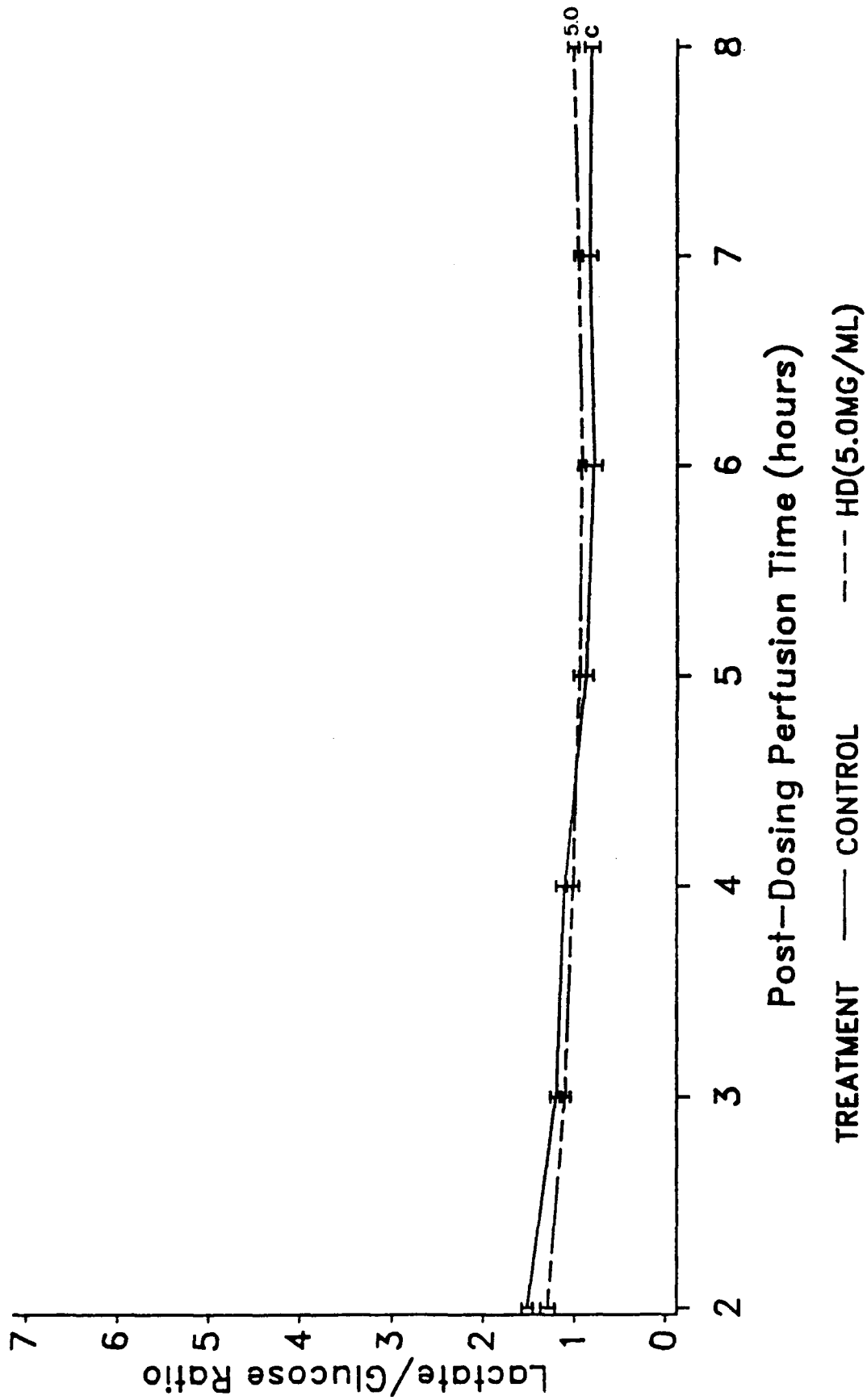
FIGURE 60. Graph Illustrating L/GU of 5.0 mg/ml of XHD compared to control.

Lactate/Glucose Ratio

Post-Dosing Perfusion Time (hours)

TREATMENT ——— CONTROL   - - - HD(5.0MG/ML)
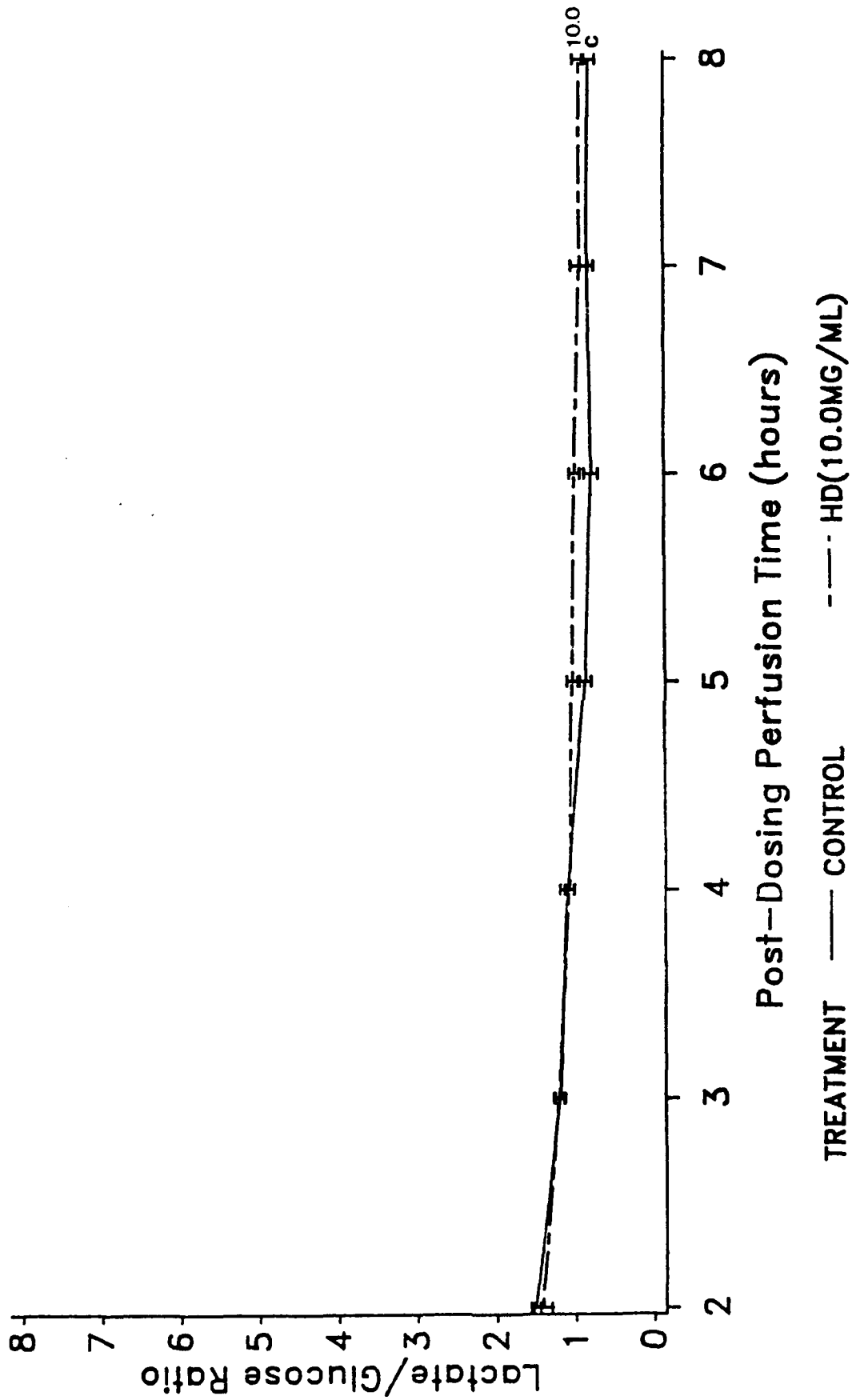
FIGURE 61. Graph Illustrating L/GU of 10.0 mg/ml of XHD compared to control.
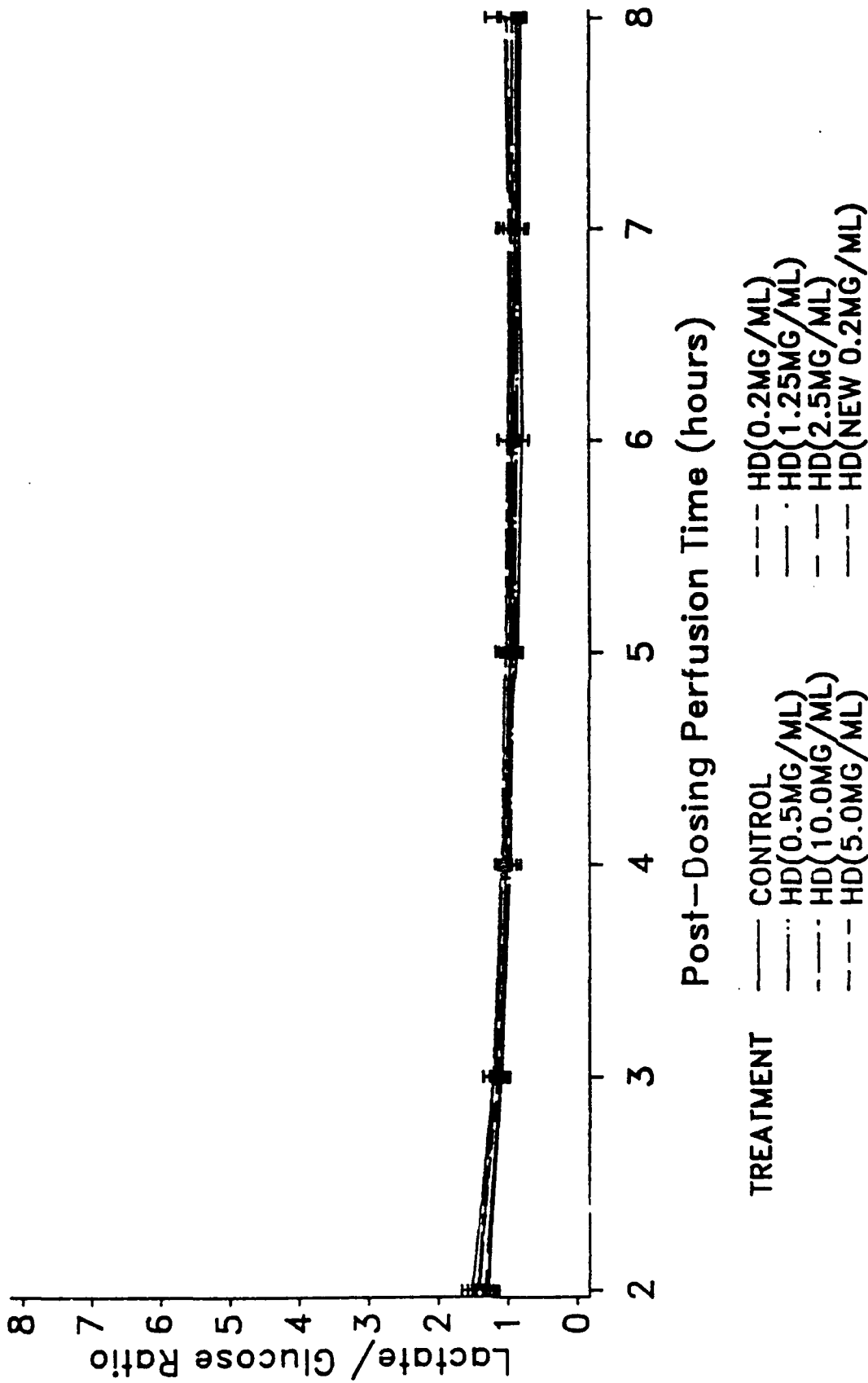
FIGURE 62. Graph Illustrating L/GU of all concentrations of XHD compared to control.
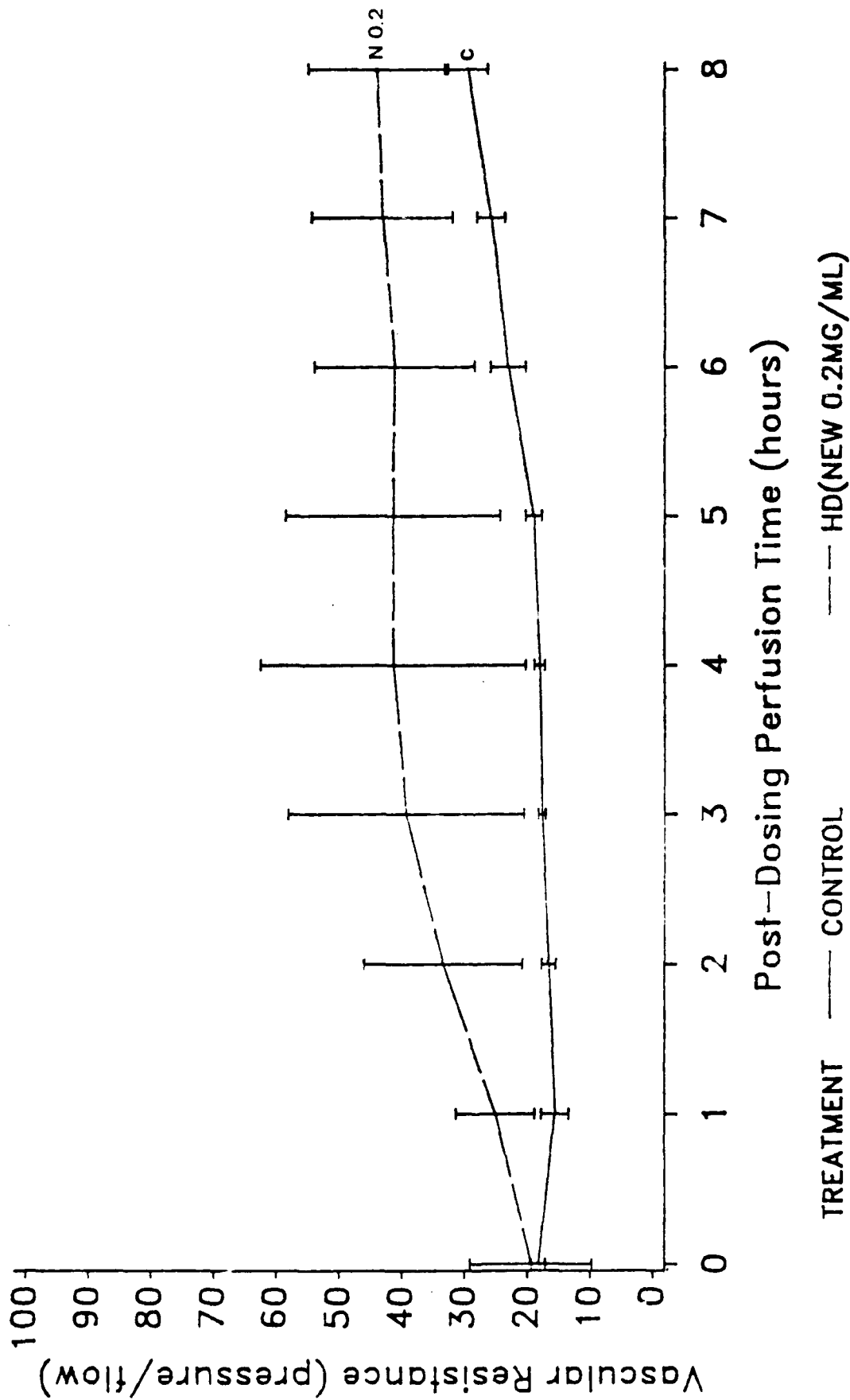
FIGURE 63. Graph illustrating VR of the new 0.2 mg/ml of XHD compared to control.
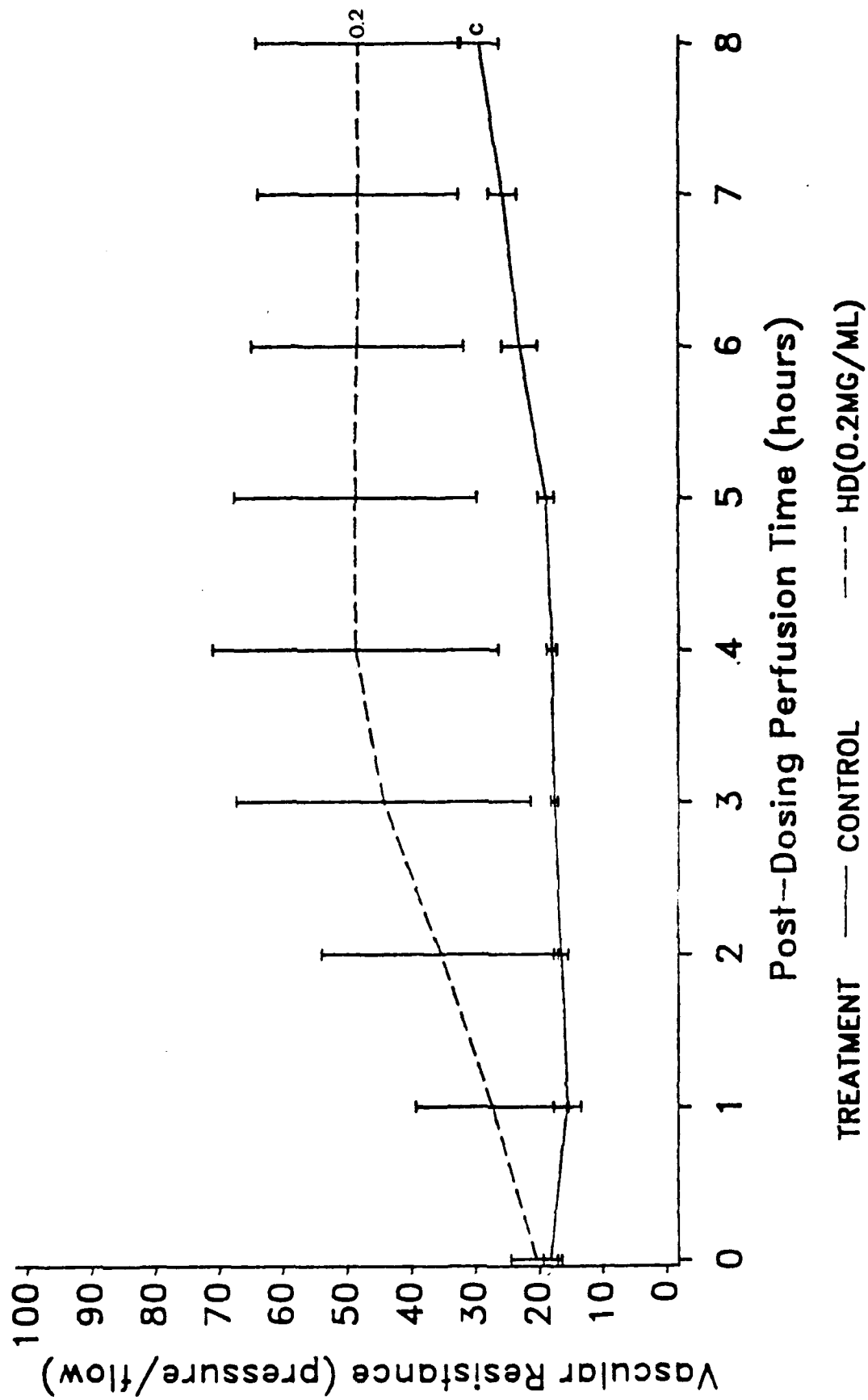
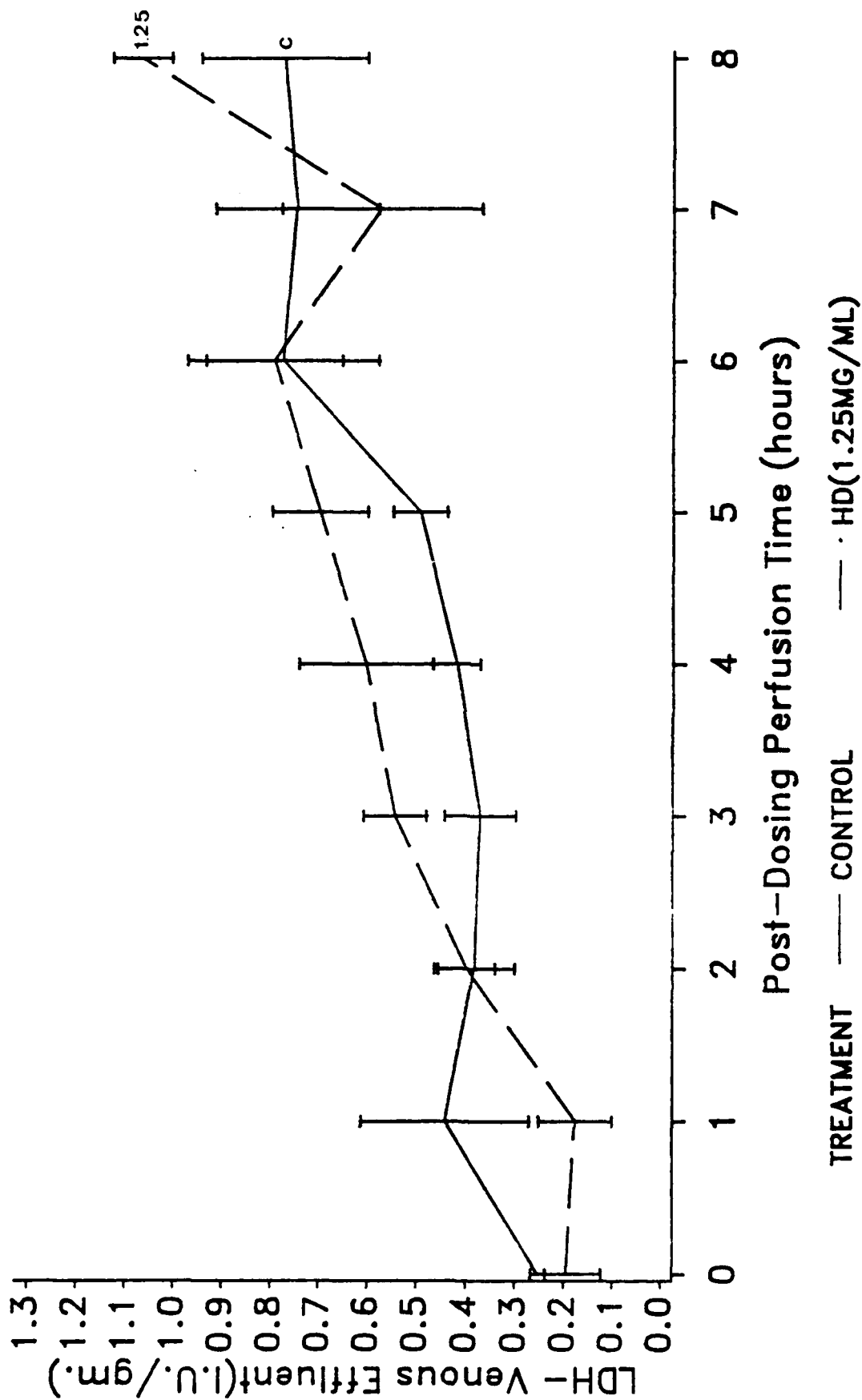FIGURE 64. Graph illustrating VR of 0.2 mg/ml of XHD compared to control.

TREATMENT ——— CONTROL ----- HD(0.2MG/ML)

Post-Dosing Perfusion Time (hours)

Vascular Resistance (pressure/flow)
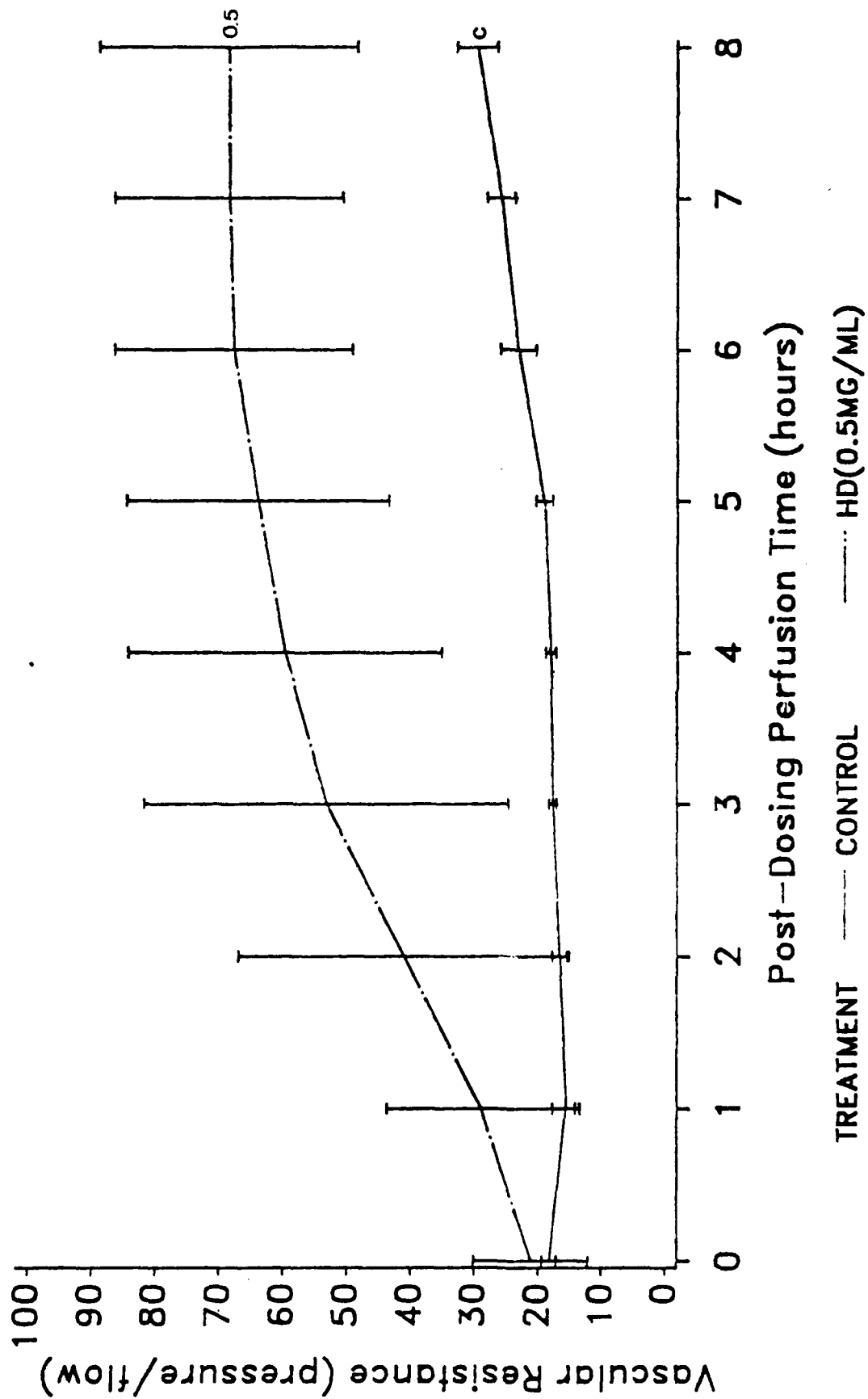
FIGURE 65. Graph illustrating VR of 0.5 mg/ml of XHD compared to control.

FIGURE 66. Graph illustrating VR of 1.25 mg/ml of XHD compared to control.

111

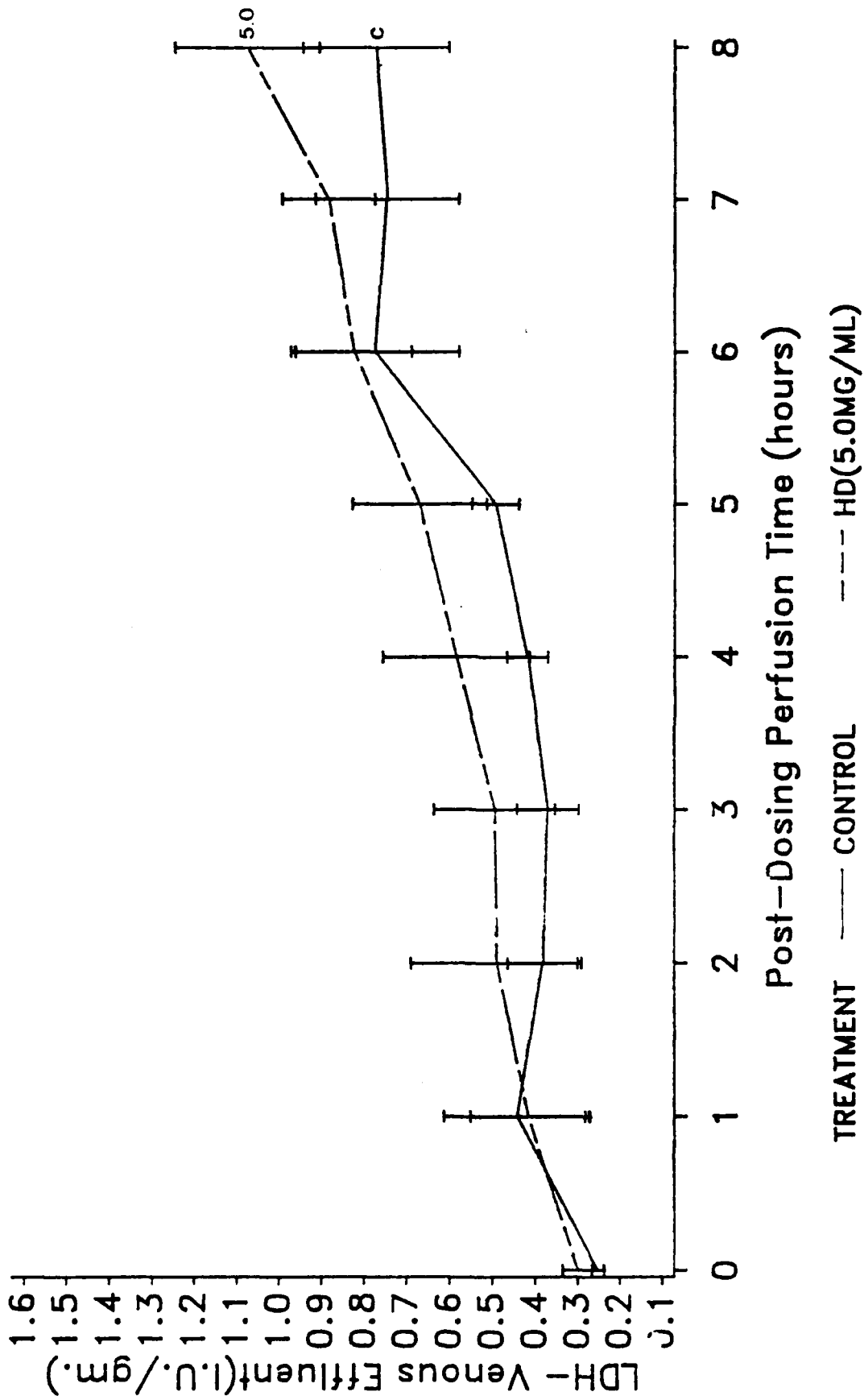FIGURE 67. Graph illustrating VR of 2.5 mg/ml of XHD compared to control.

TREATMENT — CONTROL — — HD(2.5MG/ML)

Post-Dosing Perfusion Time (hours)

Vascular Resistance (pressure/flow)

FIGURE 68. Graph illustrating VR of 5.0 mg/ml of XHD compared to control.
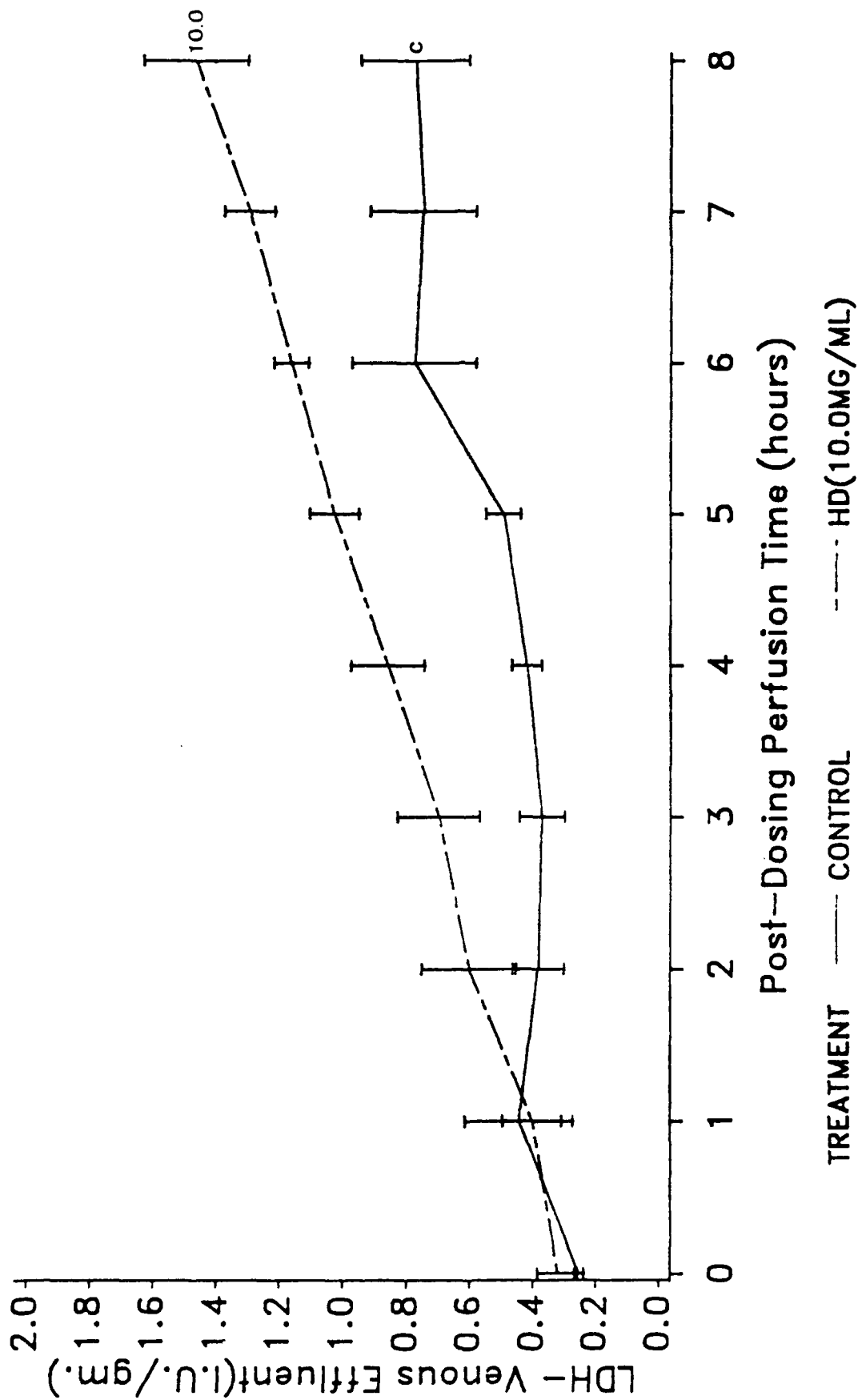
113

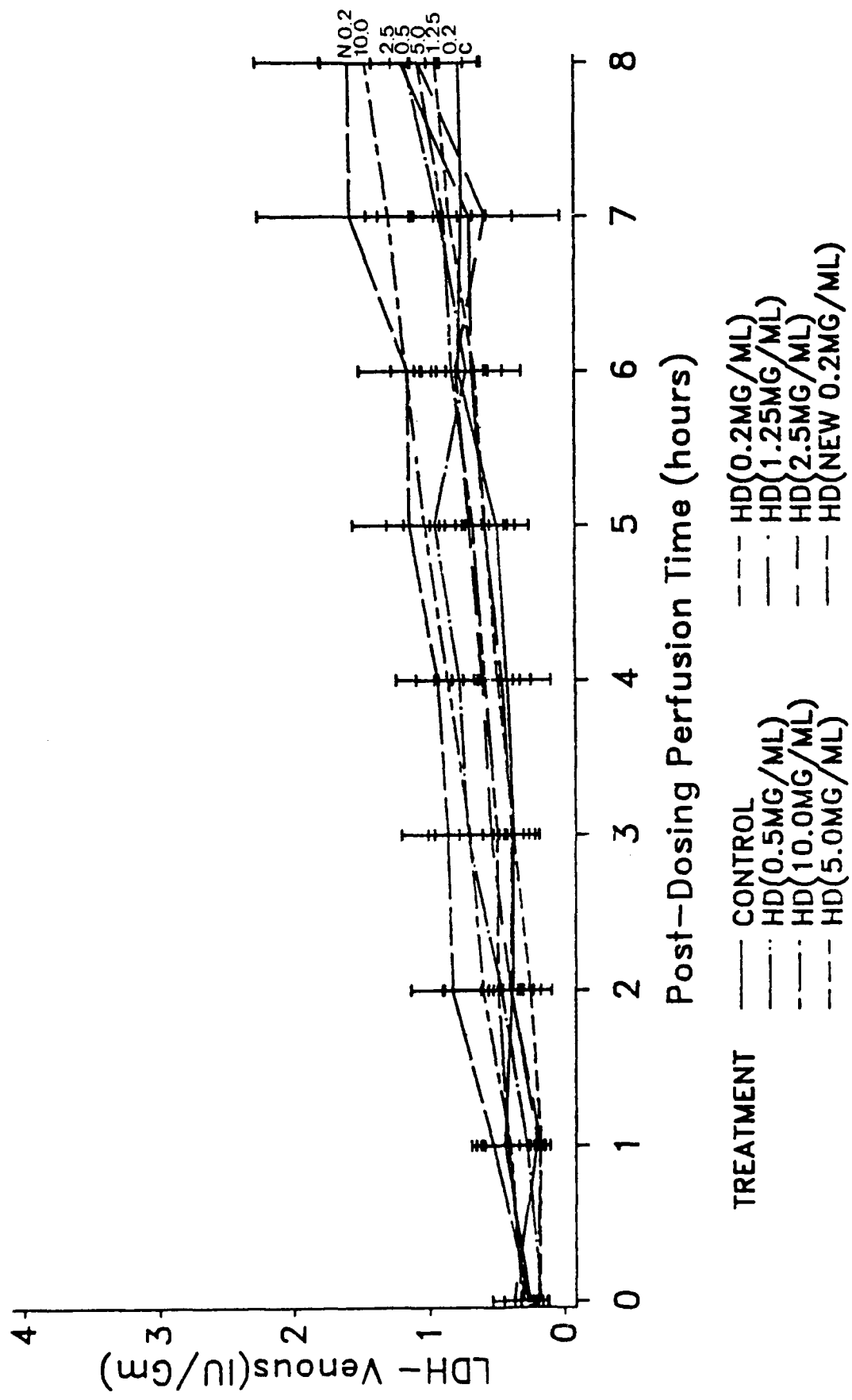FIGURE 69. Graph illustrating VR of 10.0 mg/ml of XHD compared to control.

114

FIGURE 70. Graph illustrating VR of all concentrations of XHD compared to control.

115

FIGURE 71. Graph illustrating LDH of the new 0.2 mg/ml of XHD compared to control.

FIGURE 72. Graph Illustrating LDH of 0.2 mg/ml of XHD compared to control.

117

FIGURE 73. Graph illustrating LDH of 0.5 mg/ml of XHD compared to control.

FIGURE 74. Graph Illustrating LDH of 1.25 mg/ml of XHD compared to control.

119
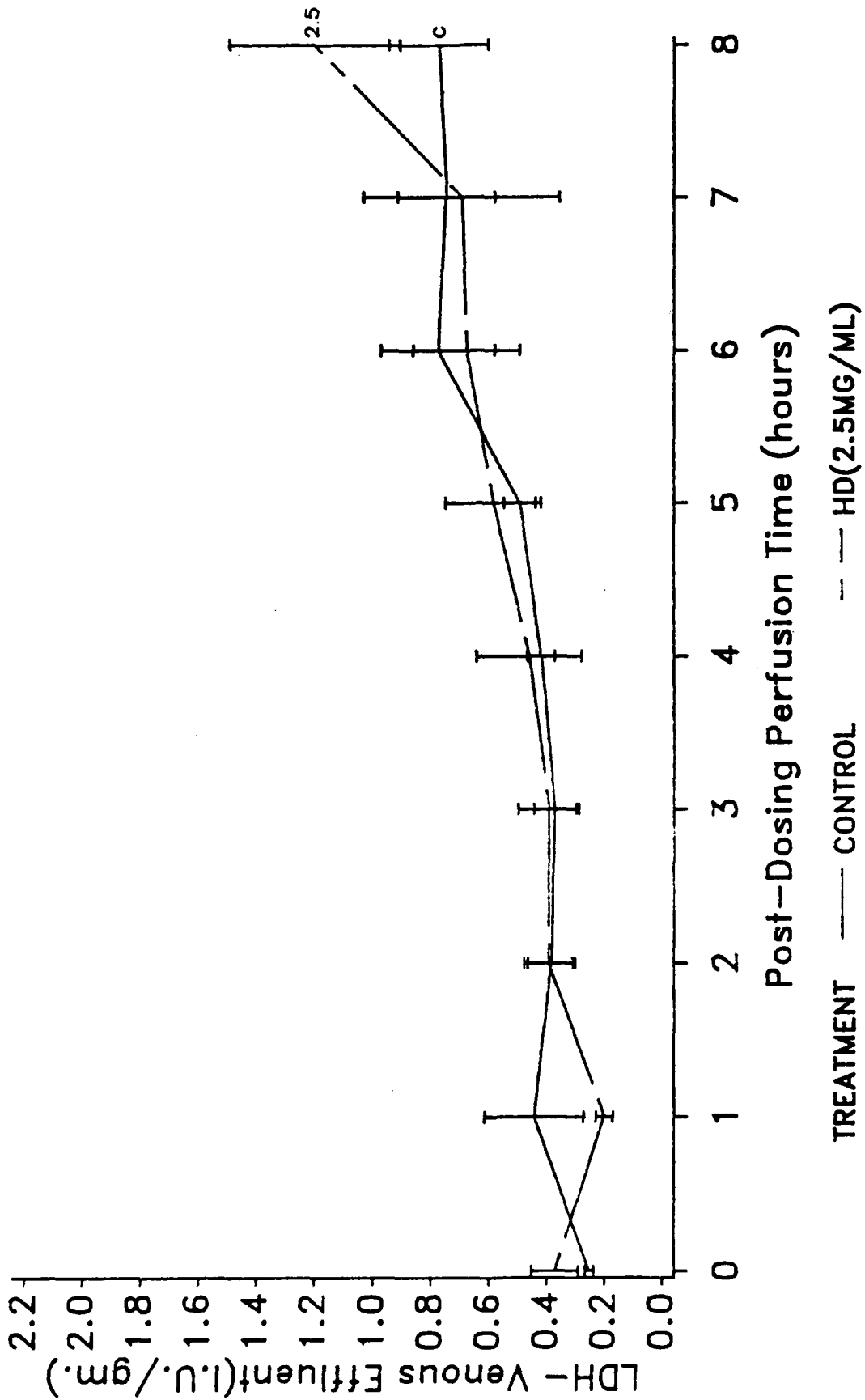
FIGURE 75. Graph illustrating LDH of 2.5 mg/ml of XHD compared to control.

TREATMENT —— CONTROL —— HD(2.5MG/ML)

FIGURE 76. Graph illustrating LDH of 5.0 mg/ml of XHD compared to control.

TREATMENT ——— CONTROL ———— HD(5.0MG/ML)

121

FIGURE 77. Graph illustrating LDH of 10.0 mg/ml of XHD compared to control.

FIGURE 78. Graph illustrating LDH of all concentrations of XHD compared to control.

123

FIGURE 79. A 0.2 mg/ml of XHD treated IPPSF demonstrating typical intracellular epidermal edema (arrows). (X700)
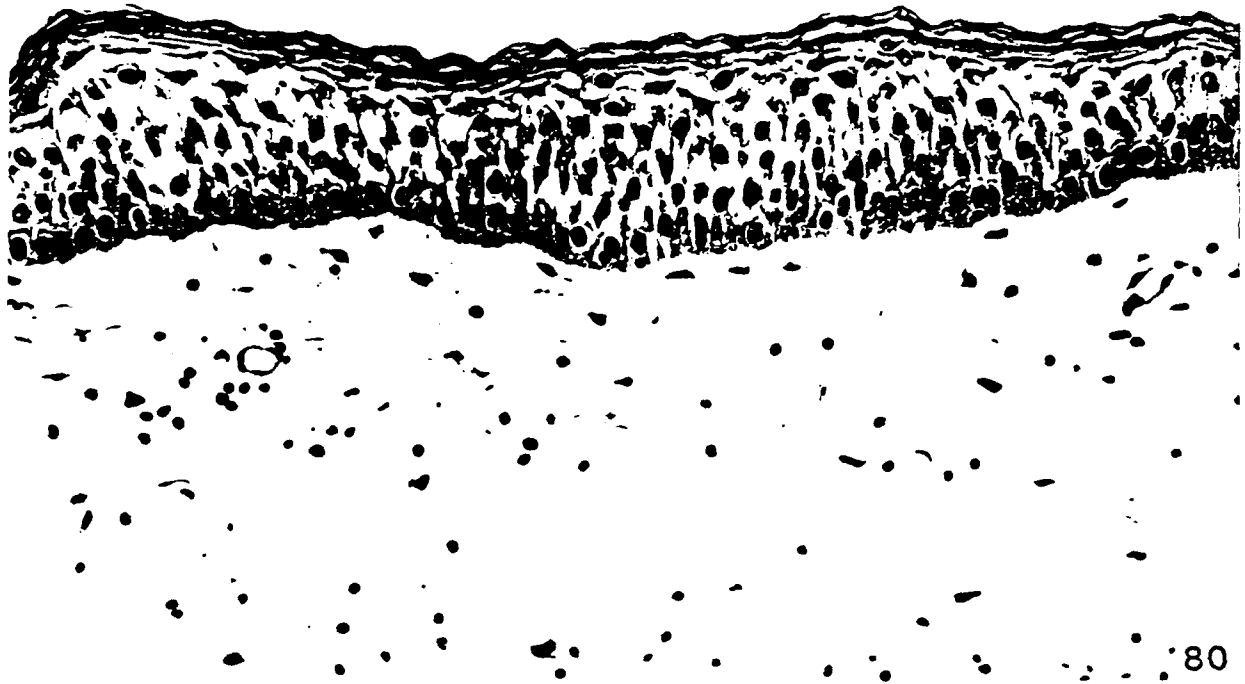
FIGURE 80. LM of 0.2 mg/ml of XHD primarily showing intercellular edema. (X350)
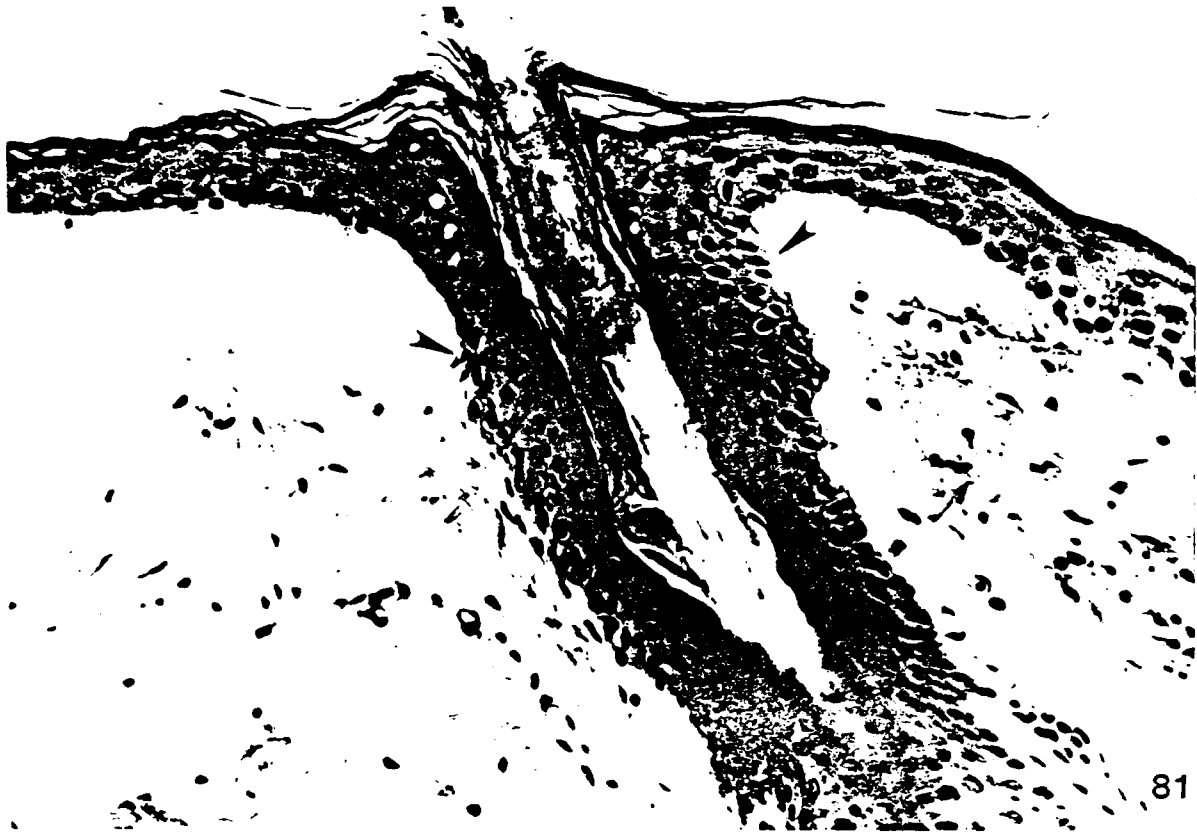
FIGURE 81. LM of an IPPSF treated with 0.2 mg/ml of XHD depicting epidermal-dermal

separation (arrows) on either side of a hair follicle. (X350)

FIGURE 82. TEM of a 0.2 mg/ml of XHD showing intercellular edema (arrow) and blown-out mitochondria (M) in the stratum basale layer (SB). Note that the nucleolar pleomorphism (N) found in normal IPPSF's can be seen in the stratum spinosum layer. (X5,700)
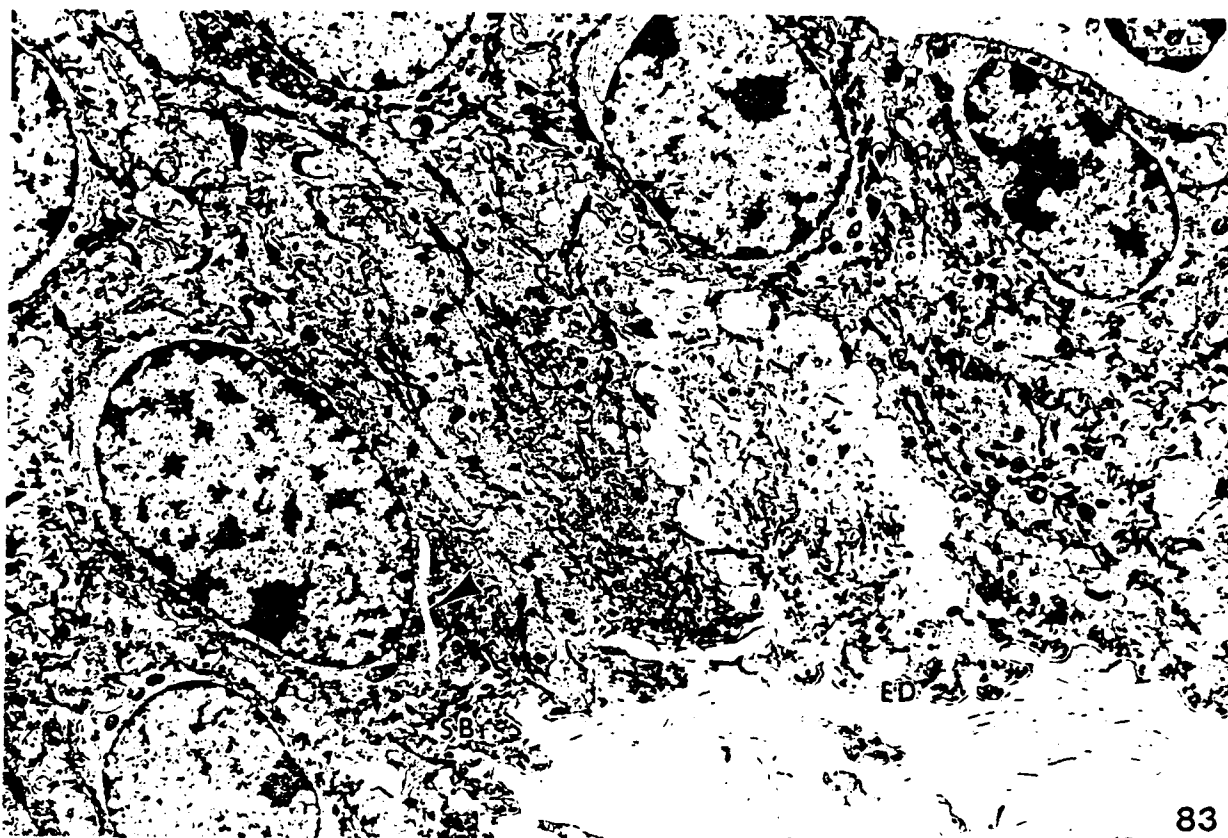
FIGURE 83. TEM of a 0.2 mg/ml of XHD demonstrated a normal epidermal-dermal

junction (ED) and well preserved organelles. Note the dilated endoplasmic

reticulum (arrow) present in the stratum basale cell (SB). (X5,700)

FIGURE 84. Light micrograph of a typical 0.5 mg/ml of XHD-treated IPPSF. Note slight intercellular (large arrow) and intracellular epidermal edema (small arrow). (X350)
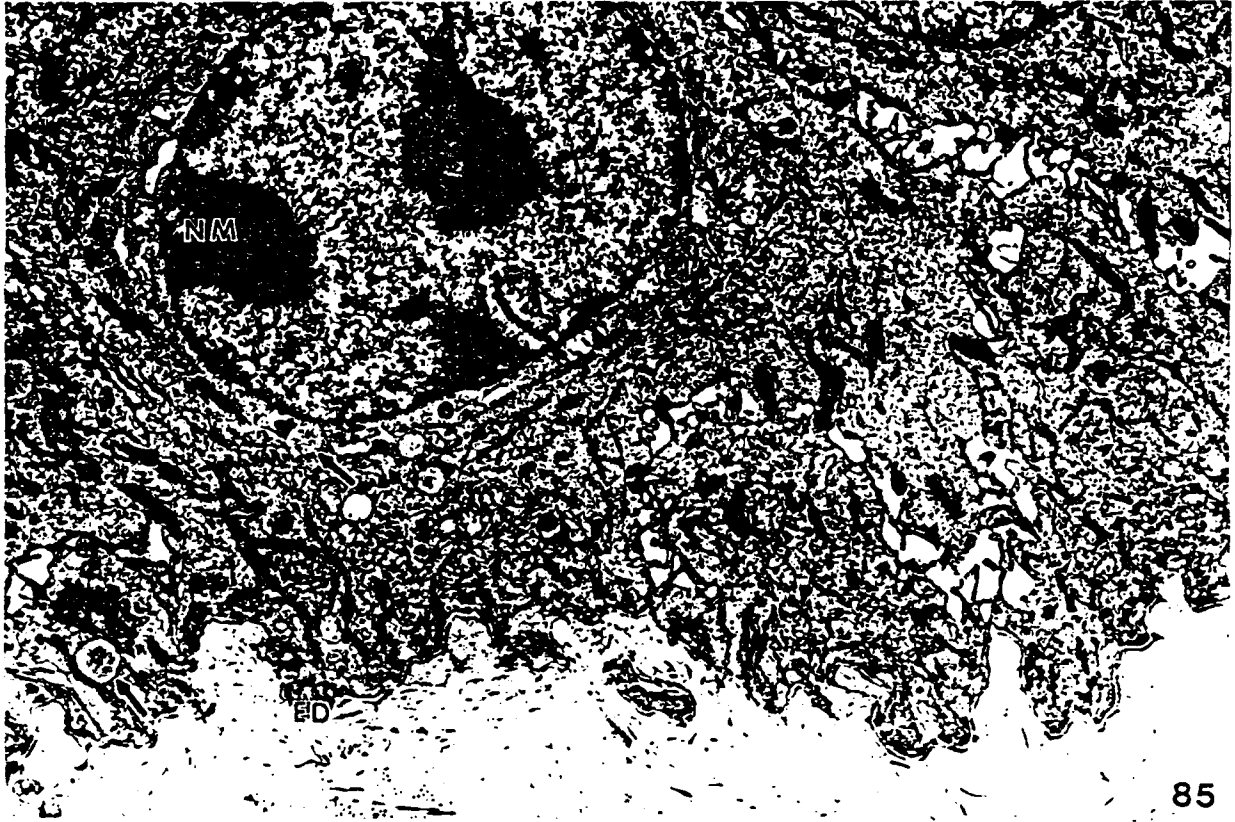
FIGURE 85. Electron micrograph of a 0.5 mg/ml of XHD flap demonstrating normal

epidermal-dermal junction (ED). Note cytoplasmic inclusions of lipid (arrow)

and nucleolar margination (NM). (X8,360)

FIGURE 86. Electron micrograph of a 0.5 mg/ml of XHD flap depicting slight intercellular edema (ID). Note the nucleolar margination. Most nucleoli have an enlarged granular center (arrows) surrounded by dense fibrillar component (F). Also, note the nucleolar caps and margination present in adjacent cells. (X4,560)

FIGURE 87. Light micrograph showing normal stratum corneum (SC), with intracellular
(arrows) and slight intercellular edema in an IPPSF treated with 1.25 mg/ml
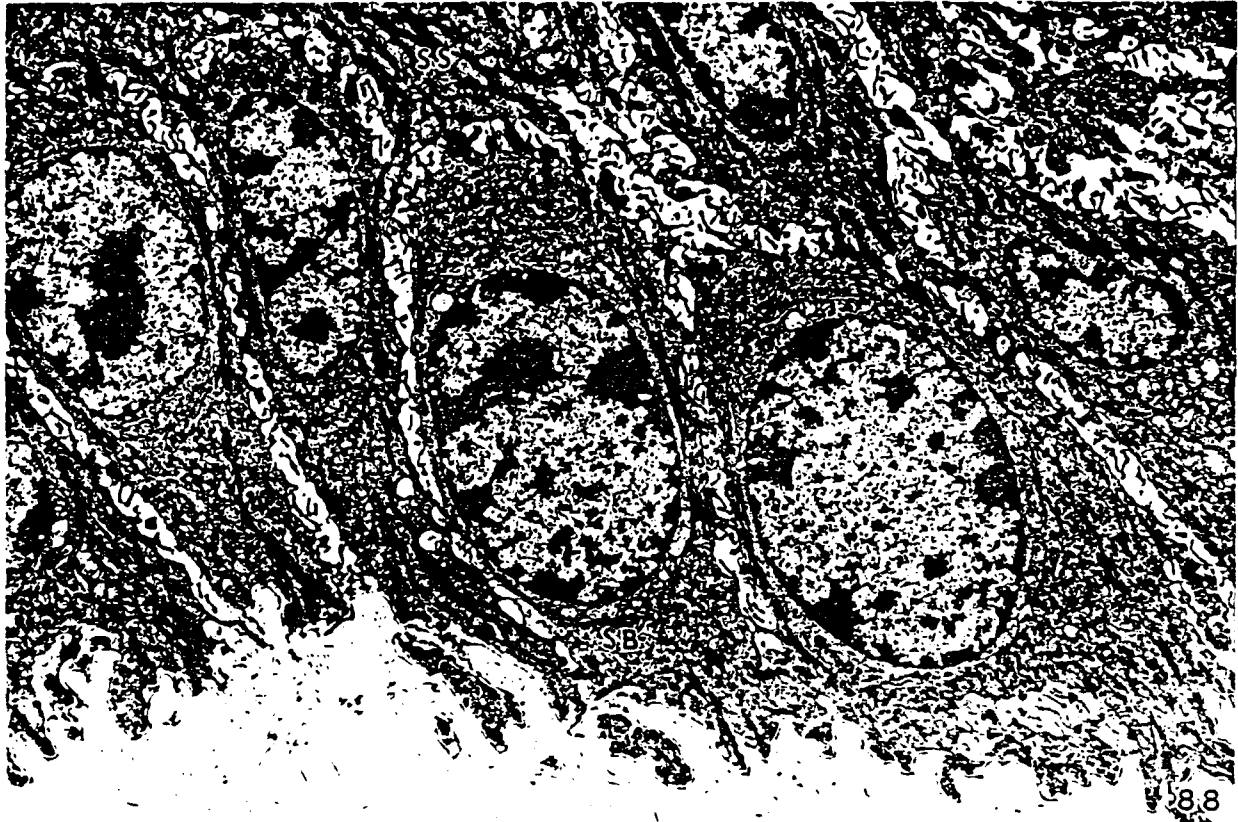of XHD. (X350)

FIGURE 88. Transmission electron micrograph of a 1.25 mg/ml of XHD-treated flap. Note
that the epidermal-dermal junction is intact and the stratum basale (SB) and
stratum spinosum (SS) cells appear normal. (X5,700)

FIGURE 89. Transmission electron micrograph demonstrating
the normal appearance of the upper stratum
spinosum (SS), stratum granulosum (SG) and
stratum corneum (SC) layers in an IPPSF treated
with 1.25 mg/ml of XHD. (X4,560)

FIGURE 90. Transmission electron micrograph of a 2.5 mg/ml

of XHD-treated IPPSF showing a Langerhans cell

process (L) traversing through the stratum basale

(SB) and stratum spinosum (SS) cell layers. Note

the numerous tonofilaments and organelles
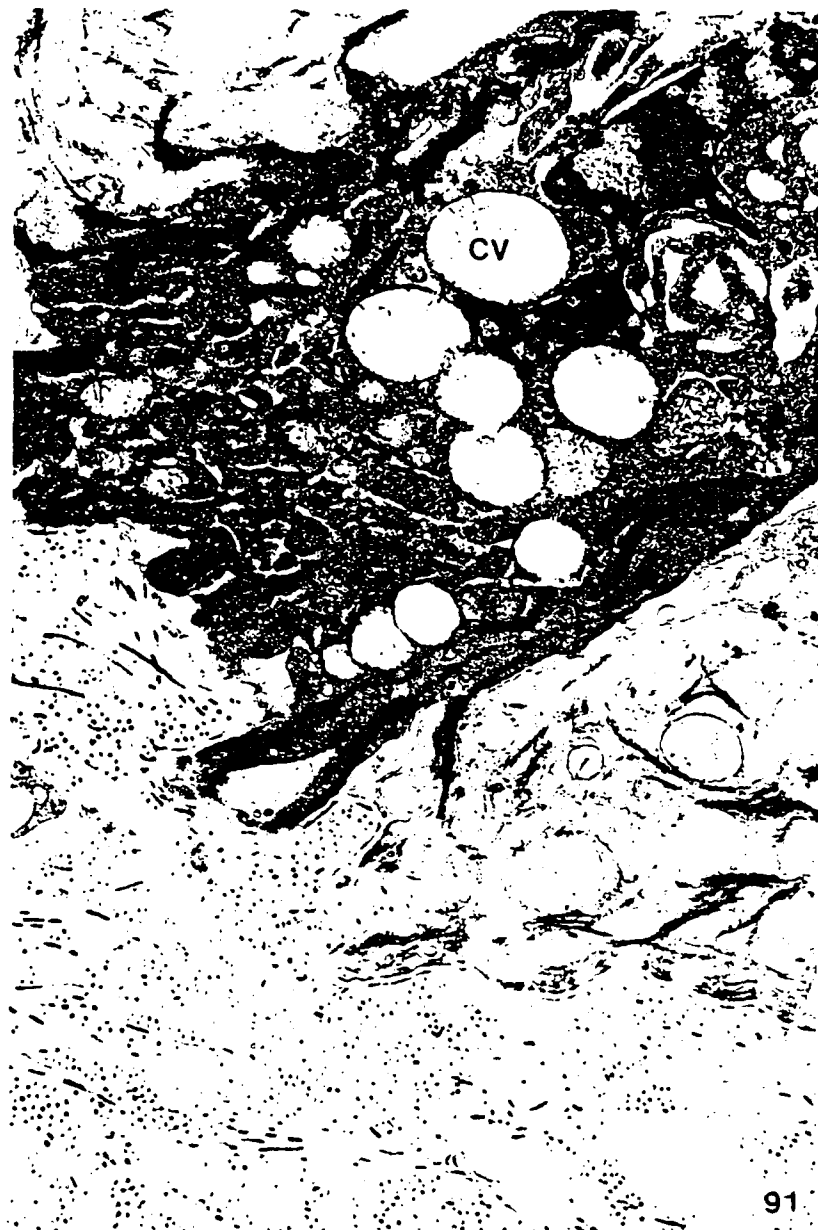
typically present in normal IPPSF's. (X8,360)

135

FIGURE 91. Another example of a 2.5 mg/ml of XHD-treated flap showing a dark degenerative stratum basale cell with large cytoplasmic vacuoles (CV), probably remnants of damaged mitochondria. (X13,490)
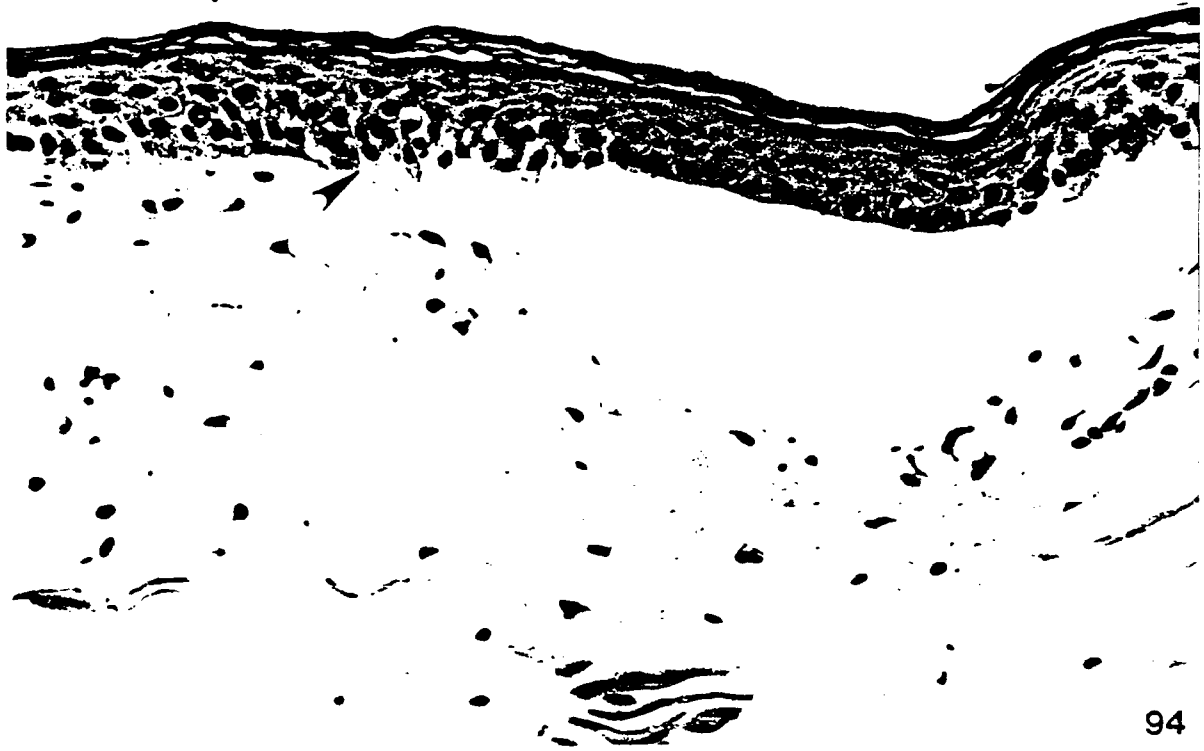
136

FIGURE 92. Light micrograph of a 5.0 mg/ml of XHD showing subepidermal vesiculation

(V) and pyknotic stratum basale cells. (X403)

FIGURE 93. Light micrograph of a 5.0 mg/ml of XHD showing epidermal-dermal

separation (arrow) and intercellular and intracellular epidermal edema.

(X403)

FIGURE 94. Light micrograph of a 5.0 mg/ml of XHD flap exhibiting a focal lesion of epidermal-dermal separation (arrow). (X403)
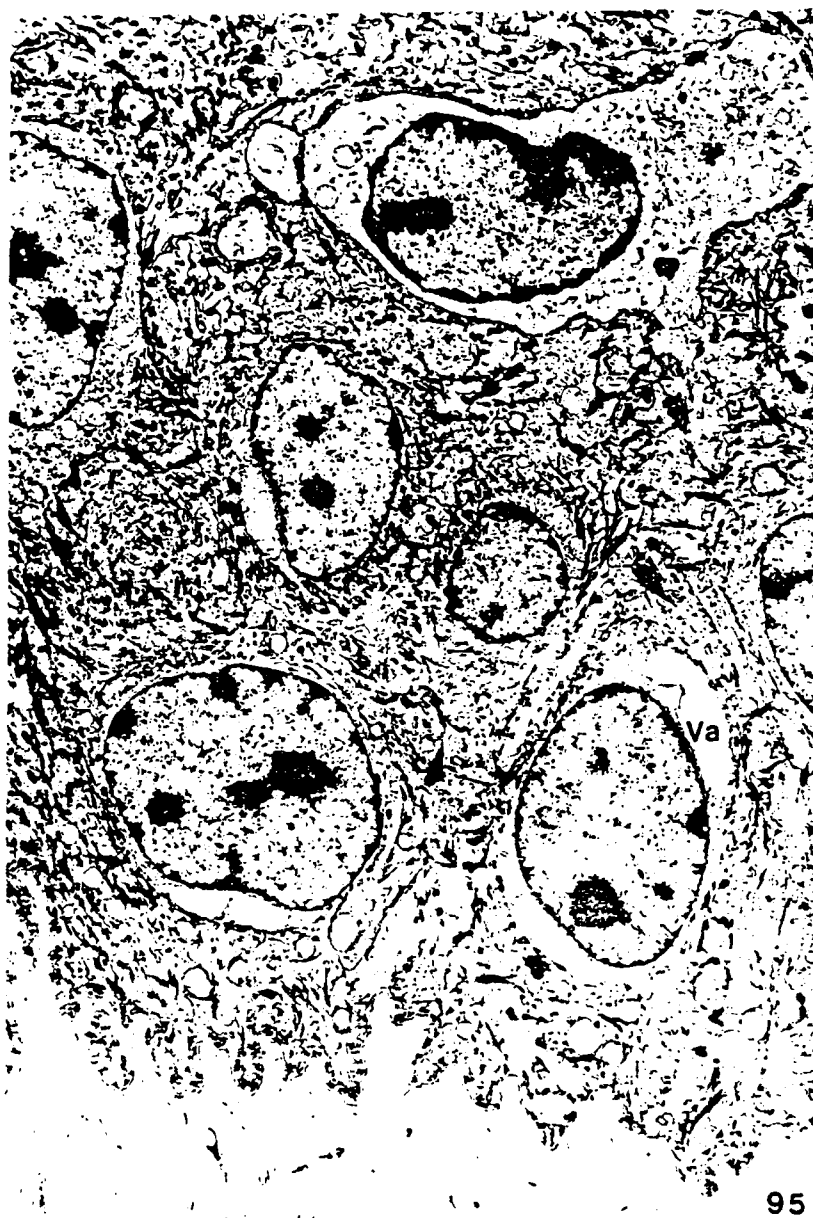
FIGURE 95. Transmission electron micrograph of a 5.0 mg/ml of XHD depicting damaged mitochondria which eventually coalesce, forming a large crescent-shaped vacuole (Va). (X4,560)
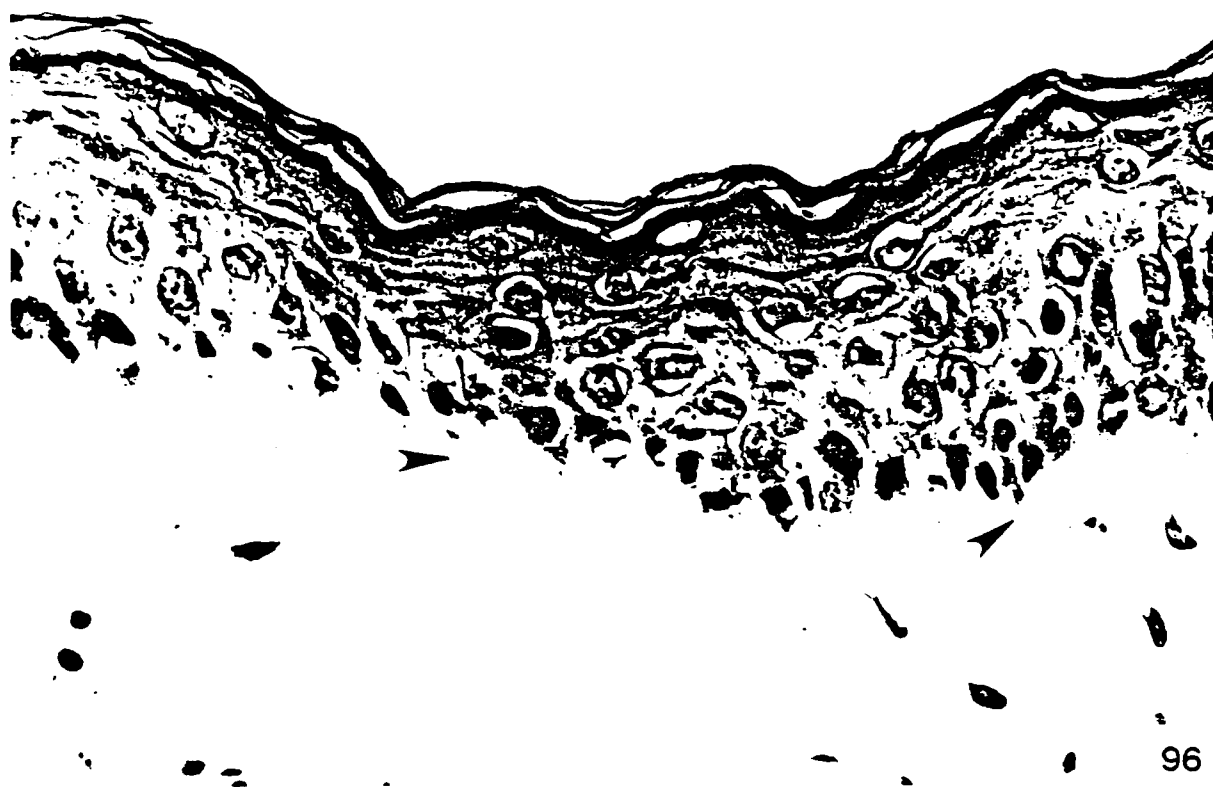
FIGURE 96. Light micrograph of a 10.0 mg/ml of XHD showing basement membrane

separation (arrows) and pyknotic stratum basale cells. (X805)

FIGURE 97. Light micrograph of another 10.0 mg/ml of XHD showing a complete

separation of the epidermal-dermal junction (arrows), pyknotic nuclei, and

inflammatory cells. Note that the upper stratum spinosum, stratum

granulosum, and stratum corneum appear normal. (X350)

FIGURE 98. Transmission electron micrograph of a 10.0 mg/ml of XHD showing pyknotic cells (P), large cytoplasmic vacuoles (CV), and damaged organelles. (X5,700)
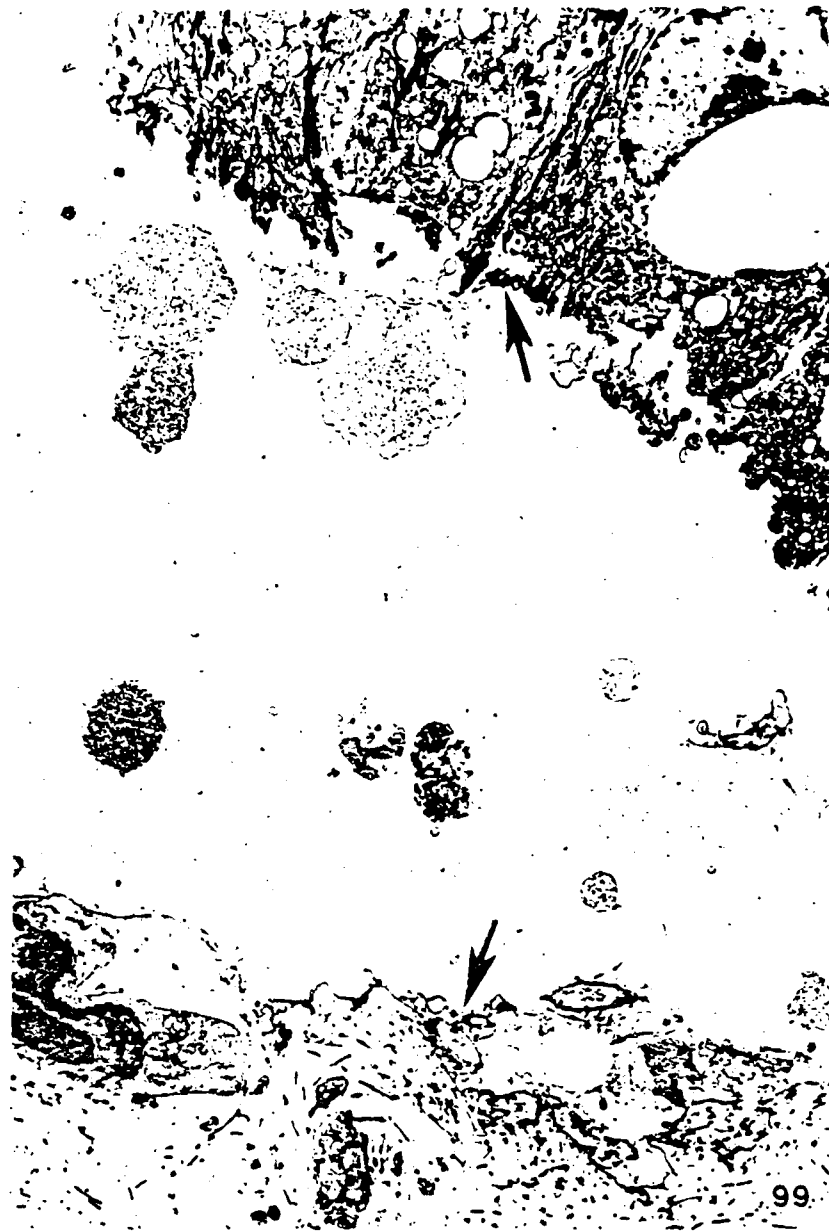
FIGURE 99. Transmission electron micrograph of another 10.0

mg/ml of XHD showing epidermal-dermal

separation (arrows). (X4,560)